H. A. HATİPOĞLU

EXPERIMENTAL AND NUMERICAL INVESTIGATION OF SHEET METAL HYDROFORMING (FLEXFORMING) PROCESS

HASAN ALİ HATİPOĞLU

SEPTEMBER 2007

METU 2007

EXPERIMENTAL AND NUMERICAL INVESTIGATION OF SHEET METAL HYDROFORMING (FLEXFORMING) PROCESS

A THESIS SUBMITTED TO
THE GRADUATE SCHOOL OF NATURAL AND APPLIED SCIENCES
OF
MIDDLE EAST TECHNICAL UNIVERSITY

BY

HASAN ALİ HATİPOĞLU

IN PARTIAL FULFILLMENT OF THE REQUIREMENTS
FOR
THE DEGREE OF MASTER OF SCIENCE
IN
MECHANICAL ENGINEERING

SEPTEMBER 2007

Approval of the thesis:

EXPERIMENTAL AND NUMERICAL INVESTIGATION OF SHEET METAL HYDROFORMING (FLEXFORMING) PROCESS

submitted by **H. ALİ HATİPOĞLU** in partial fulfillment of the requirements for the degree of **Master of Science in Mechanical Engineering, Middle East Technical University** by,

Prof. Dr. Canan Özgen _____
Dean, Graduate School of **Natural and Applied Sciences**

Prof. Dr. Kemal İder _____
Head of Department, **Mechanical Engineering Dept., METU**

Prof. Dr. Zafer Dursunkaya _____
Supervisor, **Mechanical Engineering Dept., METU**

Prof. Dr. –Ing. A. Erman Tekkaya _____
Co-Supervisor, **Manufacturing Engineering Dept., ATILIM UNI.**

Examining Committee Members:

Prof. Dr. Engin Kılıç _____
Mechanical Engineering Dept., METU

Prof. Dr. Zafer Dursunkaya _____
Mechanical Engineering Dept., METU

Prof. Dr. –Ing. A. Erman Tekkaya _____
Manufacturing Engineering Dept., ATILIM UNI.

Asst. Prof. Dr. Serkan Dağ _____
Mechanical Engineering Dept., METU

Assoc. Prof. Dr. Hakan Gür _____
Metallurgical Engineering Dept., METU

Date: _____

I hereby declare that all information in this document has been obtained and presented in accordance with academic rules and ethical conduct. I also declare that, as required by these rules and conduct, I have fully cited and referenced all material and results that are not original to this work.

H.Ali Hatipoğlu

ABSTRACT

EXPERIMENTAL AND NUMERICAL INVESTIGATION OF SHEET METAL HYDROFORMING (FLEXFORMING) PROCESS

Hatipoğlu, H. Ali
M.S., Department of Mechanical Engineering
Supervisor: Prof. Dr. Zafer Dursunkaya
Co- Supervisor: Prof. Dr. A. Erman Tekkaya

September 2007, 138 pages

Sheet metal hydroforming(flexforming) is a process generally used in the manufacturing of aerospace parts in which a rubber diaphragm forms the sheet on a die with the help pressurized fluid and by this aspect it is different from the conventional stamping process. Some defects occur in the parts that are manufactured by this method and they are not different from the general sheet metal forming defects. Wrinkling, tearing and springback are among those defects. Variety of parts makes difficult to encounter these defects arising the detailed investigation of this process.

In this work, the flexforming process was modeled by finite element method in order to investigate the operation windows of the problem. Various two and three-dimensional models were established with and without diaphragm, using explicit and implicit approach for time integration and using solid and shell elements for the blank. Using the material Aluminum 2024-T3 alclad sheet alloy, three basic experiments were conducted: Bending of a straight flange specimen, bending of a

contoured flange specimen and bulging of a circular specimen. By these experiments the effects of blank thickness, die bend radius and forming pressure have been investigated. Experimental results were compared with finite element results to verify the computational models. Then, three selected aerospace sheet parts were analyzed and success of the model in the real life applications is proved.

Keywords: Hydroform, Flexform, Wrinkling, Tearing, Springback, Finite element method.

ÖZ

SAC METAL HİDROFORM (FLEXFORM) PROSESİNİN DENEYSEL VE SAYISAL İNCELENMESİ

Hatipoğlu, H. Ali
Yüksek Lisans, Makina Mühendisliği Bölümü
Tez Yöneticisi: Prof. Dr. Zafer Dursunkaya
Yardımcı Tez Yöneticisi: Prof. Dr. A. Erman Tekkaya

Eylül 2007, 138 sayfa

Sac metal hidroform (flexform) prosesi genellikle uçak parçalarının imalatında kullanılan, sıvı ortamın basıncıyla hareket eden kauçuk bir diyaframın kalıp üzerindeki sacı şekillendirdiği ve bu yönüyle yaygın olan sac metal presleme prosesinden farklılaşan metal şekillendirme yöntemidir. Bu yöntemle üretilen parçalarda bazı sorunlarla karşılaşılmaktadır ki bunlar bilinen sac metal şekillendirme sorunlarından farksızdır. Kırışma, yırtılma ve geri yaylanma bu sorunlar arasındadır. Parça çeşitliliğinin çok olması bu sorunlarla başa çıkmayı güçleştirmekte ve prosesin detaylı incelenmesi gereğini ortaya çıkarmaktadır.

Bu çalışmada, flexform prosesi deneysel ve sayısal olarak incelenmiştir. Sayısal yöntem olarak sonlu eleman yöntemi kullanılmıştır. İki ve üç boyutlu, diyaframlı ve diyaframsız, açık ve kapalı yaklaşımın kullanıldığı, sac için tuğla ve kabuk elemanların kullanıldığı birçok model oluşturulmuştur. Alüminyum 2024-T3 alaşım malzemesi kullanılarak üç temel deney yapılmıştır: Düz flanşa sahip bir parçanın bükülmesi, konturlu flanşa sahip bir parçanın bükülmesi ve dairesel bir parçanın şişirilmesi. Bu deneylerle sac kalınlığının, kalıp büküm yarıçapının ve şekillendirme basıncının parçanın şekline etkileri incelenmiştir ve sayısal analiz

sonuçlarının doğruluğu sınanmıştır. Daha sonra üretimdeki üç örnek uçak parçası seçilerek analizleri yapılmış ve modelin gerçek uygulamalarda da başarılı olduğu ispatlanmıştır.

Anahtar Kelimeler: Hidroform, Flexform, Kırışma, Yırtılma, Geri yaylanma, Sonlu eleman yöntemi.

To My Father

ACKNOWLEDGMENTS

I would like to express my deepest gratitude and appreciation to my supervisor Prof. Dr. Zafer Dursunkaya and my co-supervisor Prof. Dr. –Ing.A.Erman Tekkaya for their support, encouragement and guidance throughout this study.

This study was carried out as a research project with the project name "Optimization of Hydroforming Process" at Turkish Aerospace Industries (TAI). I would like to thank Naki POLAT and Arif Köksal who give the opportunity to work in this project. Also, thank Halit Ulular for providing the necessary equipment for the experimental study; İsmail Ünver and Hakkı Çevik for conducting the experiments; Nevzat Akgün, Tufan Sezenöz and Gökhan Ertem for the material characterization tests.

In addition, I should thank Andre Stühmeyer from CADFEM for his technical support about software using.

I would also like to thank to my colleague İ. Erkan Önder, whose suggestions made great contributions to this work.

I would like to send best wishes to my colleagues Koray Demir, Alper Güner and Emrah Demirci.

Finally, I would like to thank my family for their unyielding support and love.

TABLE OF CONTENTS

CHAPTER 1

INTRODUCTION

1.1 Motivation

Having a closer look to the aircraft sheet parts, it is seen that they have contoured surfaces mostly (Figure 1.1). For the manufacturing of these parts, conventional stamping in which a punch forms the sheet over a die, comes to mind firstly. However, this process is costly for the aircraft companies because there are many different parts that have to be manufactured in small batches. Therefore, flexforming process is used instead.

Flexforming is a type of hydroforming process in which the sheet metal is forced to take the shape of a rigid die by the action of fluid pressure, which acts through a rubber diaphragm (Figure 1.2). The advantages of the process are that there is only a single rigid die providing low die costs, the easy modification of the dies after design changes leading to fast tryouts, and finally high quality parts with less damage of the sheet (less wrinkling and tearing than occurs in conventional stamping). The disadvantages are that special presses are needed to stand for the high pressures (up to 80 MPa) in the pressure chamber and that controlling the final geometry of the part is more challenging than in conventional stamping.

The failure modes of the process are wrinkling, tearing and springback (Figure 1.3). Semi-empirical methods and experience are not sufficient to predict these defects before forming. Therefore, some detailed numerical analysis is needed for the optimization of the process.

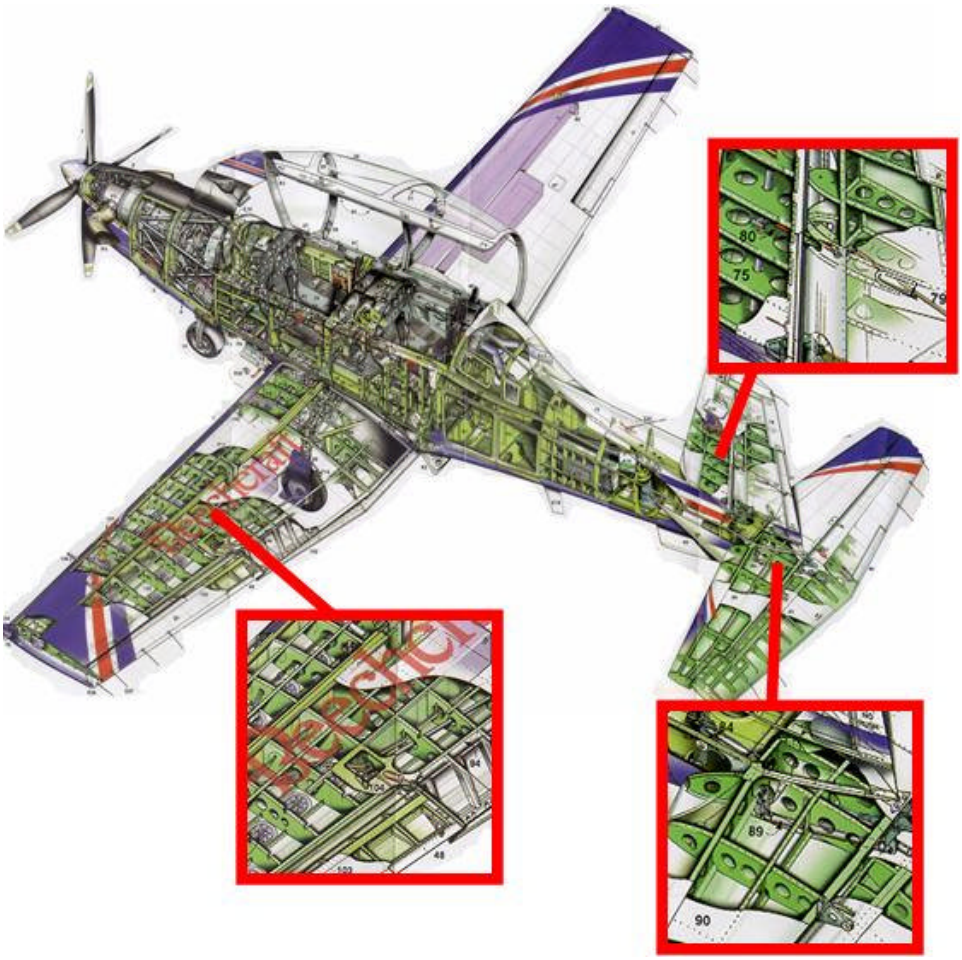

Figure 1.1 Closer look to the aircraft sheet parts

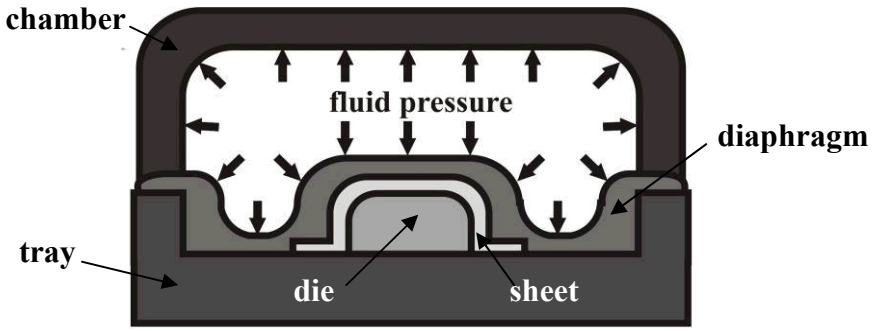

Figure 1.2 Schematic representation of the flexforming process.

Figure 1.3 Failure modes of the process: a) tearing b) wrinkling c) springback

1.2 Aim and scope of this study

In this study, it is aimed to model the flexforming process in order to predict the defects of the formed parts beforehand. This helps to make the necessary design changes of the dies and the blanks earlier and provides time, work and material savings with the elimination of trial and error procedure (Figure 1.4).

Finite Element Method is used for the numerical analysis. Various two and three-dimensional models are established with and without diaphragm, using explicit and implicit approach for time integration and using solid and shell elements for the blank. Using the material Aluminum 2024-T3 alclad sheet alloy, three basic experiments are conducted: Bending of a straight flange specimen, bending of a contoured flange specimen and bulging of a circular specimen. By these experiments the effects of blank thickness, die bend radius and forming pressure have been investigated. Experimental results are compared with finite element results to verify the computational models. Then, three selected aerospace sheet parts are analyzed and success of the model in the real life applications is proved.

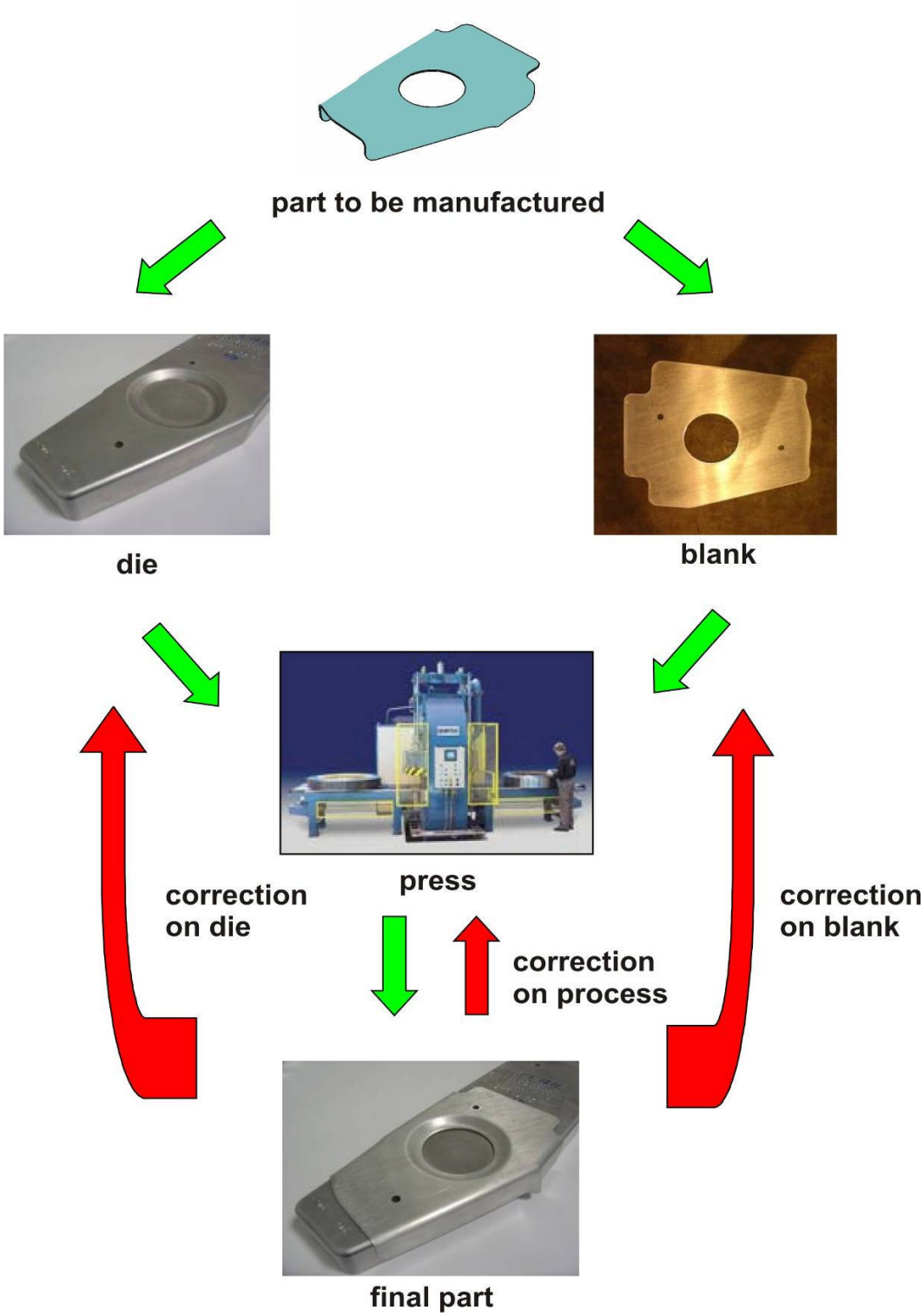

Figure 1.4 Trial and error procedure of the flexforming process

1.3 Content of this study

The whole study can be divided into six chapters. In the first chapter, general information about the study will be given. The next chapter is the literature survey, which will include the past studies about the subject. Chapter 3 is dedicated to finite element method (FEM) and its theoretical background. In the fourth chapter, experimental analysis and material characterization will be presented. In chapter 5, numerical modeling features will be explained and numerical results will be given with comparing experimental results. Chapter 6 contains the three real applications in which the model is used for the simulations. Finally, conclusions and future work will be the content of the last chapter.

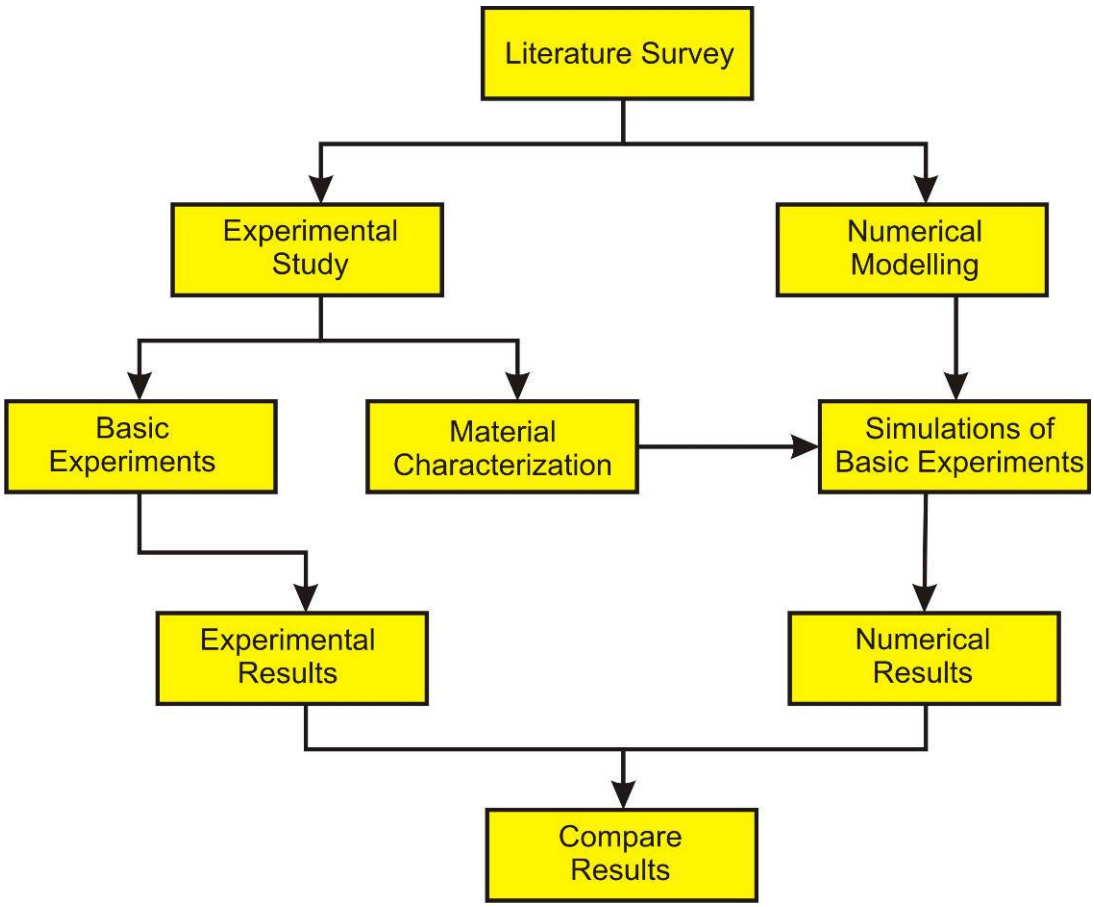

Figure 1.5 Content of the Study

CHAPTER 2

LITERATURE SURVEY

2.1 Introduction

This chapter is devoted to the literature survey and is a preparation to the main subject. Firstly, sheet metal hydroforming types will be introduced in which the working fluid forms the sheet in different ways. Secondly, the place of flexforming process among those will be situated and the past studies about the flexforming process will be cited. Then, some information will be given about the sheet metal formability concepts that will be frequently used in the subsequent chapters. Lastly, studies about the sheet metal forming simulation and springback prediction will be reviewed.

2.2 Sheet Metal Hydroforming Processes

Figure 2.1-a shows the conventional stamping process which contains a rigid die and a rigid punch, a rigid blank holder and a deformable sheet part. Punch moves downwards and forces the sheet that is hold by the blank holder to take the shape of the die. In sheet metal hydroforming processes a working fluid media takes the place of one of the rigid tools providing soft-tooling.

In the first type, the blank holder is replaced by a fluid pressure with a thin rubber diaphragm transferring the pressure to the blank flange. This process is shown in Figure 2.1-b and is known as “deep drawing process with fluid-assisted blank holding” [22]. This soft-blank holder reduces friction considerably and provides high Limiting Drawing Ratios (LDR). The disadvantage is that a fluid blank-holding device is required and the productivity is reduced a little.

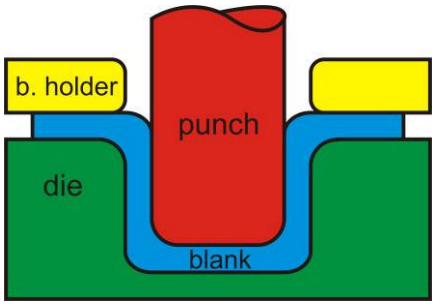

(a) conventional stamping

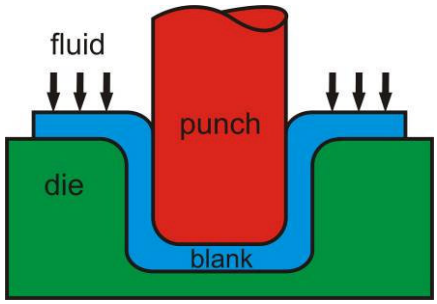

(b) deep drawing with fluid-assisted blank holding

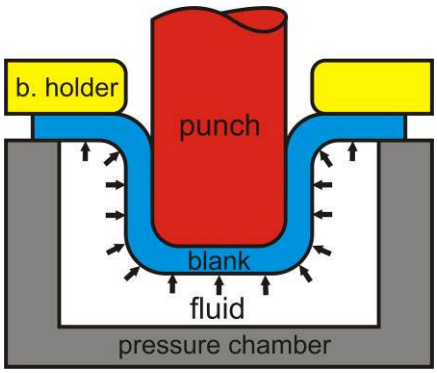

(c) hydromechanical deep drawing

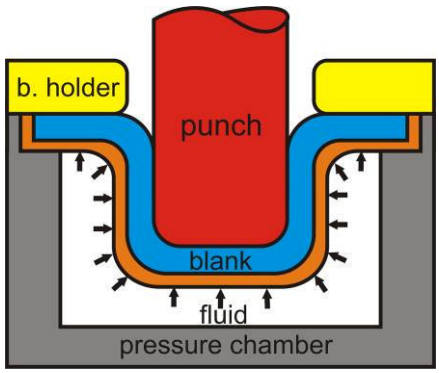

(d) hydromechanical deep drawing with membrane

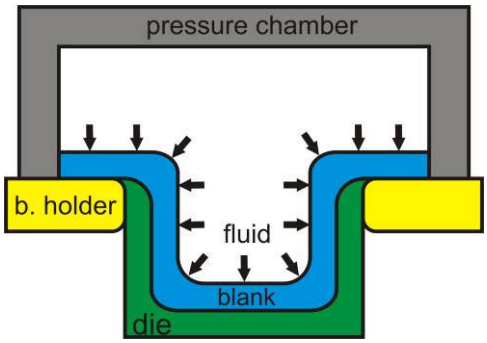

(e) internal high pressure forming

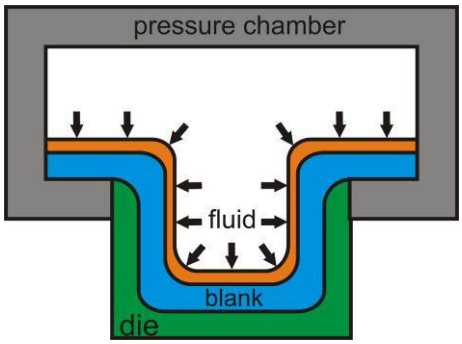

(f) flexforming (with membrane)

Figure 2.1 Sheet metal hydroforming processes

Second type of hydroforming processes replaces the rigid die with fluid which is acting through a membrane (Figure 2.1-d). In this process, again punch moves downwards, but this time the fluid applies a supporting counter pressure to the sheet

acting like a soft die. This process is known as “hydromechanical deep drawing process” [23]. The fluid pressure is controlled by a device and adjusting this pressure is very important for the part quality. If the pressure is not sufficiently high, wrinkles will appear in the part and if the pressure is too high, the part may be damaged by rupture. In another version of this process, there is no membrane and an O-ring is used for preventing the flow out of the fluid on the flange (Figure 2.1-c).

The hydromechanical deep drawing process has the following advantages:

- The counter pressure causes friction forces between the punch and the sheet, which act as part of forming forces. It prevents local thinning and provides uniform thickness distribution of the sheet.

- This counter pressure also serves for wrinkle prevention by acting on the unsupported regions of the sheet causing circumferential tensile stresses.

- For the O-ring type that is without membrane, the fluid between the flange and the blank holder reduces friction leading to high drawing ratios (LDR).

- Since there is only a single punch as a rigid tool and the forming stages are reduced (high LDR values), the process is very flexible and cost effective and is suitable for small batch production.

The disadvantage of the process is that the tool closure is needed and this increases the cycle time of the process. Also, higher forces are needed for stamping and blank holding compared with conventional stamping process.

In the third type, fluid pressure is used instead of rigid punch and the sheet comforms the shape of the die by the act of this soft-punch. Like in the hydromechanical deep drawing process, there are two types with and without membrane that separates the fluid media from the sheet. The one without membrane is known as HBU process (high-pressure sheet metal forming) and is shown in

Figure 2.1-e [24]. This process is suitable for complex sheet parts and small lot production. On the other hand, the process may last longer and accurate positioning of the sheet may be difficult. The one with membrane is known as the flexforming process or fluid cell forming process and is the subject of this thesis work. Different from all other types, there is no blank-holder in flexforming and the sheet is hold by attaching it to the die with the help of guide pins (Figure 2.1-f).

2.3 Past Studies about the Flexforming Process

Only few studies are known in literature about the analysis of this process. Palaniswamy et al. [4] studied reduction of springback in flexforming by using optimized blank dimensions. The sensitivity of springback on the blank dimensions for cone shaped parts is analyzed. Based on this analysis, an optimization problem is formulated that minimizes springback. Kulkarni and Prabhakar [5] conducted physical straight flanging experiments with varying bend angles and part thicknesses in flexforming. Springback results were compared with FEM simulations giving good agreement. In all these studies, rubber diaphragm was not modeled and uniform pressure was applied onto the surface of the blank. F. Vollersten et al. [9] considered this rubber diaphragm, but in a different process called “multiple membrane deep drawing” which is conceptually similar to the hydromechanical deep drawing process stated in the previous section. Deformation behaviour of the rubber diaphragm was investigated and an empirical formulation was developed for the coefficient of friction between the diaphragm and the sheet by conducting strip-drawing tests.

This work aims to investigate the modeling of flexforming process with finite element method taking into account the effect of the rubber diaphragm. Experimental work is done for a better understanding of the influence of process parameters on the final part and for the validation of simulation results. Then, the numerical model is introduced and numerical results are compared with experimental results [8].

2.4 Formability of Sheet Metals

The properties of sheet metals vary considerably depending on the base metal (steel, aluminum, copper, etc), alloying elements, heat treatment, gage and level of cold work. Thus, formability of sheet metals also varies depending on the material properties and the deformation conditions. Therefore, a compromise must be made between functional requirements of the part and forming properties of the available materials.

There are potential formability problems typically associated with each forming operation. The major problems are tearing, wrinkling and springback.

2.4.1 Tearing and Thickness Distribution

During forming, material flows on the sheet from one region to the other according to the tool geometry resulting the local thinning or thickening. The sheet may fracture at those locations where local thinning is high. This defect is called “tearing”. Homogenous thickness distribution is important for high quality of the sheet parts, but this is difficult to obtain.

2.4.2 Wrinkling

Some regions of the sheet part experience compressive plane stresses during deformation. If these stresses exceed a critical value instability occurs and the sheet buckles at these regions. These wavy regions are called as “wrinkles”. Blank Holder Force should be increased to avoid wrinkling.

2.4.3 Springback

There are two deformation types during forming: The elastic deformation in which the part deforms temporarily and the plastic deformation in which the part deforms permanently. Every part first experiences elastic deformation and then plastic deformation if sufficient load is applied. The recovery of the elastic deformation causes shape distortions of the sheet and the final part shapes will be a little different from desired. This phenomenon is called "springback" and is a challenging problem to solve for industry.

In the following paragraphs, the definitions of some sheet metal forming concepts that will be frequently used in the subsequent chapters are given.

2.4.4 Limiting Drawing Ratio (LDR)

The limiting drawing ratio, generally speaking, can be defined as the ratio of optimum initial area of the blank to the mean cross-sectional area of die and punch. Maximum drawing ratio is an important numerical value to determine the required number of drawing steps. For cylindrical cup drawing process with circular cross-section, drawing ratio can be defined by the following equation:

$$\beta = \frac{A_0}{A_i} = \sqrt{\frac{\pi r_0^2}{\pi r_i^2}} = \frac{r_0}{r_i} \tag{2.1}$$

where

A_0 is initial blank area

A_i is mean cross-sectional area of punch and die

r_0 is the initial radius of blank

r_i is the average of punch radius (r_p) and die cavity radius (r_d)

For non-circular cross-section, equivalent drawing ratio can be defined as the ratio of initial blank area and mean cross-sectional area of punch and die.

The limiting drawing ratio is dependent on many factors like the tool geometry, lubrication conditions, and the amount of blank holding forces, sheet thickness, and material properties (especially the R and n value).

2.4.5 Anisotropy

Due to their crystallographic structure and the characteristic of the rolling process, sheet metals generally exhibit a significant anisotropy of mechanical properties [25]. The variation of their plastic behavior with direction is assessed by a quantity called Lankford parameter of anisotropy coefficient [26]. This coefficient is usually determined by uniaxial tensile tests on sheet specimens in the form of a strip. The anisotropy coefficient (r) is defined by

$$r = \frac{e_2}{e_3} \tag{2.2}$$

where ε_2; ε_3 are the strains in the width and thickness directions, respectively

Experiments show that "r" depends on the in-plane direction. If the tensile specimen is cut having its longitudinal axis parallel to the rolling direction, the coefficient r_{90} is obtained. The average of the r-values obtained for different directions in the plane of the sheet metal represents the coefficient of normal anisotropy r_n. The coefficient of normal anisotropy is obtained from equation

$$r_n = \frac{r_0 + 2 \cdot r_{45} + r_{90}}{4} \tag{2.3}$$

where

r_0 is anisotropy factor in rolling direction (RD)

r_{45} is anisotropy factor in 45° direction relative to RD

r_{90} is anisotropy factor in 90° direction relative to RD

A measure of the variation of normal anisotropy with the angle to the rolling direction is given by the quantity,

$$\Delta r = \frac{r_0 + r_{90} - 2 \cdot r_{45}}{2} \tag{2.4}$$

where

r_0 is anisotropy factor in rolling direction (RD)

r_{45} is anisotropy factor in 45° direction relative to RD

r_{90} is anisotropy factor in 90° direction relative to RD

known as planar anisotropy (Figure 2.2).

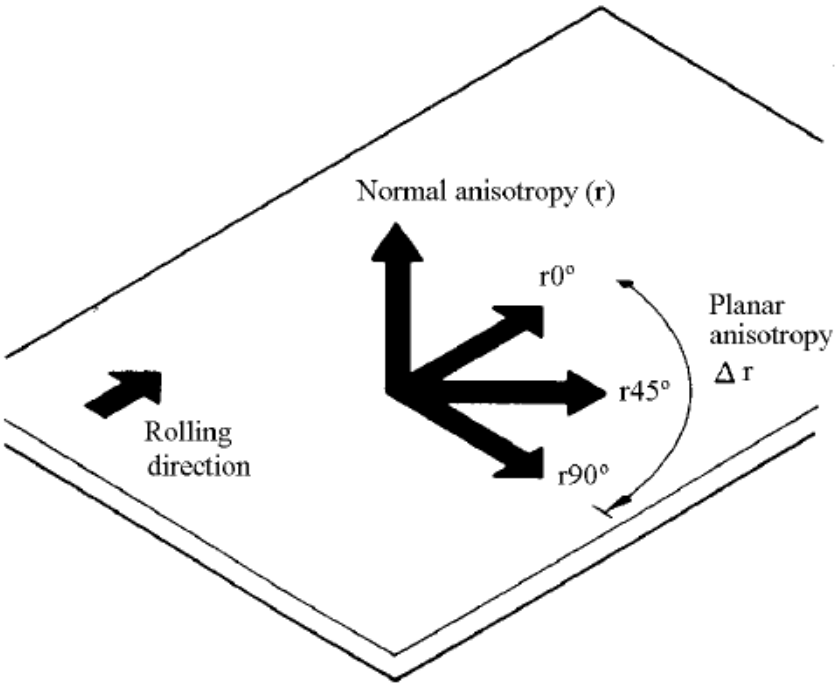

Figure 2.2 Sheet orientation relative to Normal and Planar Anisotropy (Hosford, W.F., et al. 1983)

2.4.6 Forming Limit Diagram

Maximum values of principal strains ε_1 and ε_2 can be determined by measuring the strains at fracture on sheet components covered with grids of circles. The research in this field was pioneered by Keeler, based on the observations of Gensamer [25]. During forming, the initial circles of the grid become ellipses. Keeler plotted the maximum principal strain against the minimum principal strain obtained from such ellipses at fracture of parts after biaxial stretching. By this way, a curve limiting the tolerable range is obtained.

Later Goodwin plotted the curve of tension/compression domain by using different mechanical tests. In this case, transverse compression allows obtaining high values of tensile strains like in rolling or wire drawing.

The diagrams of Keeler and Goodwin together give the values of ε_1 and ε_2 at fracture. Those strain values can be used to determine forming limit diagram (FLD) that is seen in Figure 2.3 [25].

Keeler and Goodwin also suggested an empirical formula that was obtained from experimental trials on standard steel test specimens. This curve is only a function of work hardening exponent (n) and thickness (in mm), and it has been used for about twenty years and has yielded numerous successful results. However, it is not verified for the materials whose work hardening exponent is more than 0.21 and steel with a thickness in excess of 5mm. It is also not suitable for aluminum and new steels [11].

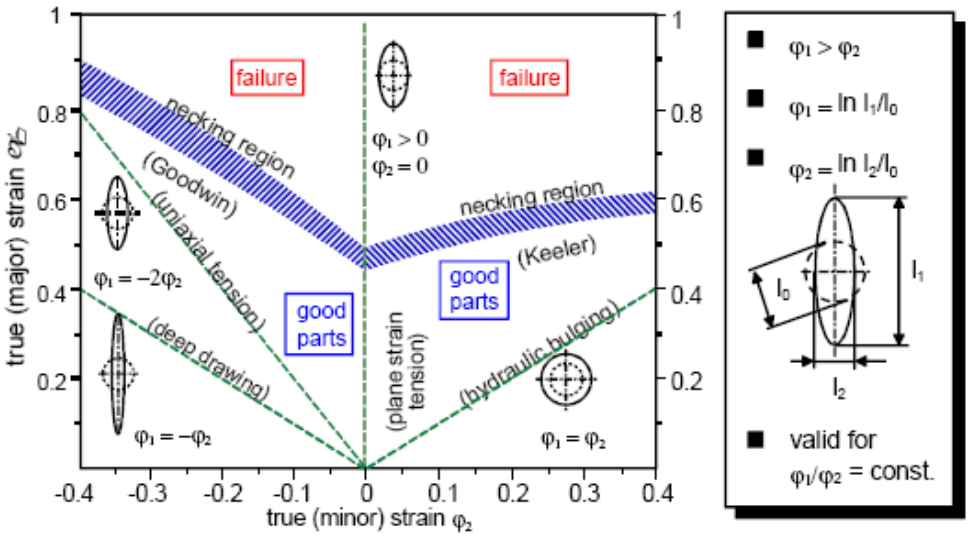

Figure 2.3 Forming Limit Diagram according to the Goodwin and Keeler

2.5 Sheet Metal Forming Simulation

Attempts of numerical approximate solution of sheet metal forming go back to 1980's. The very first numerical solutions of sheet forming processes have been obtained by finite difference methods (FDM) [27]. These methods are, however, restricted to axisymmetrical problems. In the nineties, attempts have been made to replace FDM with FEM in general three-dimensional deep drawing problems. This is due to the serious drawback of not applying boundary conditions in a general manner as it could be done elegantly in the finite element method, FDM could not be established.

The real break-through of the numerical approximation of sheet metal processes was possible through the application of the finite element method done by Wang and Budianski, Wifi, Gotoh and Ishise [25]. In those applications, they used either elasto-plastic or rigid plastic material law and element types were membrane or continuum. Up to this point, all studies are static implicit or static explicit type.

The dynamic explicit methods have their roots in the study of Belytschko and Mullen in 1977. It is interesting that explicit time integration methods, which are

applicable to the solution of the dynamic equations of motion of a finite element model, would be used to simulate an essentially static problem, such as a typical sheet metal forming operation. In finite element simulations with explicit time integration methods, however, it is generally agreed that the computational effort usually becomes enormous and impractical when the actual time duration of the slow physical event is used., provided that the mass densities have not been fictitiously increased. To reduce the computer's effort, the duration of the computer simulation can be reduced, or equivalently the loading rate can be increased. The challenge for the analyst is therefore to artificially speed up the process in the computer simulation to achieve computational efficiency, but at the same time to keep the dynamic effects minimal. [7]

2.6 Springback Prediction

Numerous studies have been conducted to focus on springback from experimental, analytical or numerical viewpoints. Due to the poor accuracy of analytical methods, finite element simulations have been widely used to predict the springback. A complete review on springback studies was presented in [Wagoner, 2002]. Finite element analyses of springback are sensitive to the numerical parameters such as mesh size, element definition, time integration scheme and contact algorithm [Li D., et al., 2002; Papeleux and Ponthot, 2002]. The analyses of springback are also sensitive to the materials such as hardening law, the evolution of elastic modulus during the forming process and the normal anisotropic coefficient R [Kulkarni, 2004; Badis et al., 2005]. Most of studies were carried out with static implicit method to predict the springback [Nilsson, 1997; Forcellese et al., 1998].

The prediction of accurate stress is far more sensitive than the prediction of accurate strain, which is why springback prediction remains a topic for discussion, but forming simulation is generally regarded as being at an acceptable industrial level for quite some time already. In order to achieve an accurate and reliable stress prediction, there is sensitivity to a number of different parameters, some physical, and some purely numerical. Each of these parameters addressed individually will

perhaps only have a limited impact on the results, but by addressing a number of them, it is possible to have reliably accurate and predictive simulation results. [2]

CHAPTER 3

REVIEW OF FINITE ELEMENT METHOD

3.1 Introduction

In this study, finite element method is used for the numerical analyses. The finite element method, a powerful numerical technique, has been applied in the past years to a wide range of engineering problems. Although much FE analysis is used to verify the structural integrity of designs, more recently FE has been used to model fabrication processes. When modeling fabrication processes that involve deformation, such as Sheet Metal Forming, the deformation process must be evaluated in terms of stresses and strain states in the body under deformation including contact issues. The major advantage of this method is its applicability to a wide class of boundary value problems with little restriction on work piece geometry [14].

This chapter aims to give background information about the concepts of finite element method mentioned in Numerical Modeling Chapter (Chapter 5). These are discretization, material models, time integration schemes, contact algorithms and codes used in the analyses.

3.2 Discretization

A mathematical model is discretized by dividing it into a mesh of finite elements. Thus a fully continuous field is represented by a piecewise continuous field by a finite number of nodal quantities and simple interpolation within each element.

3.2.1 Elements

Two-dimensional quadrilateral solid, three-dimensional hexahedron solid and quadrilateral shell elements are the element types used in this study (Figure 3.1).

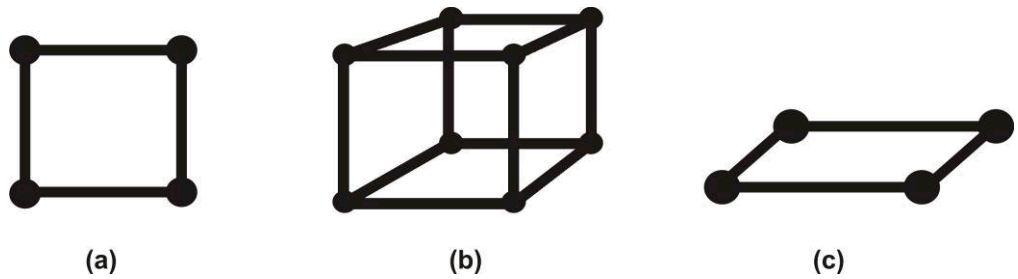

Figure 3.1 Element types used in the analyses. (a) two-dimensional quadrilateral solid element (b) three-dimensional hexahedron solid element (c) quadrilateral shell element

Two-dimensional quadrilateral solid element is a four-noded isoparametric element with bilinear interpolation. Each node has two degrees of freedom in translation and no degree of freedom in rotation. The stiffness of this element is formed using four-point Gaussian integration. This element can be used in the plane strain and axisymetric applications.

Three-dimensional hexahedron solid element is an eight-noded isoparametric element with trilinear interpolation. Each node has three degrees of freedom in translation and no degree of freedom in rotation. The stiffness of this element is formed using eight-point Gaussian integration.

Quadrilateral shell element is a shell element with global displacements and rotations as degrees of freedom. Bilinear interpolation is used for the coordinates, displacements and the rotations. The membrane strains are obtained from the displacement field; the curvatures from the rotation field. The stiffness of this element is formed using four-point Gaussian integration on element plane and user specified number of Gaussian integration points through the thickness.

Special formulations are used to improve some characteristics of the elements. Followings are the brief descriptions of those formulations for solids and shells.

Solid elements:

As these solid elements uses bilinear and trilinear interpolation functions respectively, the strains tend to be constant throughout the element. This results in a poor representation of shear behavior. The shear (or bending) characteristics can be improved by using alternative interpolation functions (ASSUMED STRAIN).

For nearly incompressible behavior, including plasticity or creep, it is advantageous to use an alternative integration procedure. This CONSTANT DILATATION method eliminates potential element locking.

For rubber materials with total Lagrange procedure, HERMANN FORMULATION can be used. This is slightly more expensive because of the extra pressure degrees of freedom associated with this formulation.

When used with reduced integration, i.e. stresses are calculated only in one integration point in the middle of the element, hourglass modes are possible and hourglass control is necessary.

Shell elements:

In the THICK-SHELL formulation, the transverse shear strains are calculated at the middle of the edges and interpolated to the integration points. In this way, a very efficient and simple element is obtained which exhibits correct behavior in the limiting case of thin shells.

When used with reduced integration, i.e. stresses are calculated only in the thickness integration points in the middle of the element, hourglass modes are possible and hourglass control is necessary.

3.2.2 Mesh Transition & Adaptive Meshing

In order to improve the accuracy of the solution, finer mesh is required for the deformable bodies in the critical areas like the tooling curvatures and buckled regions. Using a transition mesh or using adaptive meshing are the ways to obtain this. Figure 3.2 shows a transition mesh. It is used between element patterns with different densities across a transverse plane.

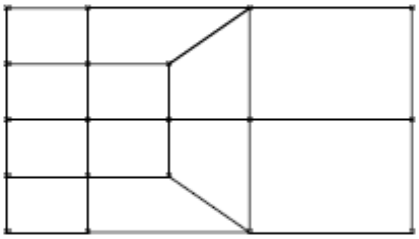

Figure 3.2 A transition mesh

On the other hand, the adaptive meshing procedure works by dividing an element and internally tying nodes to insure compatibility. Figure 3.3 shows the process for a single quadrilateral element. When adaptive meshing occurs, you can observe that discontinuities are created in the mesh. To ensure compatibility free nodes are effectively tied to end nodes of the related edge. There are two refinement criteria for adaptive meshing:

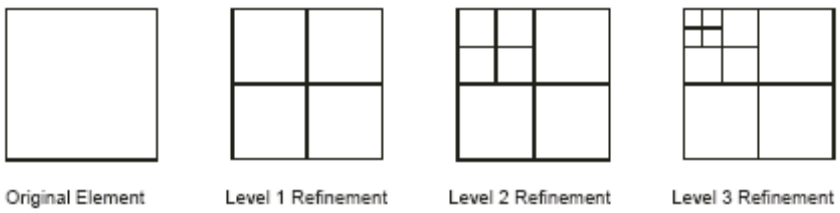

Figure 3.3 Adaptive meshing

Angle Criterion:

The solver refines an element when the variation of the angle between its normal and that of one of its neighbors exceeds a limit angle (Figure 3.4). This criterion is useful for the detection of wrinkles.

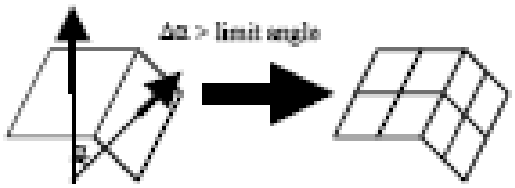

Figure 3.4 Angle Criterion

Geometrical Criterion:

The program adapts the density of the mesh to the local curvature of the tools close to the blank (Figure 3.5).

Figure 3.5 Geometrical Criterion

Adaptive meshing works only for shell elements, for solid elements transition mesh should be used.

3.3 Material Modeling

Two material behaviors are observed in this process. One is the nonlinear elastic behavior belonging to rubber diaphragm and the other is inelastic behavior belonging to the sheet metal.

3.3.1 Rubber Material

An elastomer is a polymer which shows nonlinear elastic stress-strain behavior. The term elastomer is often used to refer to materials which show a rubber-like behavior, even though no rubbers exist which show a purely elastic behavior. These materials are characterized by their elastic strain energy function. Elastomeric materials are elastic in the classical sense. Upon unloading, the stress-strain curve is retraced and there is no permanent deformation. Elastomeric materials are initially isotropic. Figure 3.6 shows a typical stress-strain curve for an elastomeric material. Calculations of stresses in an elastomeric material requires an existence of a strain energy function which is usually defined in terms of invariants or stretch ratios.

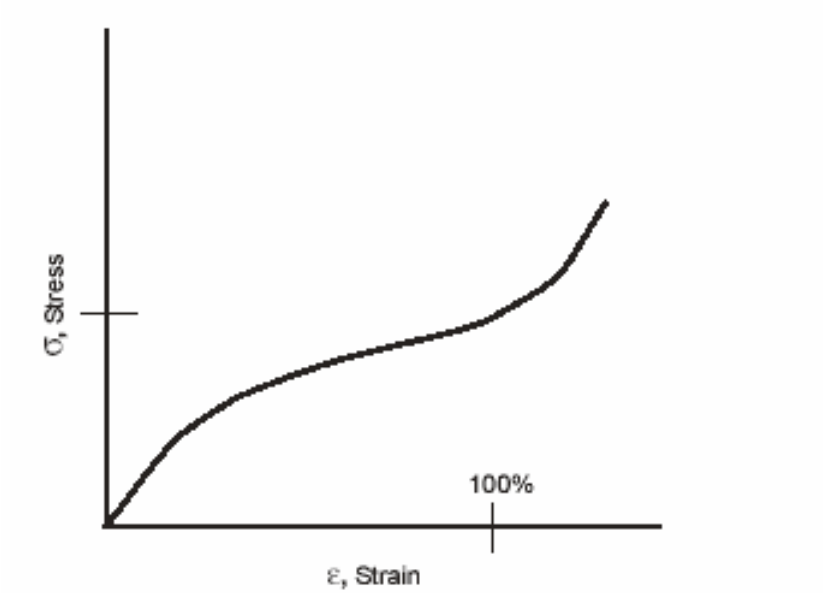

Figure 3.6 Typical stress-strain curve for an elastomeric material

Mooney-Rivlin Law is very common for modeling these kind of materials and is used in this study. In Mooney-Rivlin representation, the strain energy density function is given by:

$$W = W(I_1, I_2, I_3) = A(I_1 - 3) + B(I_2 - 3) + W(I_3)$$

Where: A and B are material parameters and $W(I_3)$ is a penalty function for incompressibility.

$$\begin{aligned} I_1 &= 3 + 2J_1 \\ I_2 &= 3 + 4J_1 - 4J_2 \\ I_3 &= 1 + 2J_1 - 4J_2 + 8J_3 \end{aligned}$$ Right Cauchy-Green strain invariants (3.1)

$$\begin{aligned} J_1 &= Tr(\mathsf{e}_{ij}) \\ J_2 &= 1/2.\mathsf{e}_{ij}.\mathsf{e}_{ij} - 1/2.J_1 \\ J_3 &= Det(\mathsf{e}_{ij}) \end{aligned}$$ Green-Langrange strain invariants (3.2)

$$S_{ij} = \frac{\partial w}{\partial \mathsf{e}_{ij}}$$ S_{ij} is the 2nd Pialo-Kirchhoff stress tensor (3.3)

3.3.1 Sheet Material

In uniaxial tension tests of most metals (and many other materials), the following phenomena can be observed. If the stress in the specimen is below the yield stress of the material, the material behaves elastically and the stress in the specimen is proportional to the strain. If the stress in the specimen is greater than the yield stress, the material no longer exhibits elastic behavior, and the stress-strain relationship becomes nonlinear. Figure 3.7 shows a typical uniaxial stress-strain curve. Both the elastic and inelastic regions are indicated.

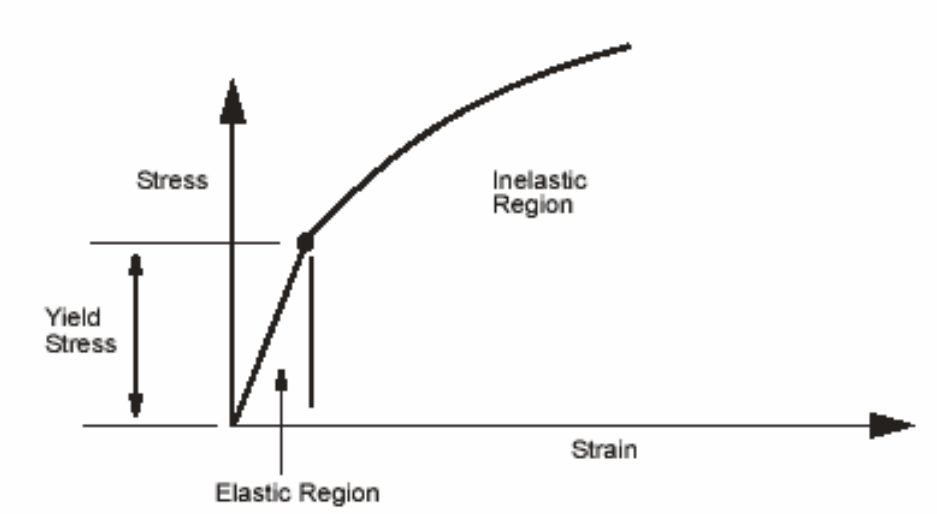

Figure 3.7 Typical stress-strain curve for a metal

The yield stress of a material is a measured stress level that separates the elastic and inelastic behavior of the material. The magnitude of the yield stress is generally obtained from a uniaxial test. However, the stresses in a structure are usually multiaxial. A measurement of yielding for the multiaxial state of stress is called the yield condition. Depending on how the multiaxial state of stress is represented, there can be many forms of yield conditions. For example, the yield condition can be dependent on all stress components as in the case of von Mises yield condition. The von Mises criterion states that yield occurs when the effective (or equivalent) stress (σ) equals the yield stress (σy) as measured in a uniaxial test.

For an isotropic material:

$$s = \sqrt{(s_1 - s_2)^2 + (s_2 - s_3)^2 + (s_1 - s_3)^2} / \sqrt{2} \tag{3.4}$$

where s_1, s_2 and s_3 are the principal Cauchy stresses.

In addition to yield stress, another rule that characterize the plastic material behavior is the hardening rule. It is represented by a hardening curve (stress-plastic strain) in which its slope relates the incremental stress to incremental plastic strain

in the inelastic region and dictates the conditions of subsequent yielding. The yield stress and the workhardening data must be compatible with the procedure used in the analysis. Isotropic workhardening rule is assumed in this study in which the center of the yield surface remains stationary in the stress space, but that the size of the yield surface expands, due to workhardening. Hardening curve can be defined in several ways. Point list definition is used in this study in which the experimental values obtained from the uniaxial tensile test are entered.

3.4 Time Integration Schemes

Implicit and Explicit are the types of time integration schemes used in finite element method.

3.4.1 Implicit

For the implicit method, the solution for the displacement vector at time, $t+\Delta t$, is sought based upon equilibrium conditions based upon time, $t+\Delta t$. If the Houbolt method is assumed then equilibrium equations take on the following form:

$$\left(\frac{2}{\Delta t^2}\widetilde{M}+\frac{11}{6\Delta t}\widetilde{C}+\widetilde{K}\right)\widetilde{U}^{t+\Delta t}=$$

$$R^{t+\Delta t}+\left(\frac{5}{\Delta t^2}\widetilde{M}+\frac{3}{\Delta t}\widetilde{C}\right)\widetilde{U}^{t}-\left(\frac{4}{\Delta t^2}\widetilde{M}+\frac{3}{2\Delta t}\widetilde{C}\right)\widetilde{U}^{t-\Delta t}+\left(\frac{1}{\Delta t^2}\widetilde{M}+\frac{1}{3\Delta t}\widetilde{C}\right)\widetilde{U}^{t-2\Delta t} \tag{3.5}$$

For implicit calculation, the equation is not solved using the whole desired displacement; the displacement and the load conditions are broken up into several steps called increments. For each increment, the solution of the sets of non linear equations requires iterations, called Newton iterations. Typically, the implicit load/displacement increments are 100 to 1000 times larger than explicit time step.

3.4.2 Explicit

For the explicit method, a solution to the displacement vector at time, $t+\Delta t$, is sought based upon the equilibrium conditions at time, t. If the central difference method is assumed then equilibrium equations take on the following form:

$$\left(\frac{1}{\Delta t^2}\widetilde{M}+\frac{1}{2\Delta t}\widetilde{C}\right)U^{t+\Delta t}=\widetilde{R}^t-\left(\widetilde{K}-\frac{2}{\Delta t^2}\widetilde{M}\right)\widetilde{U}^t-\left(\frac{1}{\Delta t^2}\widetilde{M}-\frac{1}{2\Delta t}\widetilde{C}\right)\widetilde{U}^{t-\Delta t} \tag{3.6}$$

where: $\widetilde{M},\widetilde{C},\widetilde{K}$ are the mass, damping and stiffness matrices, respectively.

$\widetilde{U}$ and $\widetilde{R}$ are the displacement and external load vectors, respectively.

In explicit calculation, the state of the simulation is continuously calculated; the time is broken up to a large number of steps called cycles and the state of the simulation is calculated for each cycle. The interval between two cycles is called the time step. A local time step is associated with each element. This element time step ΔTel is equal to the time taken by an elastic wave to pass through the element. Hence it depends on the size, density and elastic modulus of the element.

$$\Delta Tel=\frac{L}{c} \tag{3.7}$$

where L: characteristic length, c: sound speed

c and L depend on element type.

For shell elements:

$$c=\sqrt{\frac{E}{\mathsf{r}(1-\mathsf{n}^2)}} \tag{3.8}$$

where E : elastic modulus, r : density, n : Poisson's ratio

$$L = \frac{(1+\beta)A}{\max(L_1, L_2, L_3, (1-\beta)L_4)} \tag{3.9}$$

where β =0 for quadrilateral shell elements and 1 for triangular shell elements, A is the area and $L_i (i = 1...4)$ is the length of the sides defining the shell elements.

For solid elements:

$$c = \sqrt{\frac{E(1-\nu)}{\rho(1+\nu)(1-2\nu)}} \tag{3.10}$$

$$L = \frac{V}{A\max} \tag{3.11}$$

where V is the volume and Amax is the area of the largest side of the element.

A global time step ΔT used for the calculation, is computed from these element time steps. Only the time step of deformable elements is being used for the calculation of the global time step. Stability of the explicit method is ensured if the global time step is lower than the smallest element time step.

Although metal forming processes can be considered as quasi-static processes, the dynamic explicit approach handles these processes as slow-dynamic problems. However, it is agreed that the computational effort usually becomes enormous and impractical when the actual time duration and the actual mass of the slow physical event is used. Therefore, two tricks can be applied in order to save computational time:

1- The global time step ΔT can be increased by increasing the mass of the elements whose time step is smaller than a defined value. This is called “mass scaling” and reduces the computation time. However, it should be used cautiously since increasing the mass of the elements increases the inertial effects, and this can lead to erroneous results.

2- The process speed can be increased artificially while keeping the dynamic effects minimal. This is called “velocity scaling” and reduces the computation time. In order to reduce the undesired effects of the artificial mass forces numerical damping is introduced.

In order to control the inertial effects and avoid unrealistic results of both “mass scaling” and “velocity scaling”, it is always required providing an adequate amount of attention. This care can be exercised with the help of kinetic energy to internal energy ratio. Previous studies have shown that the kinetic energy of the material should be less than one percent of the internal energy.

3.4.1 Implicit vs Explicit

Table 3.1 summarizes the differences in implicit and explicit codes [14]. Which solution scheme from implicit and explicit is superior is an object at issue. Some researchers embrace the implicit form because, from an equilibrium standpoint, it is more reliable and rigorous at each step. However, convergence is not always guaranteed. Others support the explicit form because, in spite of the fact that it is less rigorous from an equilibrium standpoint at each step, it has much more favorable convergence properties, provided that the appropriate time step is assumed. Ultimately, the nature of the application should drive the decision.

Table 3.1 Implicit vs. Explicit codes

S. No	Implicit	Explicit
1.	Large time increment can be adopted and the equilibrium is rigorously satisfied at the end of the time step.	It restricts the time increment to very small size in order to maintain the out of balance force within admissible tolerance.
2.	In some cases implicit finite element analysis may develop convergence problems associated with sudden changes on the contact conditions between work piece and tools.	The solution procedure is stable even if the deformation dependent contact problem is included in the process.
3.	Several equilibrium iterations must be performed for each time step, and for each iteration it is necessary to solve a set of linear equations.	It requires fewer computations per time step. Complex geometries may be simulated with many elements that undergo large deformations.
4.	They are not well suited to solving the interaction of a large number of nodes with rigid tooling, but they do handle the springback calculation very efficiently.	Although explicit codes are well suited to solving large sheet-forming models with large number of deformable elements, calculation of geometry after springback may be difficult.
5.	Generally favored for relatively slow problems with static or slowly varying loads.	Generally favored for fast problems such as impact and explosion.

3.5 Contact and Friction

The contact and friction are defined simultaneously for each pair of parts by declaring that one of the parts (the master) is impenetrable by the other (the slave). The contact then permanently prohibits the nodes of the slave part from penetrating the master part elements. Two types of contacts are used in this study: Penalty and Direct Constraints.

3.5.1 Penalty

The penalty method is an alternative procedure to numerically implement the contact constraints. Effectively, the penalty procedure constrains the motion by applying a penalty to the amount of penetration that occurs. The penalty approach can be considered as analogous to a nonlinear spring between the two bodies (Figure 3.8). Using the penalty approach, some penetration occurs with the amount being determined by the penalty constant or function. The choice of the penalty value can also have a detrimental effect on the numerical stability of the global solution procedure. The penalty method is relatively easy to implement and has been extensively used in explicit dynamic analysis although it can result in an overly stiff system for deformable-to-deformable contact since the contact pressure is assumed to be proportional to the pointwise penetration. The pressure distribution is generally oscillatory.

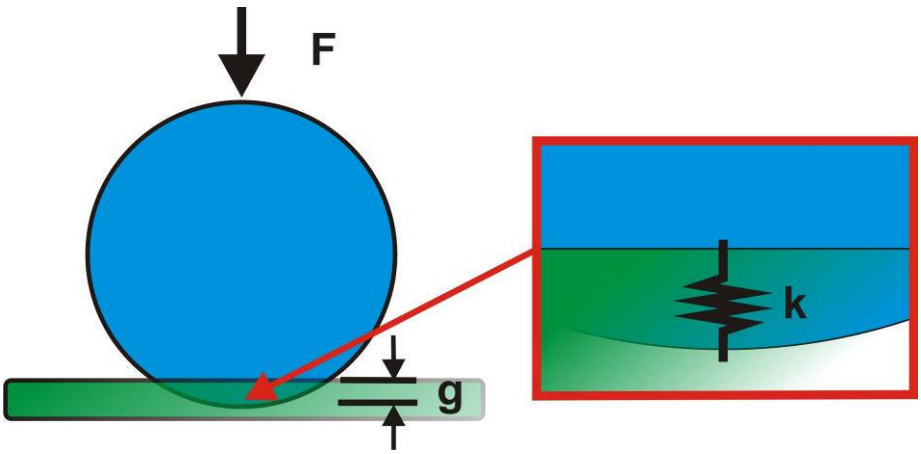

Figure 3.8 Penalty contact algorithm is identical to a spring under compression.

The penalty force is calculated as:

$$F = k.g \tag{3.12}$$

Where k is contact stiffness and g is penetration depth

For shell elements, the contact stiffness is calculated as:

$$k = \frac{SF.K.A}{d} \tag{3.13}$$

Where SF is scale factor, K is bulk modulus, A is element area and d is thickness or shortest diagonal

And for solid elements:

$$k = \frac{SF.K.A^2}{V} \tag{3.14}$$

Where SF is scale factor, K is bulk modulus, A is segment area and V is volume of element.

3.5.2 Direct Constraints

Another method for the solution of contact problems is the direct constraint method. In this procedure, the motion of the bodies is tracked, and when contact occurs, direct constraints are placed on the motion using boundary conditions, both kinematic constraints on transformed degrees of freedom and nodal forces. This procedure can be very accurate if the program can predict when contact occurs. No special interference elements are required in this procedure and complex changing contact conditions can be simulated since no a priori knowledge of where contact occurs is necessary.

3.5.3 Friction Modeling

Friction is a complex physical phenomenon that involves the characteristics of the surface such as surface roughness, temperature, normal stress, and relative velocity. The most popular friction model is Coulomb friction model and used for most applications. In this model, the friction force between pairs is calculated by:

$$F_r = \mu . F_n \tag{3.15}$$

Where F_r is friction force, F_n is normal force and μ is coefficient of friction

Examples of Coulomb's coefficient:

0.05 excellent sliding
0.1 to 0.15 conventional values
0.2 rough surface

3.6 Finite Element Codes Used in the Analyses

Finite Element codes used in the analyses are MARC-MENTAT and LS-DYNA.

MARC-MENTAT is a general purpose finite element code which has an implicit solver. The nature of the implicit solver provides good predictions of stresses and strains during deformations. It has also a large material model database including rubber material models. The disadvantage also comes from the nature of the implicit solver that has convergence problems in highly nonlinear situations.

LS-DYNA is a general purpose dynamic explicit solver which is commonly used for sheet metal forming analyses. It also contains an implicit solver for springback calculations. There are many material models including rubbers. The disadvantage is derived from its generality that numerical parameters should be adjusted well to obtain stable results.
Table 3.2 summarizes the advantages and the disadvantages of the finite element codes.

Table 3.2: Comparison of finite element codes used in the analyses

Code	**Implicit /Explicit**	**Specialty**	**Limitation**
MARC-MENTAT	Implicit	General purpose, Good accuracy, Rubber material models included	Convergence problems for highly nonlinear situations
LS-DYNA	Explicit	General Purpose, Can handle complex problems with large deformations, Large material models library	Many parameters should be adjusted for stable results

CHAPTER 4

EXPERIMENTAL STUDY

4.1 Introduction

Experimental study is done for two purposes:

1- For detecting the effects of experimental parameters such as blank thickness, forming pressure, etc. to the final shape of sheets.

2- For the validation of the finite element results belonging to the models of the experiments.

Simple basic experiments are designed with different die and blank geometries. They are conducted with changing parameters in order to form a test matrix. Numerical results are then compared with this matrix examining the success of the finite element model.

Also, material characterization is the subject of this chapter and will be explained at the end.

4.2 Experimental Setup

OUINTIS Circular Flexform Press with circular trays of 1m diameter and maximum pressure 80 MPa is used in the experiments (Figure 4.1). There is one tray at each end of the press and these shuttle in and out of the press frame, where the flexible rubber diaphragm is situated.

Figure 4.1 OUINTIS Circular Flexform Press

In the experiments ,the die is placed at the center of the circular tray (Figure 4.2-a) without the need for fixing (high pressure and friction prevents movement of the die during forming). The blank is fixed onto the die with the help of guide pins (Figure 4.2-b). The tray shuttles in the press and the sheet is formed over the rigid die with the hydraulic pressure through the diaphragm.

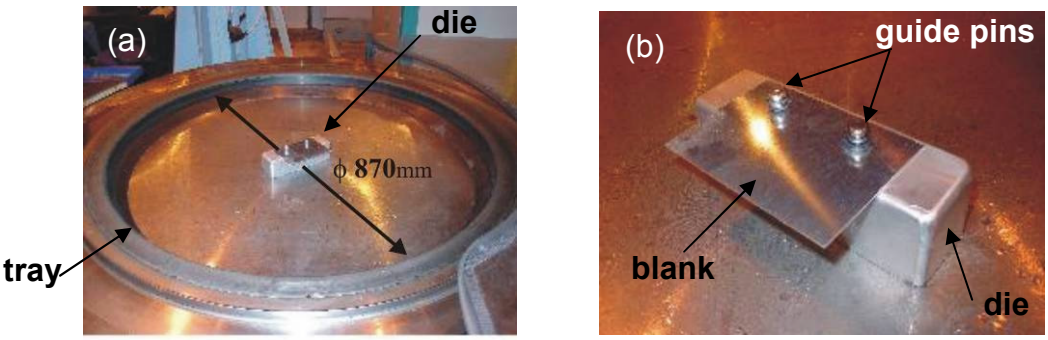

Figure 4.2 Flexform tools: (a) Tray of the flexform press with the die and the blank, (b) Guide pins for fixing the sheet onto the die

4.3 Basic Experiments

The objective of this study is to predict the defects wrinkling, tearing and springback before forming operation. For this reason, basic experiments are designed according to the simplest die-blank geometry combination that results one of these defects. These basic experiments are bending of a straight flange specimen, bending of a contoured flange specimen and bulging of a circular specimen corresponding to the springback, wrinkling and tearing defects respectively.

4.3.1 Bending of a Straight Flange Specimen (Springback)

During the bending of straight flange specimen, a rectangular blank is bended 90 degrees over a straight die. After the removal of the pressure the specimen springbacks causing a decrease in 90 degrees bend angle (Figure 4.3).

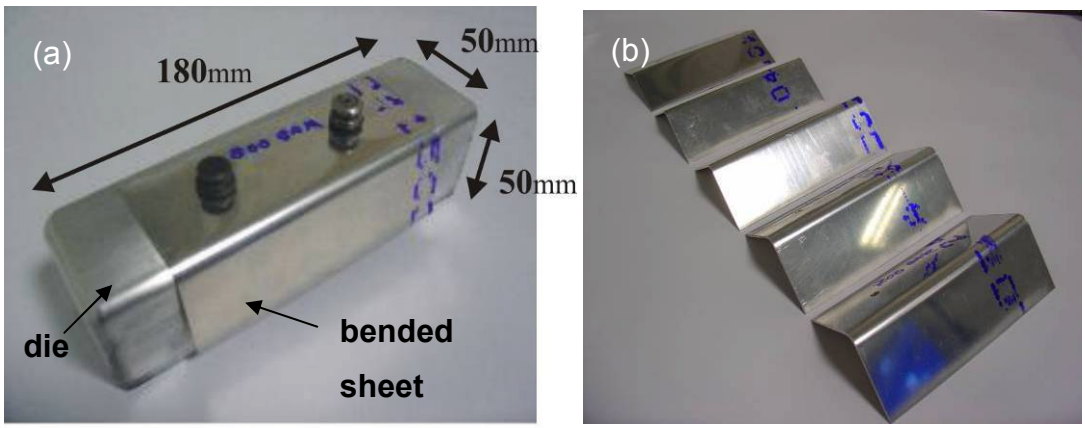

Figure. 4.3 Straight Flange Bending Specimen: (a) The die and the bended sheet (b) The deformation stages obtained with different forming pressures

4.3.2 Bending of a Contoured Flange Specimen (Wrinkling)

During the bending of contoured flange specimen, a rectangular blank is bended 90 degrees over a contoured die. This specimen has a more complex deformation with compressive strains normal to the bending plane leading eventually to wrinkle formation at the middle of the specimen (Figure 4.4).

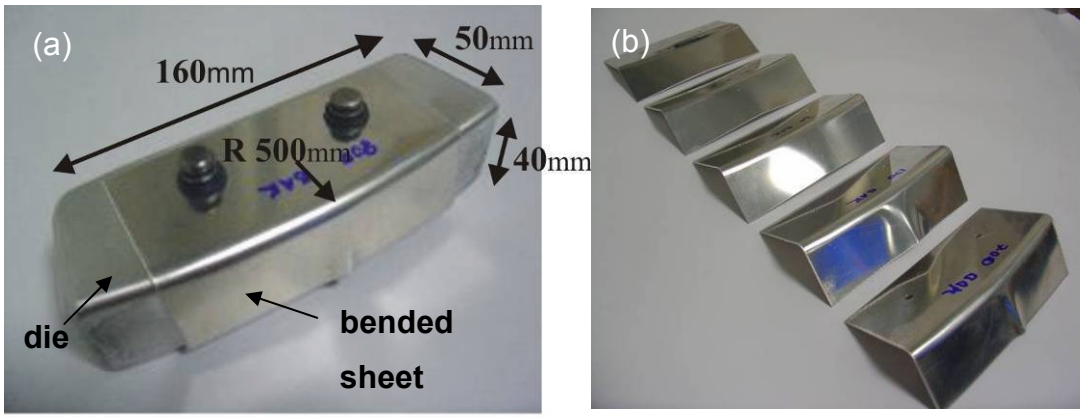

Figure. 4.4 Contoured Flange Bending Specimen: (a) The die and the bended sheet (b) The deformation stages obtained with different forming pressures

Like the straight flange specimen, contoured flange specimen also springbacks after the removal of the pressure, since this phenomenon is unavoidable.

4.3.3 Bulging of a Circular Specimen (Tearing)

During the bulging of circular specimen, a circular blank is bulged over a circular die with a hole at the center. The biaxial tension in the sheet causes tearing at a certain forming pressure (Figure 4.5).

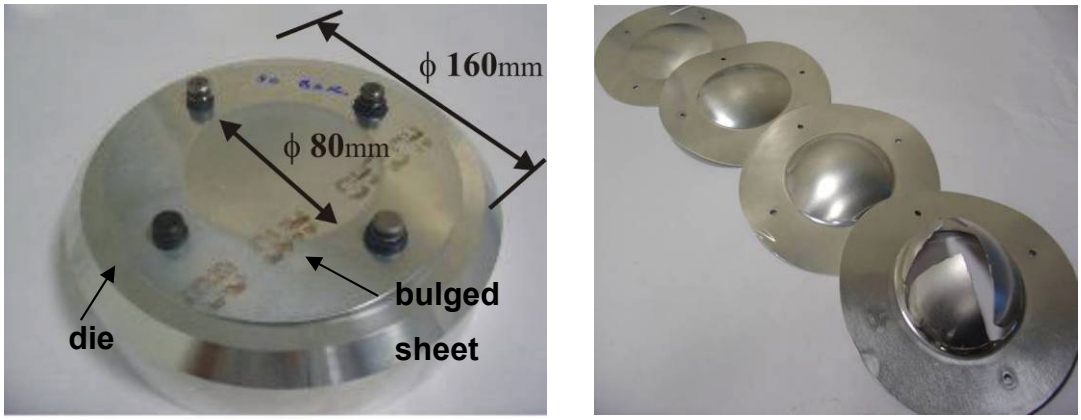

Figure. 4.5 Circular Bulging Specimen: (a) The die and the bulged sheet
(b) The deformation stages obtained with different forming pressures

4.3.4 Experimental Parameters

In order to form a test matrix, some experimental parameters are changed and different results are obtained. These experimental parameters are related to die and blank geometry and to the process. Material is not changed for the blank and Alclad Aluminum 2024-T3 is used in all experiments. This is a temper of 2024 alloy group which is noteworthy for its high toughness. Therefore, the defects like springback and wrinkling are obvious with this temper. Other experimental parameters are blank thickness (t), flange length of blank (l), orientation of blank according to the rolling direction, die bend radius (r) and the forming pressure (p). They are shown in Figure 4.6.

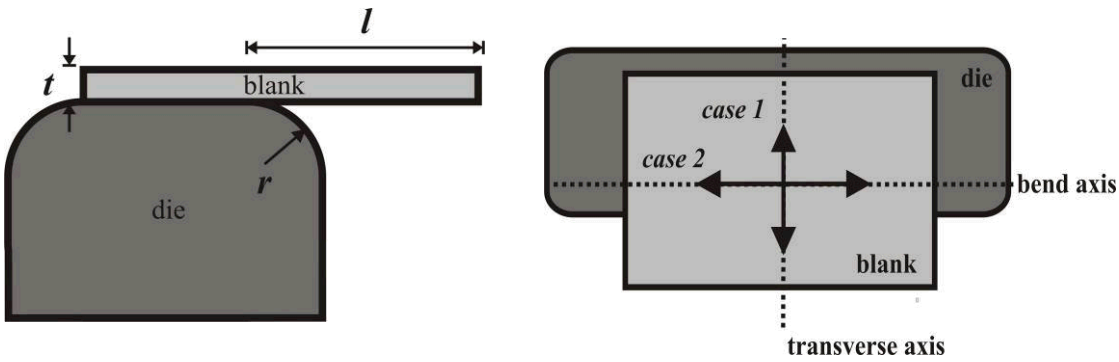

Figure 4.6 Experimental parameters: (a) blank thickness *t,* flange length *l*, die bend radius *r*, (b) rolling direction of the blank: along transverse axis(case 1) or along bend axis(case 2)

In this study, the effects of some parameters are not investigated for some basic experiments because they are not applicable or meaningless. These are listed as:

1- For the straight flange bending specimen, rolling direction and flange length parameters are not investigated since a previous study suggests that these have almost no effect on springback angle [8].
2- For the contoured flange bending specimen, rolling direction has no effect on wrinkle formation and considering the flange length is meaningless because as the flange length decreases the wrinkle disappears totally [8].
3- For the circular bulging specimen, there is no flange and changing the orientation of the blank is meaningless since the specimen is axisymetric. In addition, the die bend radius is not changed for this specimen since it is a bulging operation.

After narrowing down the experimental parameters, Table 4.1 lists the experimental parameters for basic experiments and their values.

Table 4.1 Experimental parameters and their values for basic experiments

parameter	**value**		
	straight bending	**contoured bending**	**circular bulging**
forming pressure (p) [MPa]	10, 40, 80	10, 40, 80	10,12.5,15,17.5,20
blank thickness (t) [mm]	0.6, 1, 1.6, 2	0.6, 1, 1.6, 2	0.6, 1, 1.6, 2
die bend radius (r) [mm]	2.5, 5, 7.5	2.5, 5, 7.5	5
flange length (l) [mm]	45	45	-
rolling direction	transverse axis	transverse axis	-

4.4 Experimental Results

Changing experimental parameters leads to different results. For the straight flange bending specimen, different springback angles are obtained, for the contoured flange experiment different wrinkle shapes are observed and for the circular bulging specimen different bulge depth values up to tearing are noted. All those results form a complete set of the defects seen in the process in their simplest form.

4.4.1 Bending of a Straight Flange Specimen (Springback)

The experimental results are evaluated by the springback angle defined as the angle deviation from 90 degrees which is the bend angle. The values given in Table 4.2 are the averages of five measurements at various flange locations and of three specimens. The measurements are done with using a digital protractor.

Table 4.2 Springback results of straight flange bending specimen

forming pressure (*p*) [MPa]	**die bend radius (*r*) [mm]**	**blank thickness (*t*) [mm]**	**springback [degrees] ± 0.2**
10	2.5	0.6	10.6
10	2.5	1	7.8
10	2.5	1.6	5.7
10	2.5	2	split
10	5	0.6	16.0
10	5	1	11.3
10	5	1.6	8.8
10	5	2	8.2
10	7.5	0.6	20.1
10	7.5	1	14.8
10	7.5	1.6	11.3
10	7.5	2	10.3
40	2.5	0.6	10.0
40	2.5	1	7.3
40	2.5	1.6	5.0
40	2.5	2	split
40	5	0.6	15.0
40	5	1	11.2
40	5	1.6	8.1
40	5	2	7.5
40	7.5	0.6	20
40	7.5	1	14.4
40	7.5	1.6	10.5
40	7.5	2	9.4
80	2.5	0.6	9.7
80	2.5	1	7.0
80	2.5	1.6	5.0

80	2.5	2	split
80	5	0.6	15.3
80	5	1	11.1
80	5	1.6	7.8
80	5	2	7.3
80	7.5	0.6	19.9
80	7.5	1	14.5
80	7.5	1.6	10.4
80	7.5	2	9.5

Results show that:

- Springback angle for the straight flange bending specimen is not a function of *p, t, r* but a function of *p, t/r*. Figure 4.7 shows the decreasing trend of springback angle with increasing *t/r* ratio.
- At a certain *t/r* ratio (0.8), the specimen is split from the bending line.
- Increasing the forming pressure to a certain value (40 MPa) decreases the springback angle, but then it has no effect on springback angle (Figure 4.7).

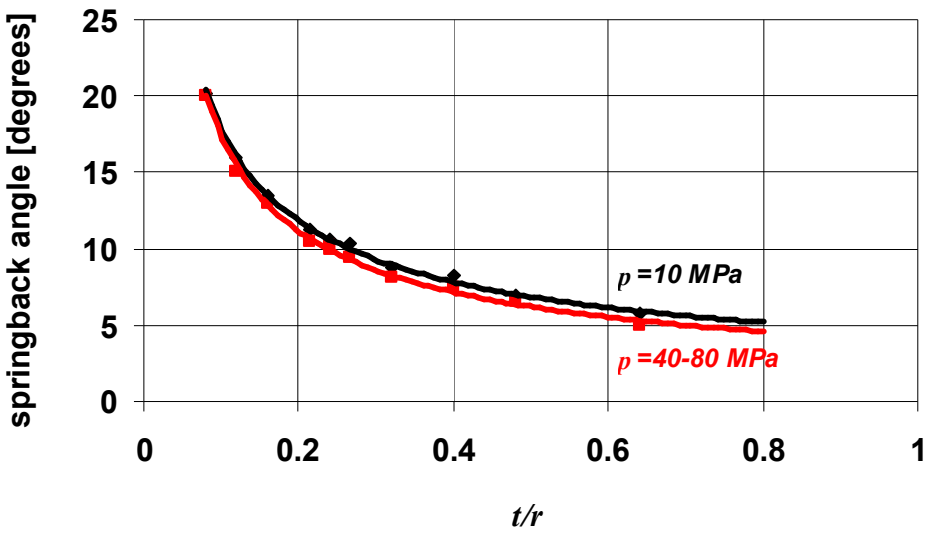

Figure 4.7 Springback angles with changing *t/r* for the straight bending specimen

4.4.2 Bending of a Contoured Flange Specimen (Wrinkling)

For the contoured flange bending specimen the wrinkle formation is used as the basic parameter for the assessment. Different wrinkle shapes are obtained with different blank thicknesses, die bend radiuses and forming pressures (Figure 4.8)

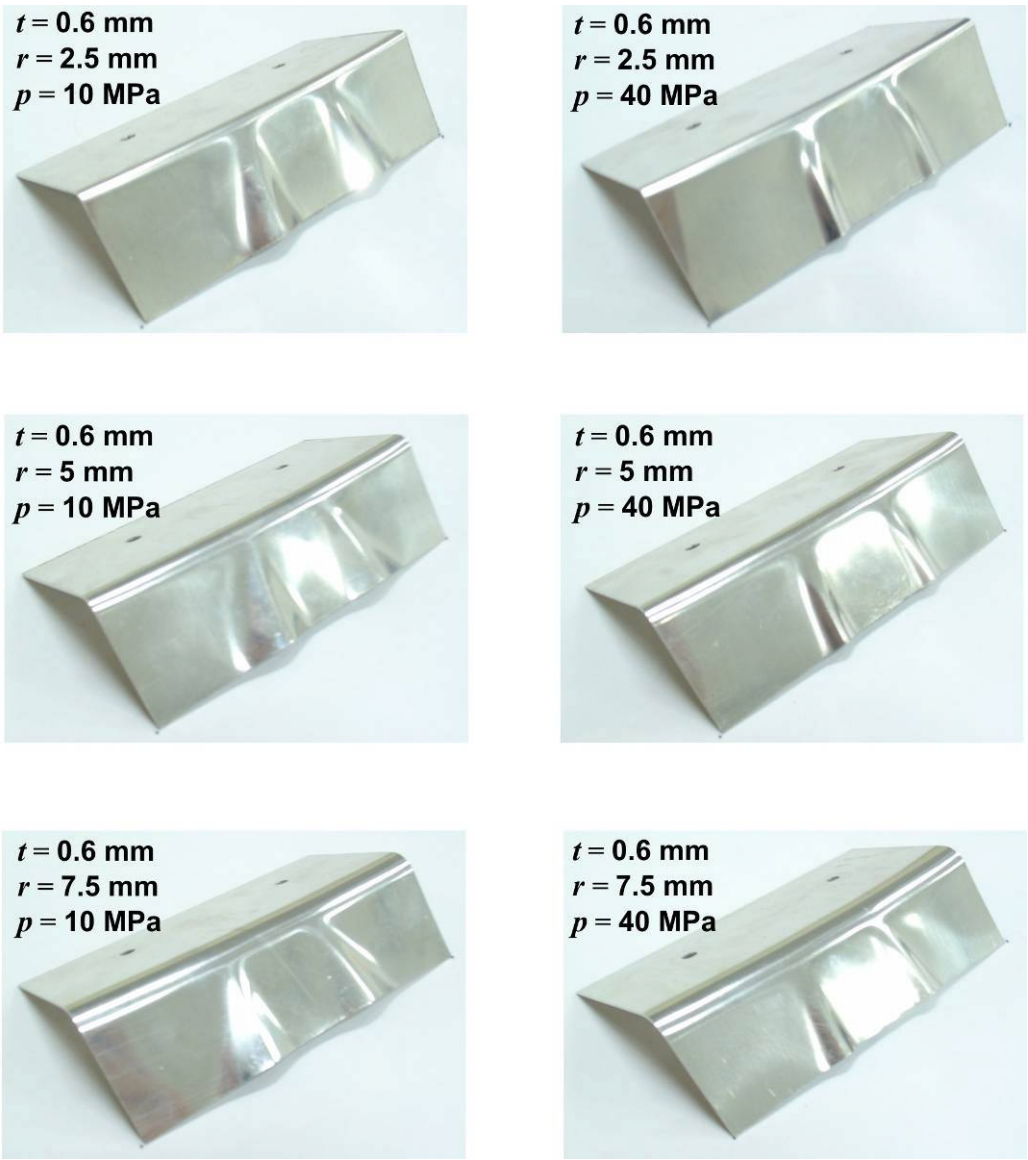

Figure 4.8 Experimental results of contoured flange bending specimen.

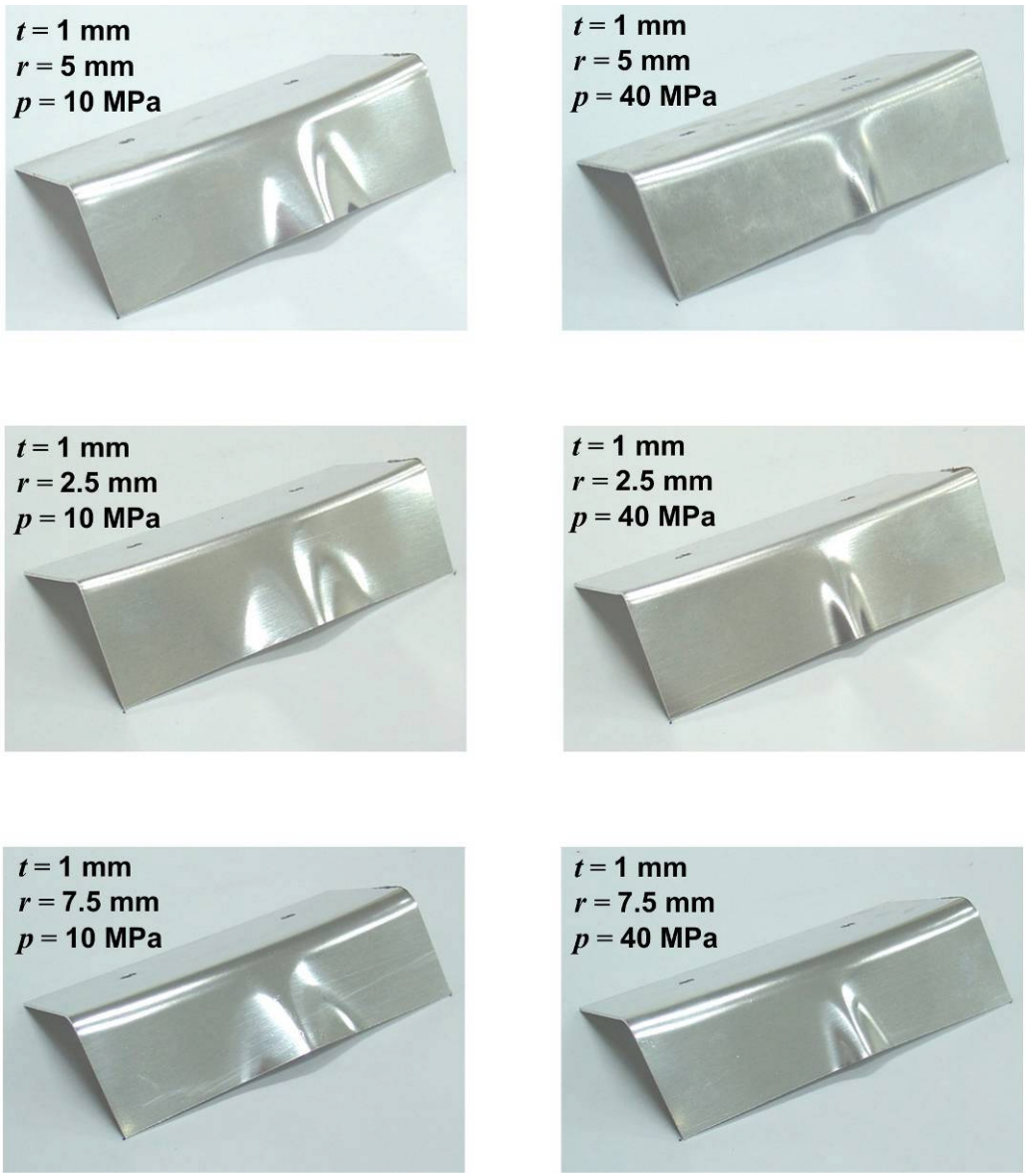

Figure 4.8 (continued)

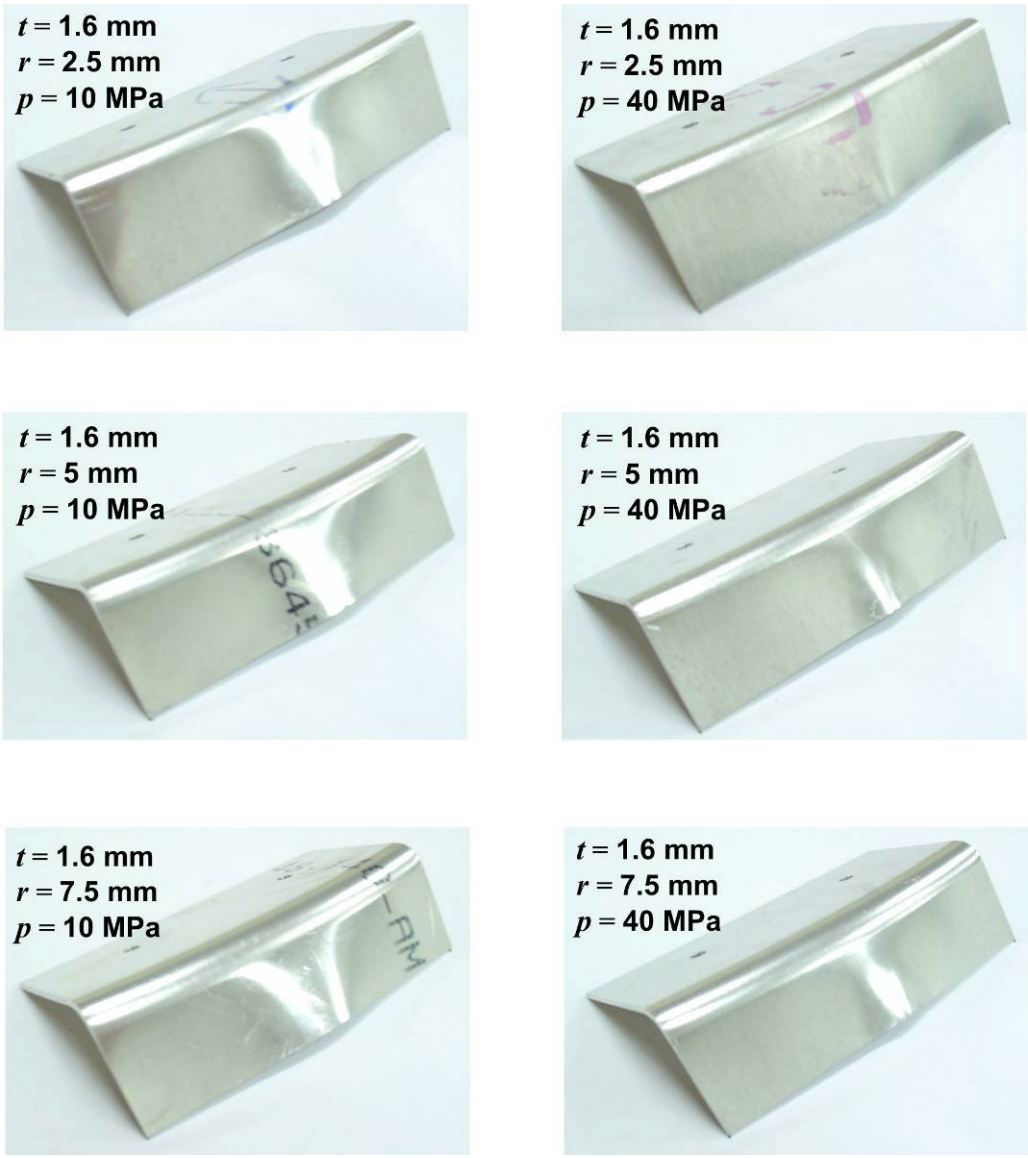

Figure 4.8 (continued)

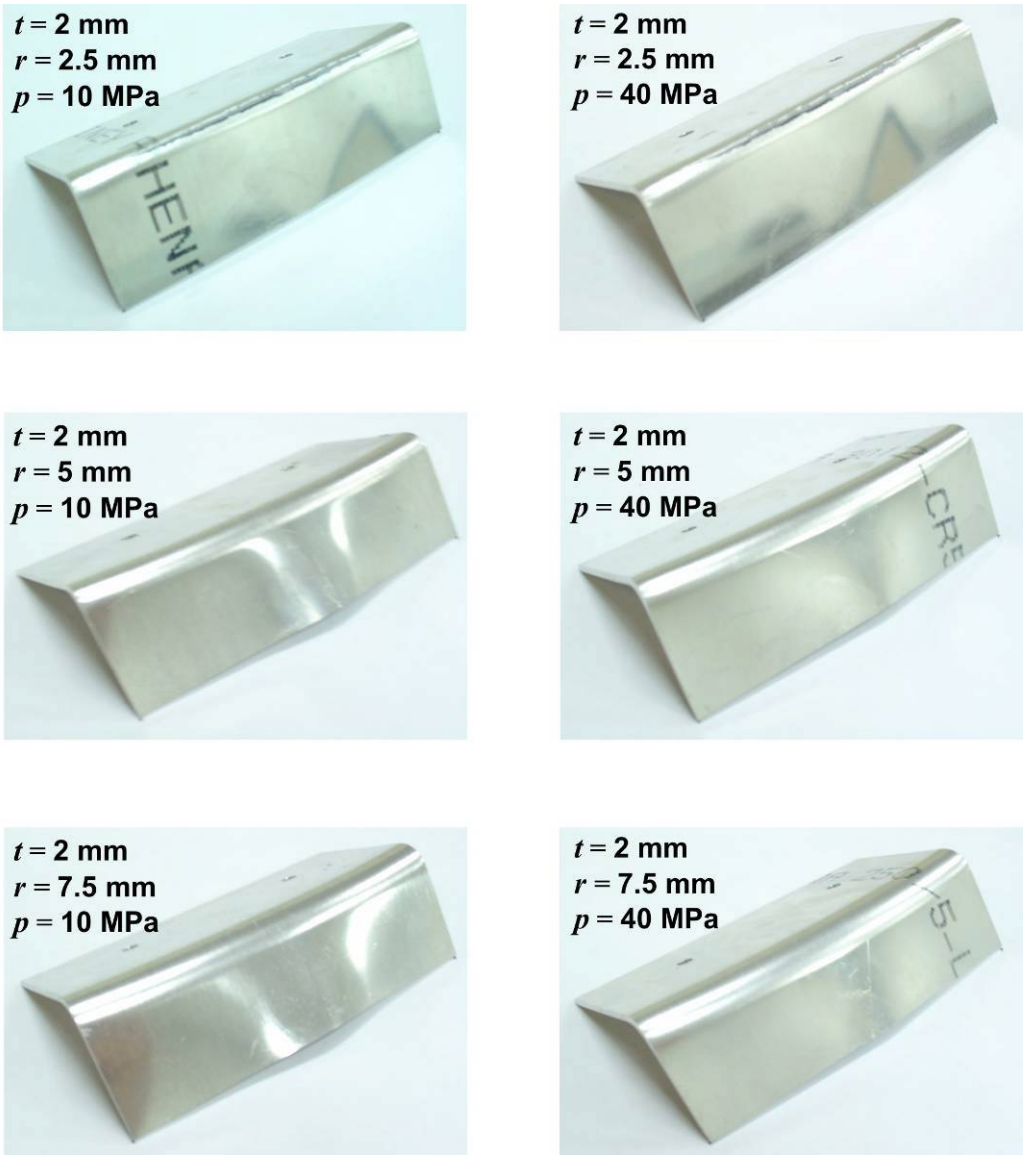

Figure 4.8 (continued)

Results show that:

- Wrinkle shape is very sensitive to the blank thickness *t* and is changing from two wrinkles to one wrinkle and eventually no wrinkle as blank gets thicker.
- Die bend radius *r* has almost no effect on the wrinkle shapes, it has effect on springback angles and splitting of the specimen as in the straight flange bending specimen.
- Increasing the forming pressure to a certain value (40 MPa) decreases wrinkle size, but then it has no effect on wrinkle shape. The wrinkle sizes at 80 MPa are almost the same as at 40 MPa.

4.4.3 Bulging of a Circular Specimen (Tearing)

For the circular bulging specimen, forming pressure and blank thickness are changed. Depth of the bulge is measured at different pressures and for different blank thicknesses. Splitting occurs at a certain forming pressure.

Table 4.3 Bulge depth results of circular bulging specimen

blank thickness (*t*) [mm]	**forming pressure (*p*) [MPa]**	**bulge depth [mm] ± 0.5**
0.6	10	15.8
0.6	12.5	split
1	10	10.4
1	12.5	12.9
1	15	15.3
1	17.5	18.5
1	20	split
1.6	10	6.6
1.6	12.5	8.4

1.6	15	1.3
1.6	17.5	11.8
1.6	20	13.6
2	10	5.0
2	12.5	5.5
2	15	6.4
2	17.5	9.1
2	20	10.6

Results show that:

- Increasing the forming pressure *p,* increases the bulge depth and at a certain forming pressure the sheet fractures as expected.
- At a certain forming pressure *p,* as the blank gets thicker the bulge depth decreases as expected.
- The specimen springbacks after unloading and has a wavy view as shown in Figure 4.9. These waves become more noticeable as the blank gets thinner.

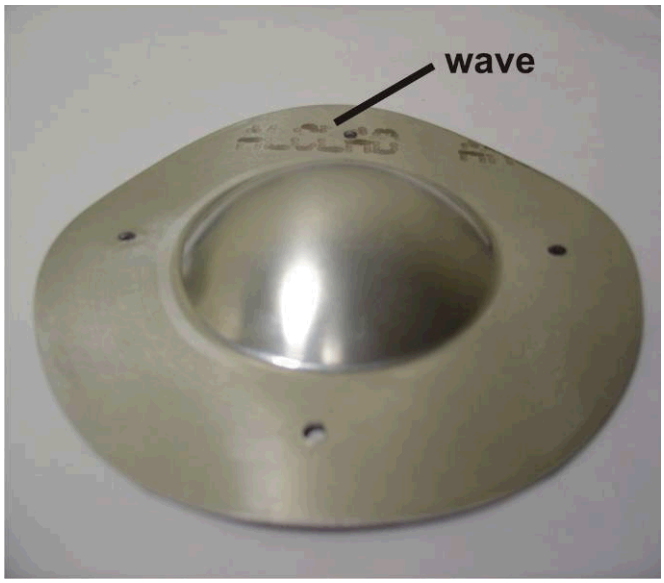

Figure 4.9 Wavy view of the circular bulging specimen.

4.5 Material Characterization

The materials in the process are Alclad Aluminum 2024 - T3 for the blank and rubber for the diaphragm. The die material is also an aluminum alloy, but no material test was done for this since its deformation is negligible and it was modeled as rigid. Uniaxial tensile tests were conducted both for the aluminum (according to ASTM E 8M) and the rubber (according to ASTM D 412) in order to obtain their material properties.

4.5.1 Aluminum Material Properties

According to the ASTM standard, tensile test specimens were punched from a 1 mm of sheet. To examine the effects of anisotropy, test specimens were punched at 0^0, 45^0 and 90^0 to the rolling direction. An Zwick model Z100 tensile testing machine was used to test the specimens in uniaxial tension as shown in Figure 4.10. The specimen was clamped between upper and lower grips and a biaxial extensometer is attached on the middle to measure both the elongation of the specimen and the transverse contraction of the specimen. The tests were run at different speeds of the Zwick machine (10 mm/min and 100 mm/min), but it was found that the material properties were rate independent (Appendix B). Figure 4.11 shows the true stress-strain plots of Alclad Aluminum 2024-T3 in three different directions.

Figure 4.10 Uniaxial tensile testing of Aluminum sheet.

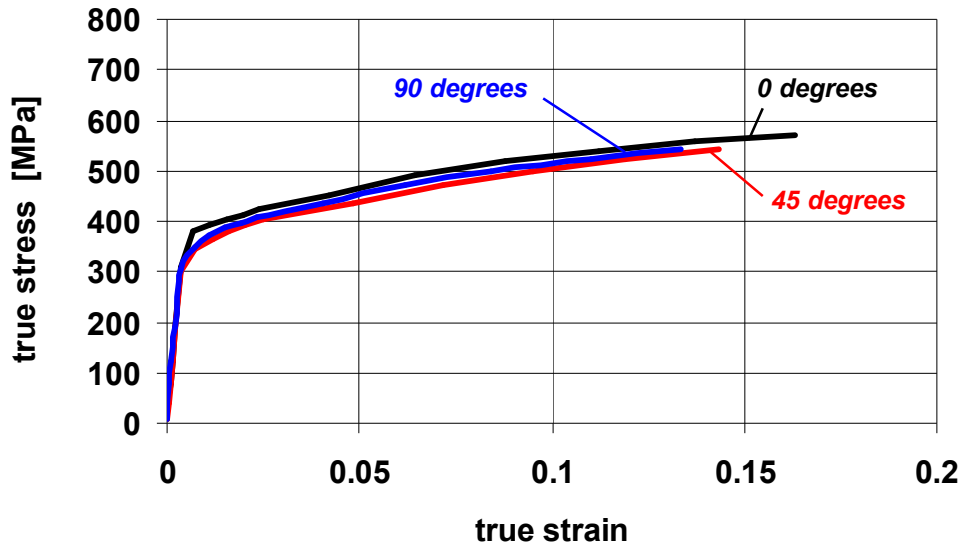

Figure 4.11 True Stress-Strain plots for Alclad Al 2024-T3 in three directions to the rolling plane.

This data will be used in the simulations for the hardening behavior of the aluminum. The other data in three directions to the rolling direction are listed in Table 4.4.

Table 4.4 Mechanical Properties of Alclad Al 2024-T3 tested in uniaxial tension at different directions.

Property	**0 degrees to RD**	**45 degrees to RD**	**90 degrees to RD**
Young's modulus	76196 MPa	77334 MPa	76009 MPa
Yield Strength(0.2 % offset)	376 MPa	335 MPa	340 MPa
Ultimate Tensile Strength	489 MPa	471 MPa	481 MPa
% Elongation to Failure	18.00	19.81	17.43
R value	0.77	0.95	0.87

Tabulated results show that Alclad Al 2024-T3 is nearly an isotropic material. Details about the uniaxial tensile tests are given in Appendix B.

4.5.2 Rubber Material Properties

Test specimens were also prepared for the rubber material according to the ASTM standard by punching from the diaphragm. A low capacity tensile testing machine is used for the uniaxial tensile test. Special grips are used for clamping the rubber specimen in which there is a mechanism that increases the holding force as the specimen elongates and prevents it from sliding. Rubber material characterization is more complex than aluminum and many tests are needed such as biaxial tension, planar tension, volumetric compression, etc in order to obtain the exact material model [20]. However, for the modeling of flexforming process, the rubber diaphragm is used as a loading element and its deformation is not as essential as the aluminum. Therefore, a simple uniaxial tensile behavior is enough to model the

rubber material. Figure 4.12 shows the engineering stress vs engineering strain plot of the rubber.

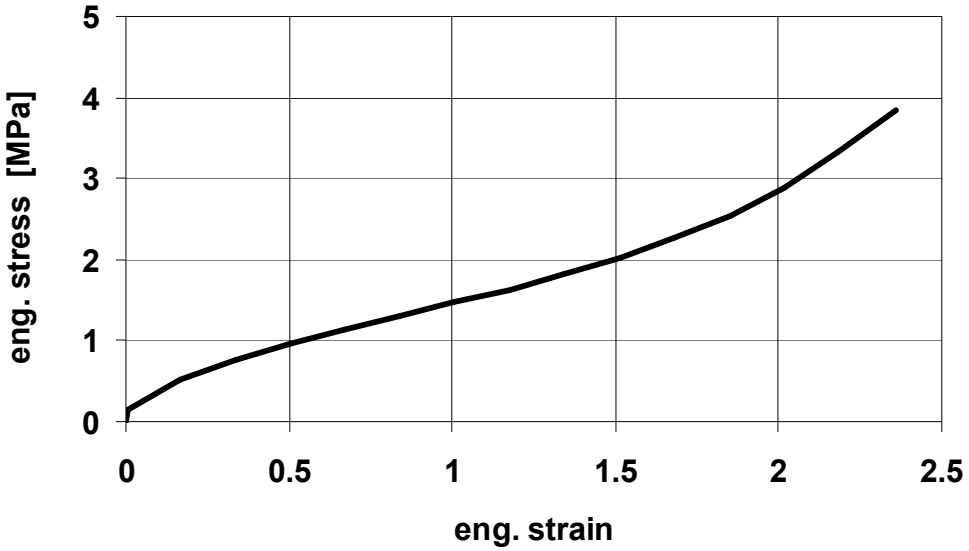

Figure 4.12 Engineering Stress-Strain plot for rubber material.

CHAPTER 5

NUMERICAL MODELING

5.1 Introduction

The aim of this study is to obtain a general numerical model which predicts the defects of the sheets before forming in the flexform press and to adjust the process parameters and make the necessary design changes of the dies and blanks accordingly. For this purpose, many numerical investigations are done by using finite element method. The study is classified according to the simulations of the basic experiments and is given in Figure 5.1. "2D, Solid, Implicit" means two-dimensional model that contains solid elements for the blank and uses static-implicit scheme for the time integration.

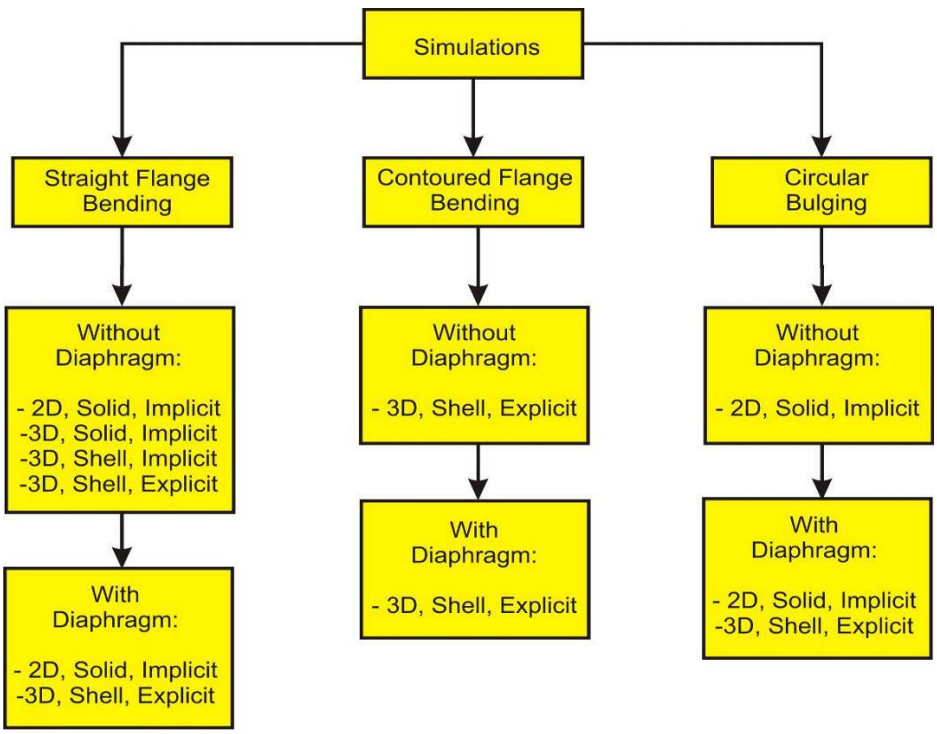

Figure 5.1 Classification of simulations.

5.2 Simulation of Straight Flange Bending Experiment

As described in Chapter 4, this experiment is the straight flange bending of a sheet over a straight die (Figure 5.2). Studies in the literature [4,5] ignore the diaphragm modeling and apply uniform pressure on sheet surface in order to simulate its effect. First analyses are made by following these studies and models are established excluding the rubber diaphragm. Simple two-dimensional plane strain models are established with solid elements and then these models are then expanded to the three-dimensional models. Also, solid elements are changed to shells and implicit scheme is changed to explicit sequentially in order to go over the modeling possibilities in hand. Then, analyses are made including the rubber diaphragm and investigating its effect. Springback prediction is the main goal in those analyses and is rather difficult to achieve since a perfect forming analysis is needed for calculating the residual stresses that provides driving forces for springback.

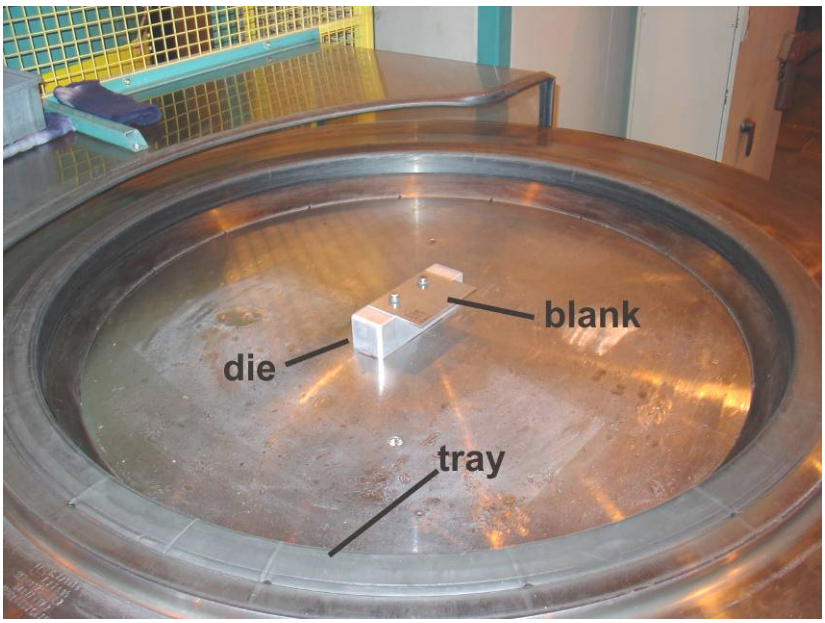

Figure 5.2 Straight Flange Bending Experiment.

5.2.1 Two-Dimensional Models without Diaphragm using Solid Elements and Static-Implicit Scheme

The specimen in this experiment is extending in the bend line direction (Figure 5.2). Therefore, two-dimensional models with plane strain assumption are established by using implicit code MARC-MENTAT. The validity of the plane strain assumption will be checked in the next section.

Figure 5.3 shows this simple model. Quadrilateral plane strain solid elements (ELEMENT TYPE 11) are used for discretization of the blank. Finer mesh is used in the bend region with a specified number of elements through the blank thickness and with a specified number of elements along the bend radius. These numbers are determined by doing a sensitivity analysis of springback angle to the number of elements through thickness and to the number of elements along the bend radius. Figure 5.4 shows the convergence of springback angle with increasing the elements through the thickness and along the bend radius for the specified experimental parameters. (t/r = 0.1, p = 10 MPa, t: blank thickness, r: die bend radius, p: forming pressure). Same analysis has made for other experimental parameters (t/r values) and minimum number of elements required through the thickness and along the bend radius are detected (Figure 5.5). More elements are needed along the bend radius for lower t/r values in which springback angle is higher. One thing that should be noted that these values are material dependent and are only valid for Al 2024 –T3 which is the material used in the experiments.

As the boundary conditions, the blank is fixed from the nodes where the guide pin is attached and direct pressure is applied onto the sheet with using FOLLOWER FORCE option in which force directions are following element normals during the deformation of the sheet.

The die is analytically described and does not need to be meshed. It is modeled as rigid and no material is defined since its deformation is negligible. An isotropic elastic-plastic material model is assigned for the aluminum blank which uses von

Mises yield surface and piecewise linear hardening rule in which points are obtained from the uniaxial tensile test of Aluminum 2024-T3.

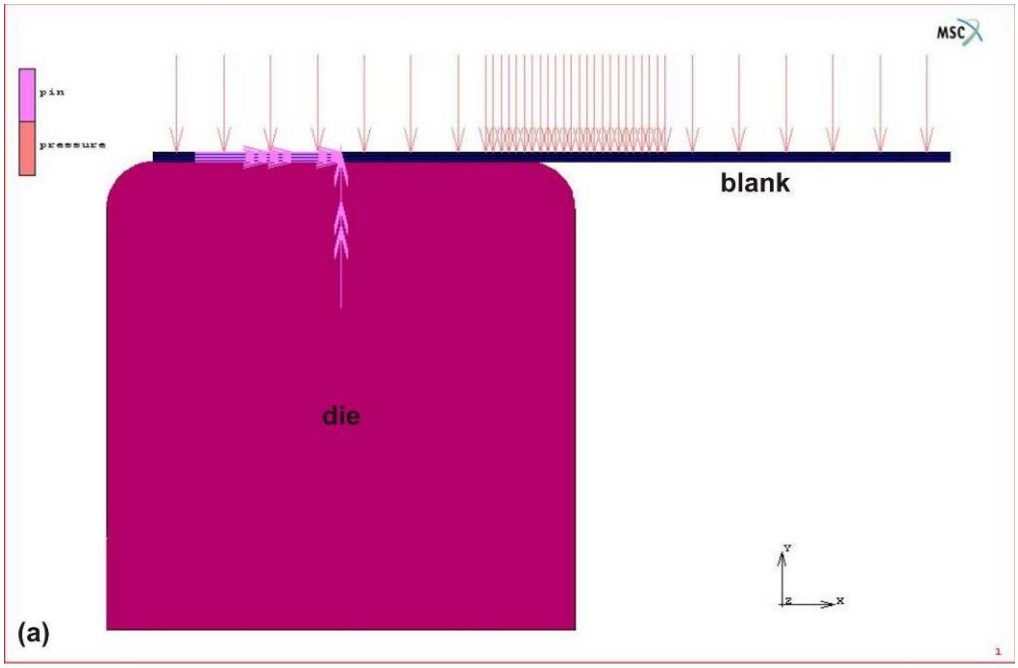

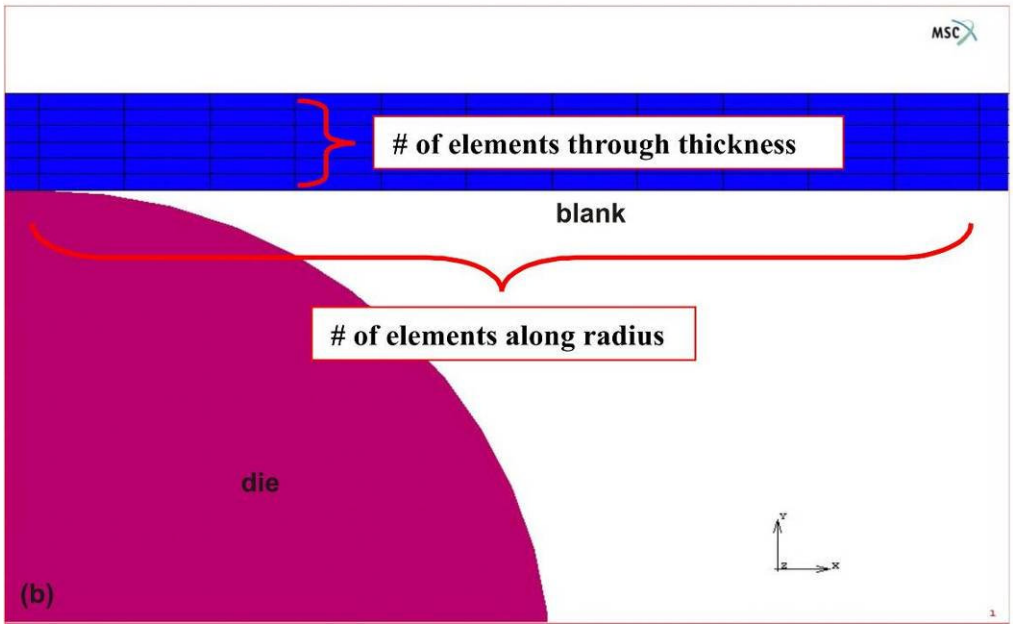

Figure 5.3 (a) Two-dimensional, without diaphragm, solid elements, static-implicit model of the straight flange bending experiment (MARC-MENTAT). (b) The bending region showing the elements through the thickness and along the bend radius.

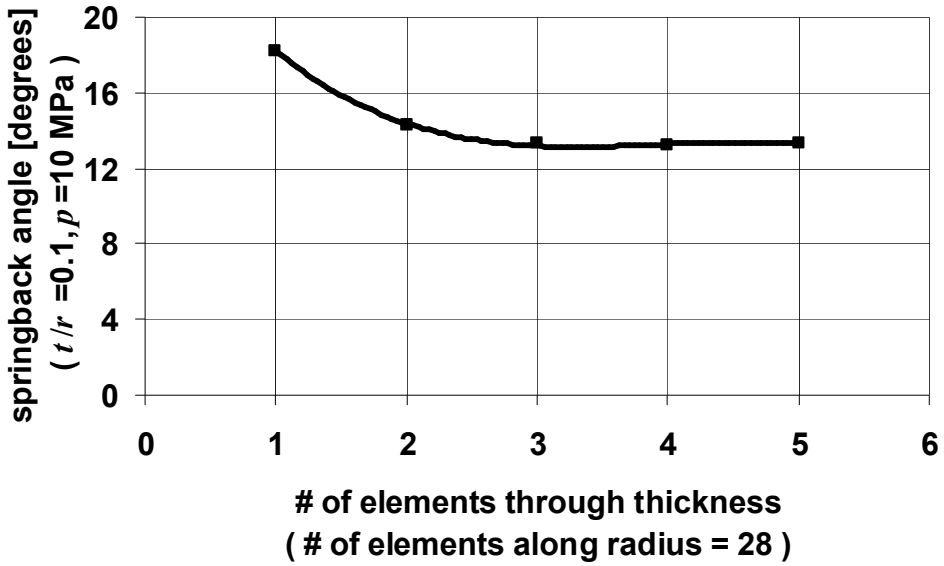

(a)

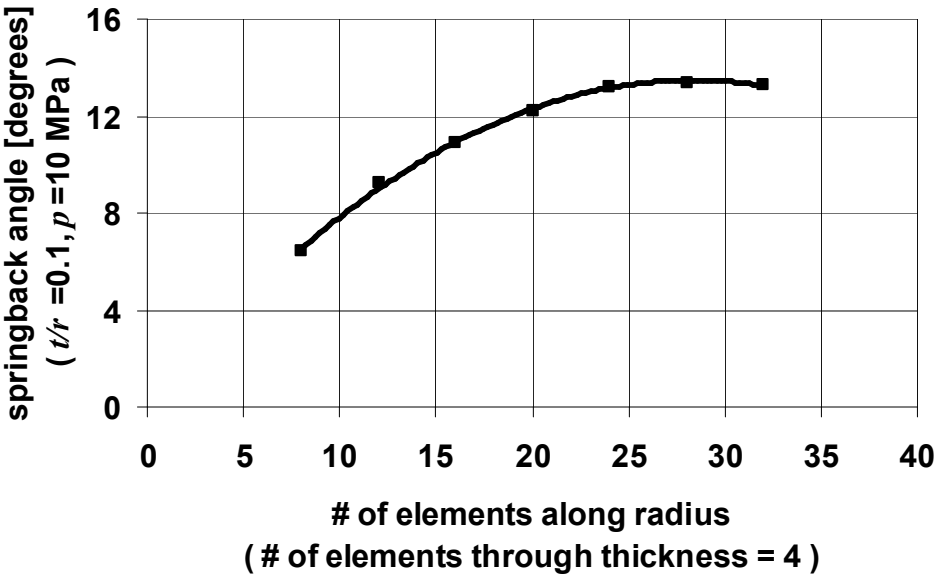

(b)

Figure 5.4 Effect of the mesh structure to the springback angle of the straight flanging specimen. (a) Effect of number of elements through the blank thickness (b) Effect of number of elements along the die bend radius.

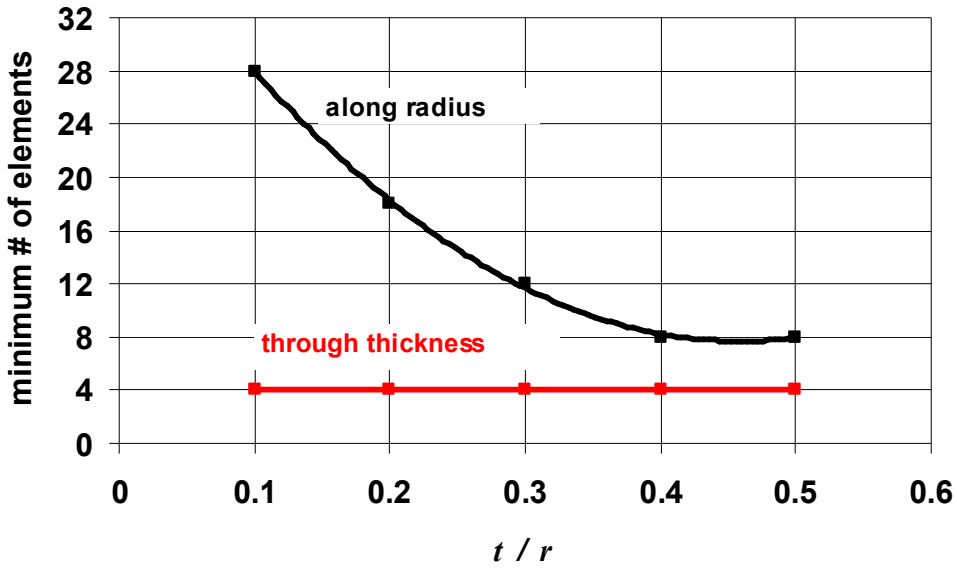

Figure 5.5 Minimum number of elements through the thickness and along the bend radius required for accurate springback prediction of straight flanging experiment for different thickness-bend radius ratios.

Direct Constraints Method and Stick-Slip Coulomb Friction Model is used for the contact between the die and the blank. Slave side is the blank and the master side is the die.

The analysis is performed in two stages as loading (forming) and unloading (springback). Adaptive time stepping is used for the loading stage in which the time step can be changed between specified minimum and maximum values according to the nonlinearity level. One-step is used for the unloading stage which is linear elastic.

The analyses are done with changing experimental parameters blank thickness, die bend radius and the forming pressure. Figure 5.6 shows the equivalent plastic strain and equivalent von Mises stress contour plots in the bending region before and after springback. The springback results are shown in Table 5.1.

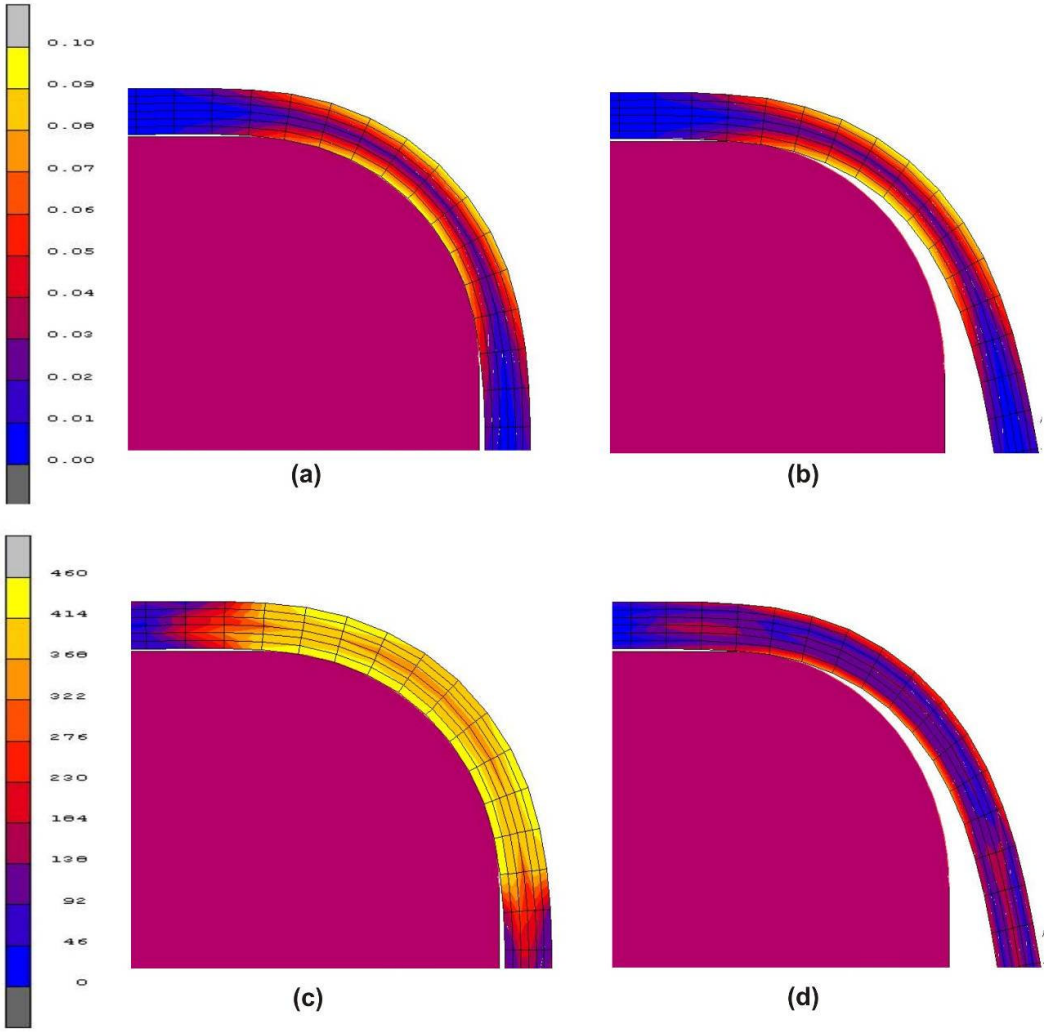

Figure 5.6 Contour plots of equivalent plastic strain and equivalent von Mises stress belonging to the straight flange bending specimen (t/r = 0.2, p = 10 MPa) before and after springback. Equivalent plastic strain distribution (a) before springback (b)after springback Equivalent von Mises stress distribution (c) before springback (d)after springback

Table 5.1 Springback angle results of the two-dimensional plane strain, without diaphragm, solid elements, static-implicit model of the straight flange bending specimen.

forming pressure (*p*) [MPa]	**die bend radius (*r*) [mm]**	**blank thickness (*t*) [mm]**	**springback [degrees]**
10	2.5	0.6	3.2
10	2.5	1	2.8
10	2.5	1.6	1.3
10	2.5	2	-
10	5	0.6	10.9
10	5	1	7.9
10	5	1.6	6.3
10	5	2	5.8
10	7.5	0.6	16.6
10	7.5	1	11.7
10	7.5	1.6	8.8
10	7.5	2	7.8

Springback angles obtained with this model are not functions of *t/r* ratio as in the case of physical experiments. Figure 5.7 shows the comparison between the experimental results and the numerical results by separating the parameters *t* and *r*.

The error of the model is defined as the angle differences between the model and the experimental results. For this model, maximum error is 6.6 degrees, minimum error is 2.4 degrees and average error is 3.3 degrees. The deviation in the results can be because of the simplifications made by assuming plane strain conditions and/or ignoring the rubber diaphragm in the model. In the next section, the validity of the plane strain condition is checked by preparing three-dimensional models.

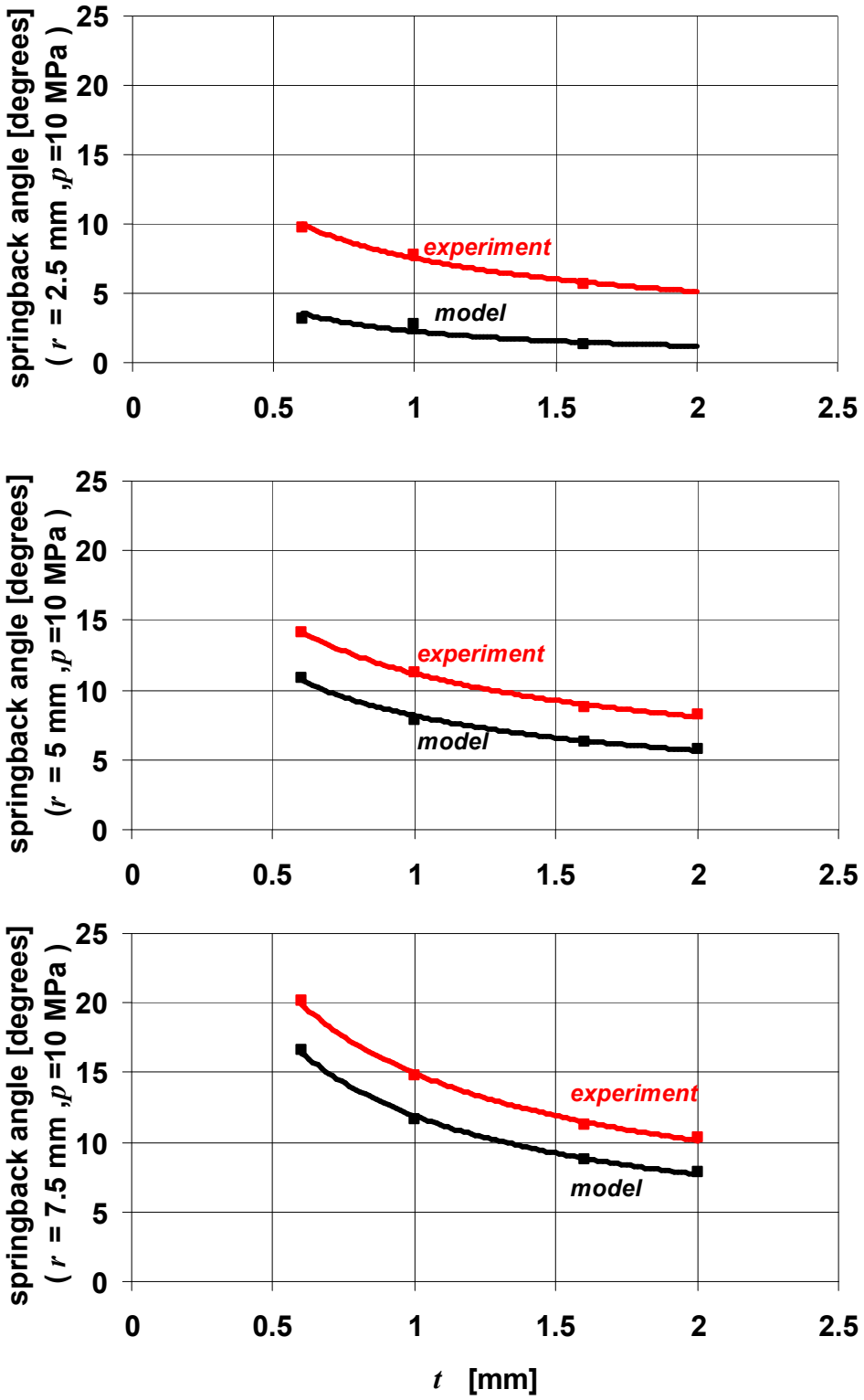

Figure 5.7 Comparison of the springback angle results of the two-dimensional, without diaphragm, solid elements, static-implicit model of the straight flange bending specimen with the experimental results.

5.2.2 Three-Dimensional Models without Diaphragm using Solid Elements and Static-Implicit Scheme

Two-dimensional models have the advantage of applying the changes easier and faster. However, they are not sufficient for constructing a general model since most sheet parts have complex shapes in which two-dimensional plane strain, plane stress or axisymetric assumptions are not valid anymore. Therefore, three-dimensional models should be prepared for full analyses.

Two-dimensional models of the previous section are expanded to the three-dimensions and the validity of the plane strain assumption is checked. Elements are changed to the three-dimensional hexahedron elements. Symmetry conditions are applied to the nodes on the x-y symmetry plane and the nodes are fixed where the guide pin is placed in the physical experiments (Figure 5.8).

As a result, total strain in the z direction (out of plane x-y) is shown in Figure 5.8. The strain is in the order of 10^{-3} at most and is seen in a small region at the end of bend. This shows that the plane strain assumption is valid in the previous analyses. Springback results are given in Table 5.2. Comparison of springback angles with two-dimensional models is given in Figure 5.9.
For the results, maximum deviation is 1.7 degrees, minimum deviation is 0.3 degrees and average deviation is 0.7 degrees.

Then, the possibility of the two-dimensional plane strain assumption being the source of the deviation from the experimental results is eliminated and one left with the assumption of excluding the diaphragm. Before, adding the diaphragm to the model, some investigations are done for this simple model by changing the element type to shells and the time integration scheme to explicit. The aim is to learn whether shell elements and explicit time integration can be used or not for accurate springback prediction.

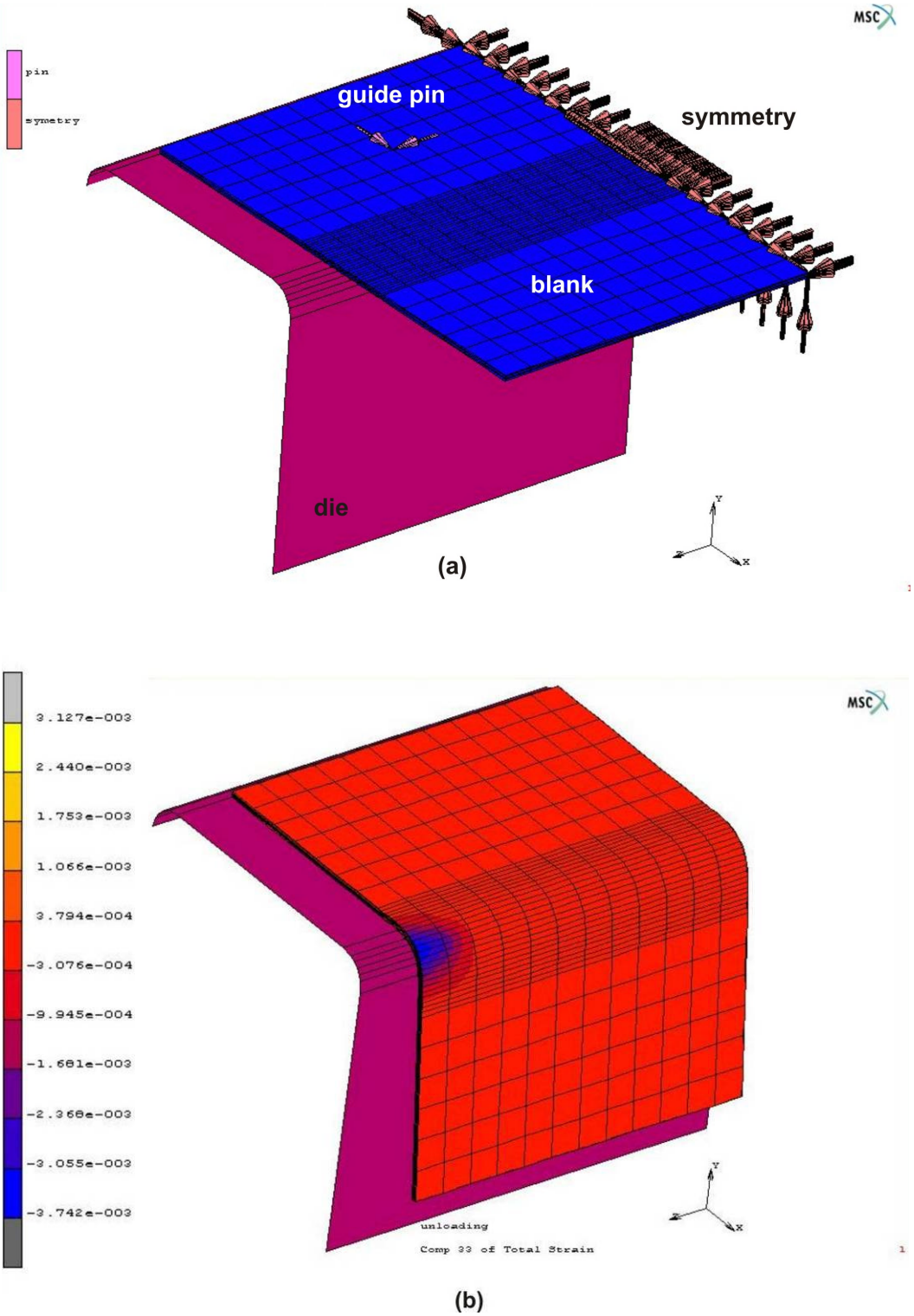

Figure 5.8 (a) Three-dimensional, without diaphragm, solid elements, static-implicit model of the straight flange bending experiment (MARC-MENTAT). (b) Contour plot of z-direction strain values after springback.

Table 5.2 Springback angle results of the three-dimensional, without diaphragm, solid elements, static-implicit model of the straight flange bending specimen.

forming pressure (*p*) [MPa]	**die bend radius (*r*) [mm]**	**blank thickness (*t*) [mm]**	**springback [degrees]**
10	2.5	0.6	2.8
10	2.5	1	1.9
10	2.5	1.6	0.3
10	2.5	2	-
10	5	0.6	10.1
10	5	1	7.3
10	5	1.6	5.8
10	5	2	5.4
10	7.5	0.6	15.9
10	7.5	1	10
10	7.5	1.6	8.2
10	7.5	2	7.5

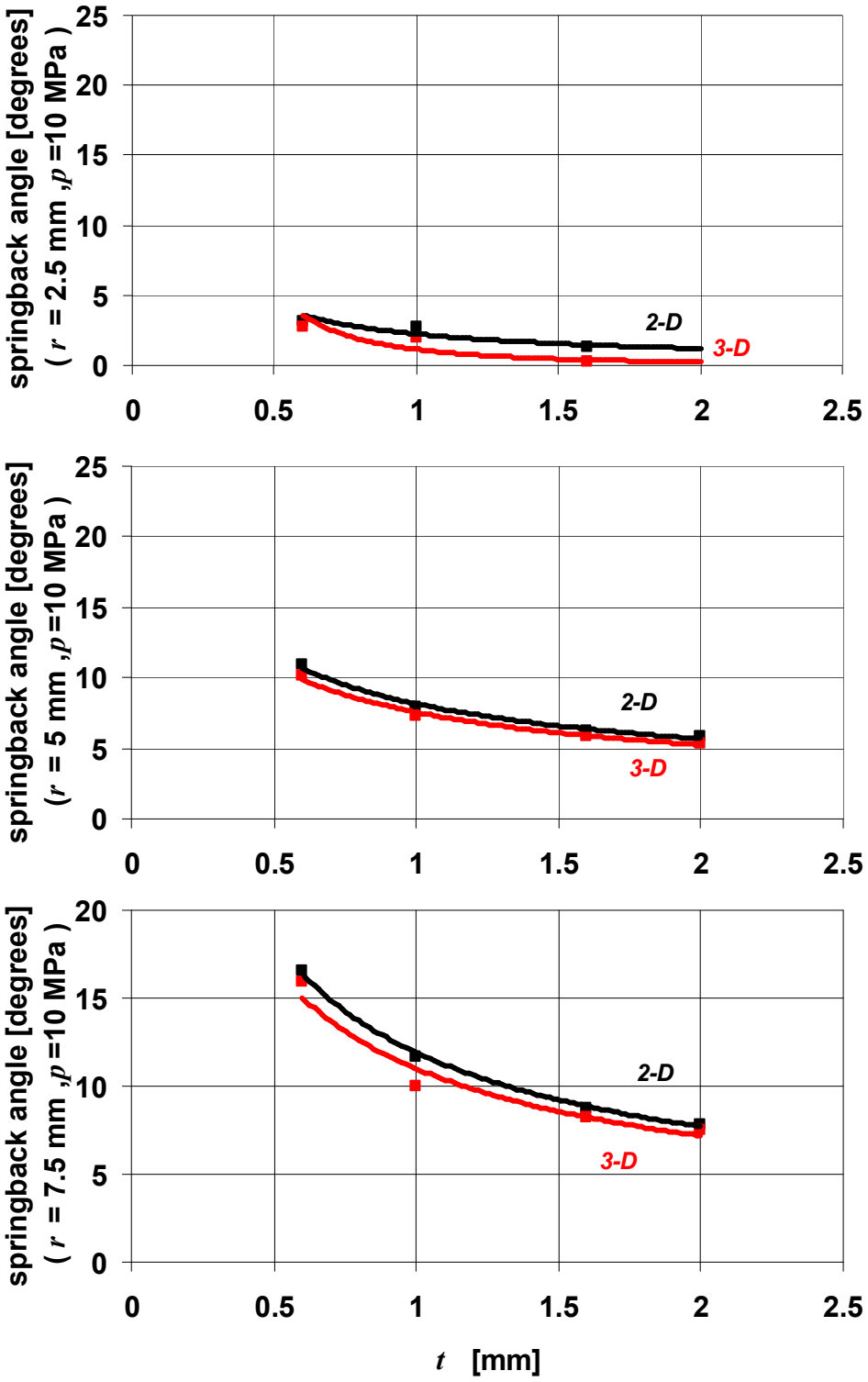

Figure 5.9 Comparison of the springback angle results of the two-dimensional, without diaphragm, solid elements, static-implicit model of the straight flange bending specimen with three-dimensional model.

5.2.3 Three-Dimensional Models without Diaphragm using Shell Elements and Static-Implicit Scheme

Extensive own computations have revealed that solid elements are despite of their better accuracy not computational efficient, so that they could be not used for the analysis of this process with the available hardware. Therefore, shell elements, which are simplified versions of solids for sheet structures, are examined. Above problem is analyzed by using shell elements this time (Figure 5.10). The elements are located only on the middle surface of the blank and five integration points are used through the thickness. Results are given in Table 5.3. There is a small deviation in the results showing that shell elements can be used instead of solids (Figure 5.11). Maximum deviation is 0.8 degrees, minimum deviation is 0.1 degrees and average deviation is 0.4 degrees.

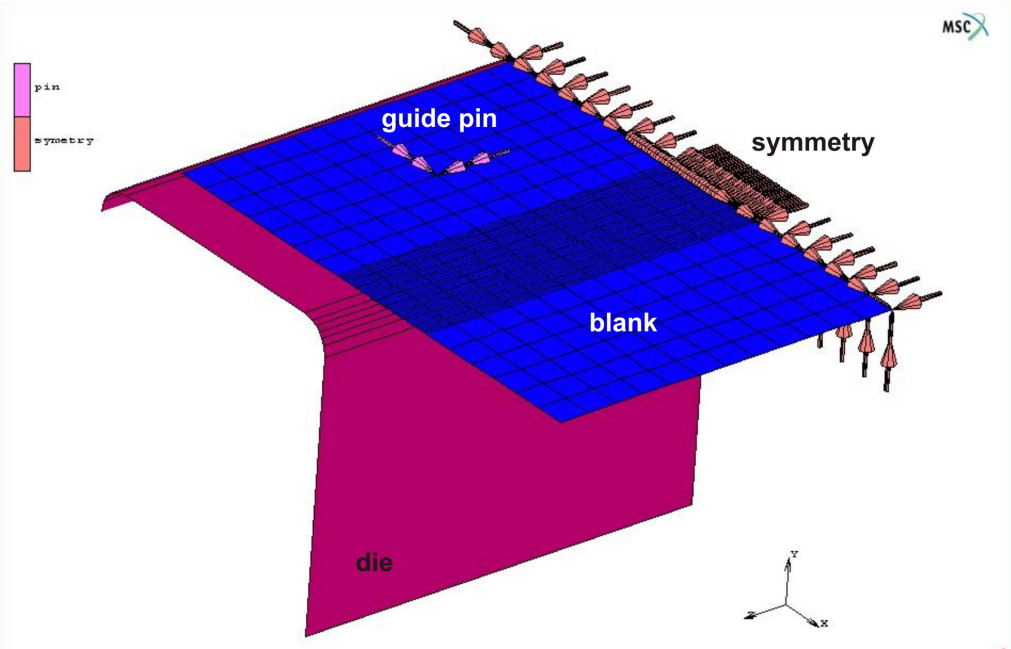

Figure 5.10 Three-dimensional, without diaphragm, shell elements, static-implicit model of the straight flange bending experiment (MARC-MENTAT).

Table 5.3 Springback angle results of the three-dimensional, without diaphragm, shell elements, dynamic-explicit model of the straight flange bending specimen.

forming pressure (*p*) [MPa]	**die bend radius (*r*) [mm]**	**blank thickness (*t*) [mm]**	**springback [degrees]**
10	2.5	0.6	2.9
10	2.5	1	1.1
10	2.5	1.6	0.4
10	2.5	2	-
10	5	0.6	10.9
10	5	1	7.6
10	5	1.6	5.6
10	5	2	5.2
10	7.5	0.6	15.1
10	7.5	1	10.8
10	7.5	1.6	8.1
10	7.5	2	7.3

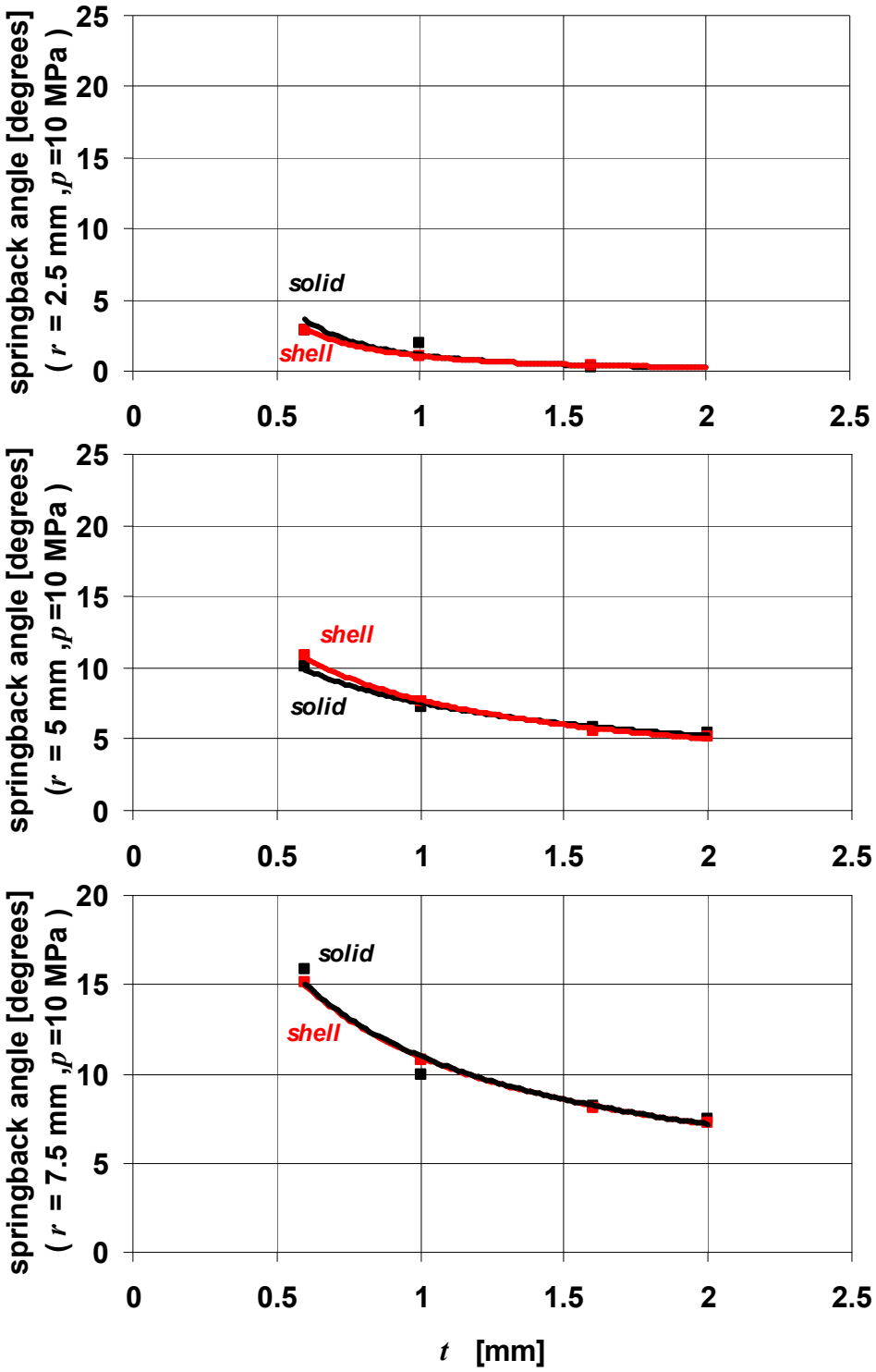

Figure 5.11 Comparison of the springback angle results of the three-dimensional, without diaphragm, solid elements, static-implicit model of the straight flange bending specimen with shell elements.

5.2.4 Three-Dimensional Models without Diaphragm using Shell Elements and Dynamic-Explicit Scheme

This problem is also solved by using a dynamic-explicit code, LS-DYNA. Figure 5.12 shows this model. Different from previous analyses, the die is also discretized with quadrilateral shell elements and material is assigned although it is modeled as rigid. The reason is the penalty contact algorithm used in those analyses. In this algorithm, the contact stiffness is calculated using the material properties of contacting pairs. For the die, same material properties are used as the blank since large material difference between pairs leads to some difficulties in contact handling which are the subjects of forward sections in which rubber diaphragm is included in the models.

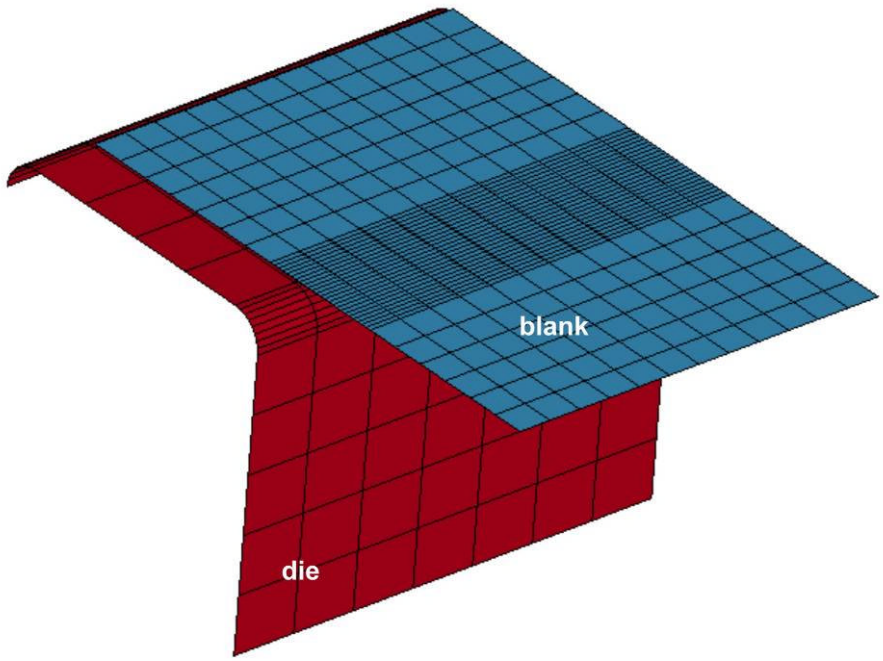

Figure 5.12 Three-dimensional, without diaphragm, shell elements, dynamic-explicit model of the straight flange bending experiment (LS-DYNA).

The global time step is calculated according to the small elements of the blank in the bend region. Mass scaling is done by increasing the mass of those elements and so that the global time step is increased and the computation time is decreased. Also

velocity scaling is done by adjusting the load curve (pressure vs time). The trend of the curve should be such that it artificially speeds up the process in the simulation while minimizing the dynamic effects [7]. In this flanging process, the load curve is divided into two regions (Figure 5.13). In the first region the loading is slow where the sheet is being bended and in the second region the loading is faster where now the sheet is stationary and supported by the die.

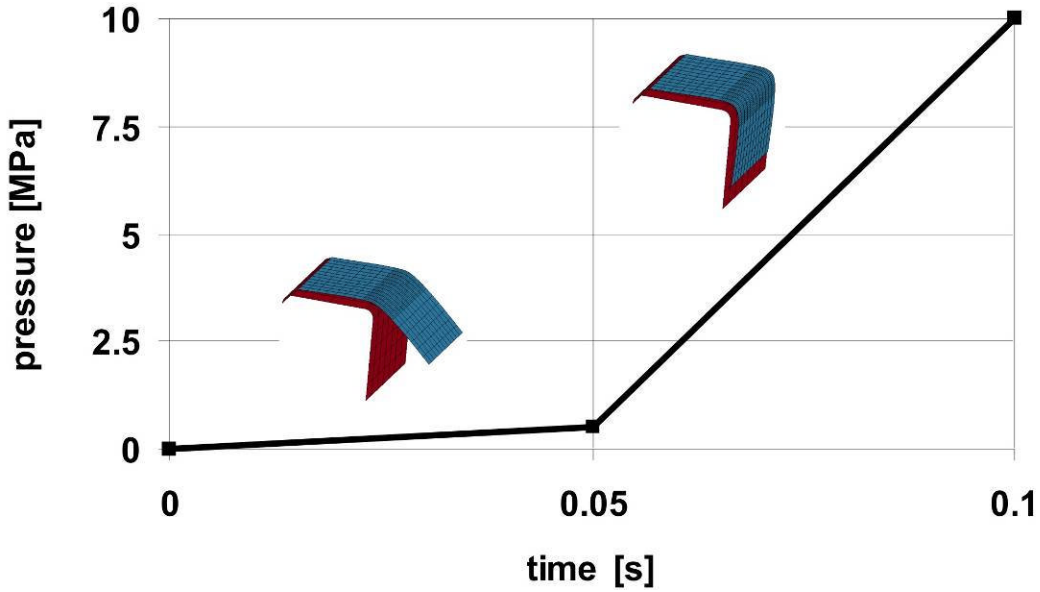

Figure 5.13 The load curve used in the three-dimensional, without diaphragm, shell elements, dynamic-explicit model of the straight flange bending experiment.

A check of kinetic energy to internal energy ratio is done in order to control inertial effects caused by mass and velocity scaling. Figure 5.14 shows that this ratio is so small that unrealistic results are avoided.

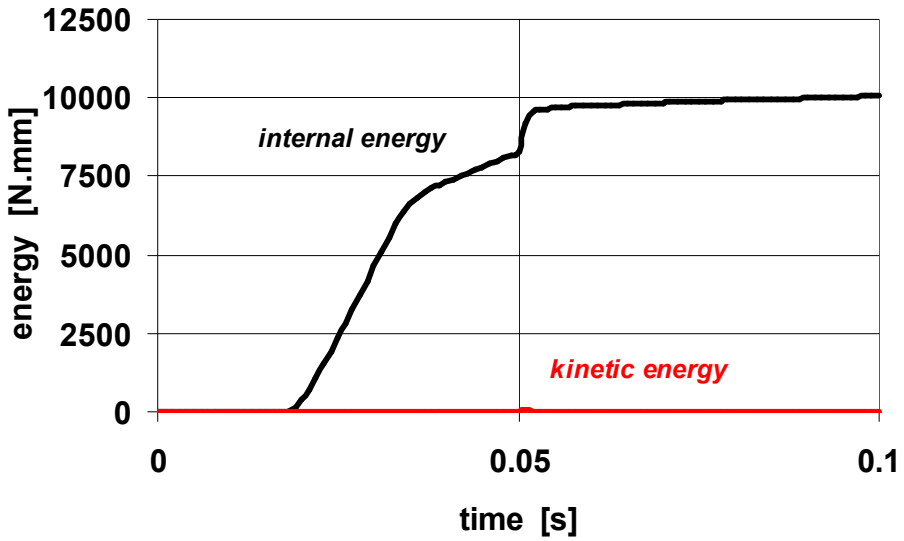

Figure 5.14 The curves of internal energy and kinetic energy of the blank in the three-dimensional, without diaphragm, shell elements, dynamic-explicit model of the straight flange bending experiment.

FORMING_ONE_WAY_SURFACE_TO_SURFACE contact type is used in which only blank nodes are checked for penetration to the die surface. Then penalty forces are applied to those nodes proportional to the penetration depth and contact is simulated.

For springback calculation, implicit scheme is used [6].

Results of this model is given in Table 5.1 and Figure 5.15 compares the dynamic-explicit results with static-implicit. Maximum deviation is 1.6 degrees, minimum deviation is 0.3 degrees and average deviation is 0.7 degrees. Then, dynamic-explicit scheme can be used instead of static-implicit for accurate springback prediction.

Table 5.4 Springback angle results of the three-dimensional, without diaphragm, shell elements, dynamic-explicit model of the straight flange bending specimen.

forming pressure (*p*) [MPa]	**die bend radius (*r*) [mm]**	**blank thickness (*t*) [mm]**	**springback [degrees]**
10	2.5	0.6	1.4
10	2.5	1	-0.3
10	2.5	1.6	-0.6
10	2.5	2	-
10	5	0.6	10.5
10	5	1	7.2
10	5	1.6	5.2
10	5	2	4.7
10	7.5	0.6	16.7
10	7.5	1	11.4
10	7.5	1.6	8.4
10	7.5	2	7.5

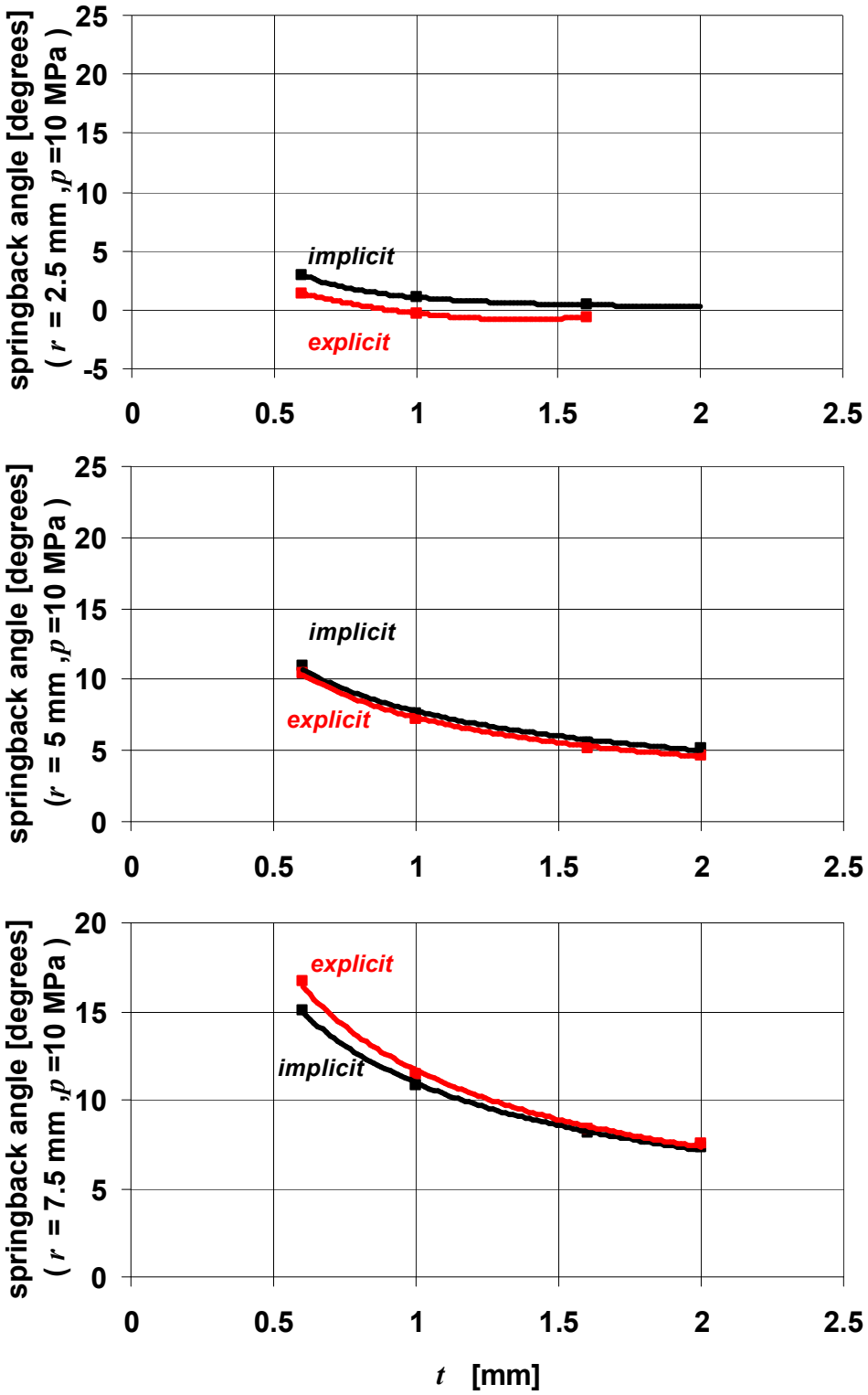

Figure 5.15 Comparison of the springback angle results of the three-dimensional, without diaphragm, shell elements, static-implicit model of the straight flange bending specimen with dynamic-explicit.

5.2.5 Two-Dimensional Models with Diaphragm using Solid Elements and Static-Implicit Scheme

The springback results of the models without diaphragm are not close to the experimental results (Figure 5.7). The reason can be the ignorance of the rubber diaphragm. Adding the rubber diaphragm into the model may lead to a change in the deformation of the sheet because of the new imposed contact conditions. To see this effect, new two-dimensional plane strain models are established including the rubber diaphragm. Figure 5.16 shows this new model.

In the real case, the press has a circular tray and a circular diaphragm. However, plane strain assumption is still valid since the die is long enough in out of plane (x-y) direction that prevents the blank from deforming in that direction by the act of rubber diaphragm. The diaphragm is meshed with quadrilateral plane strain solid elements and a finer mesh is used at the region where the die is placed. ASSUMED STRAIN, CONSTANT DILATION and HERMANN FORMULATIONS are used for the diaphragm elements. The end nodes are fixed and pressure is applied onto the outer edges of the diaphragm elements for simulating the effect of pressurized fluid. In order to compare with the old model (Section 5.2.1), which is without diaphragm, the blank mesh is kept the same.

The rubber material is described by a Mooney-Rivlin material model with two constants A and B. These constants are obtained from the uniaxial tensile test data. (A=0.4 MPa, B=0.1 MPa).

Adaptive time stepping is used for both loading and unloading stages at this time since the unloading of the rubber diaphragm is highly nonlinear.

The tray of the press is modeled together with the die as one analytical rigid body. The contacting pairs are diaphragm-die, diaphragm-blank and blank-die. Direct constraints method is used and a double-sided check is done in which the penetration of each body to the other is taken into account. Appropriate stick-slip coulomb friction coefficients are used between pairs.

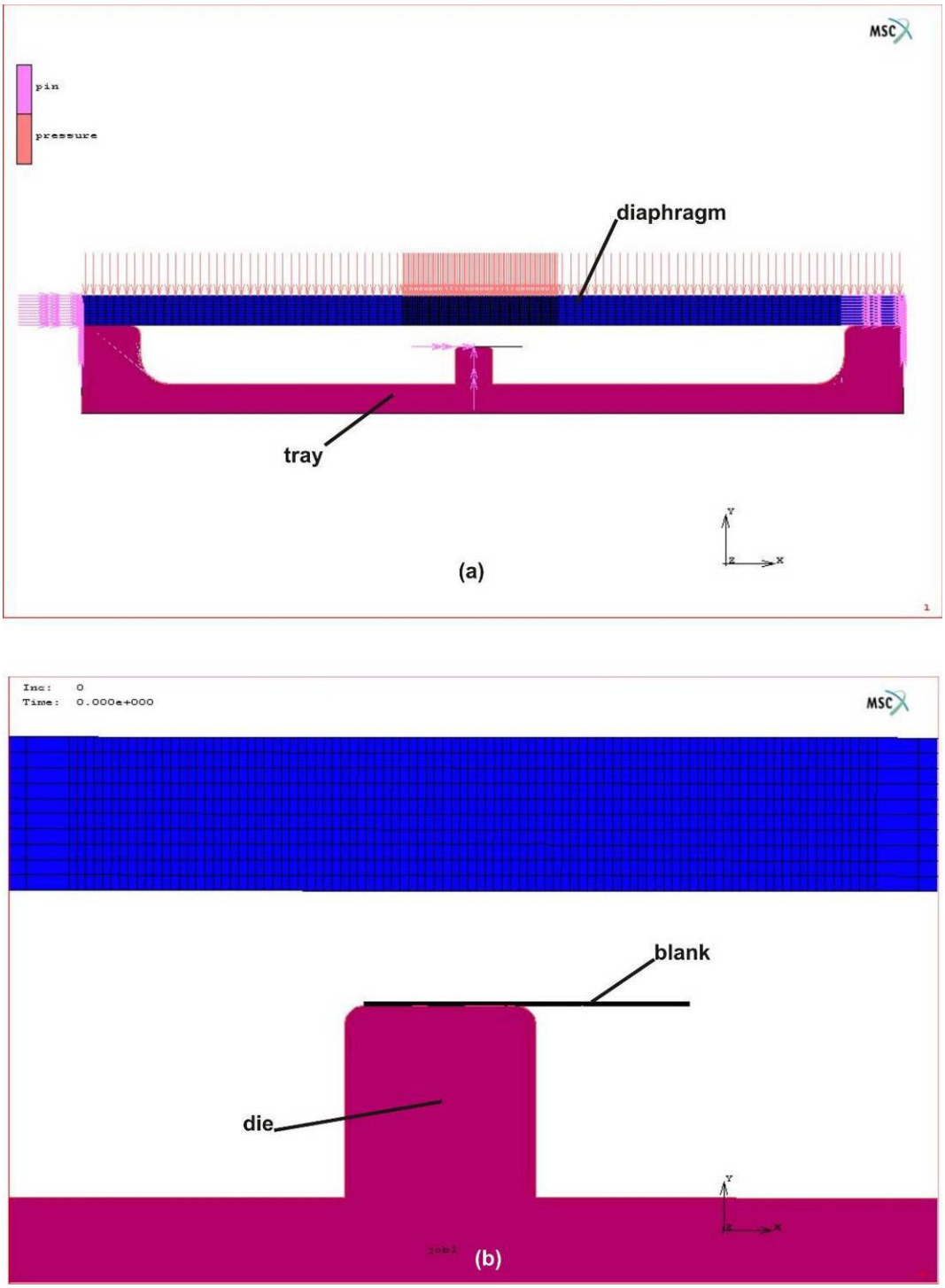

Figure 5.16 Two-dimensional, with diaphragm, solid elements, static-implicit model of the straight flange bending experiment (MARC-MENTAT). (a) whole model (b) zoom to the die and blank.

The results show that there is a change in sheet deformation with inserting the rubber diaphragm to the model. Two gaps formed in the previous analyses have disappeared with the insertion of rubber diaphragm (Figure 5.17). The reason of this difference is the non-uniform pressure distribution on the sheet surface by the act of the rubber diaphragm. Figure 5.18 shows the normal contact forces at an arbitrary stage of bending. The arrows pointing downwards belong to the sheet and upwards to the diaphragm. They are sized according to their magnitudes. The distribution is such that the forces are decreasing while moving on the sheet flange and become zero after half-length. The conclusion drawn from this analysis is that the rubber diaphragm in this process should be modeled in order to capture the deformation behavior of the sheet accurately.

Table 5.5 gives the springback results of this model and Figure 5.19 compares the results with the previous ones obtained by the model without diaphragm. The deviation in the results between these two models decreases as the die bend radius increases. The reason is the weak gap formation at higher bend radius in the model without diaphragm.

Springback angles obtained with this model are now functions of *t/r* ratio as in the case of physical experiments. In Figure 5.20, results are shown by using the parameter *t/r* and they are compared with experimental results. Although increasing forming pressure has a little effect on springback in the physical experiments that is not the case in simulations. The deviation between numerical and experimental results increases considerably as the forming pressure increases. For the forming pressure of 10 MPa, max error of the model is 3.3 degrees, min error is 1.4 degrees and average error is 2.1 degrees. For the forming pressure of 40 MPa, max error is 4.8 degrees, min error is 2.7 degrees and average error is 3.3 degrees. For the forming pressure of 80 MPa, max error is 7.3 degrees, min error is 3.8 degrees and average error is 4.8 degrees. The reason of this deviation can be explained by the discretization of the rubber diaphragm causing high local stress regions at higher pressures (higher than 10 MPa) leading to bad springback results.

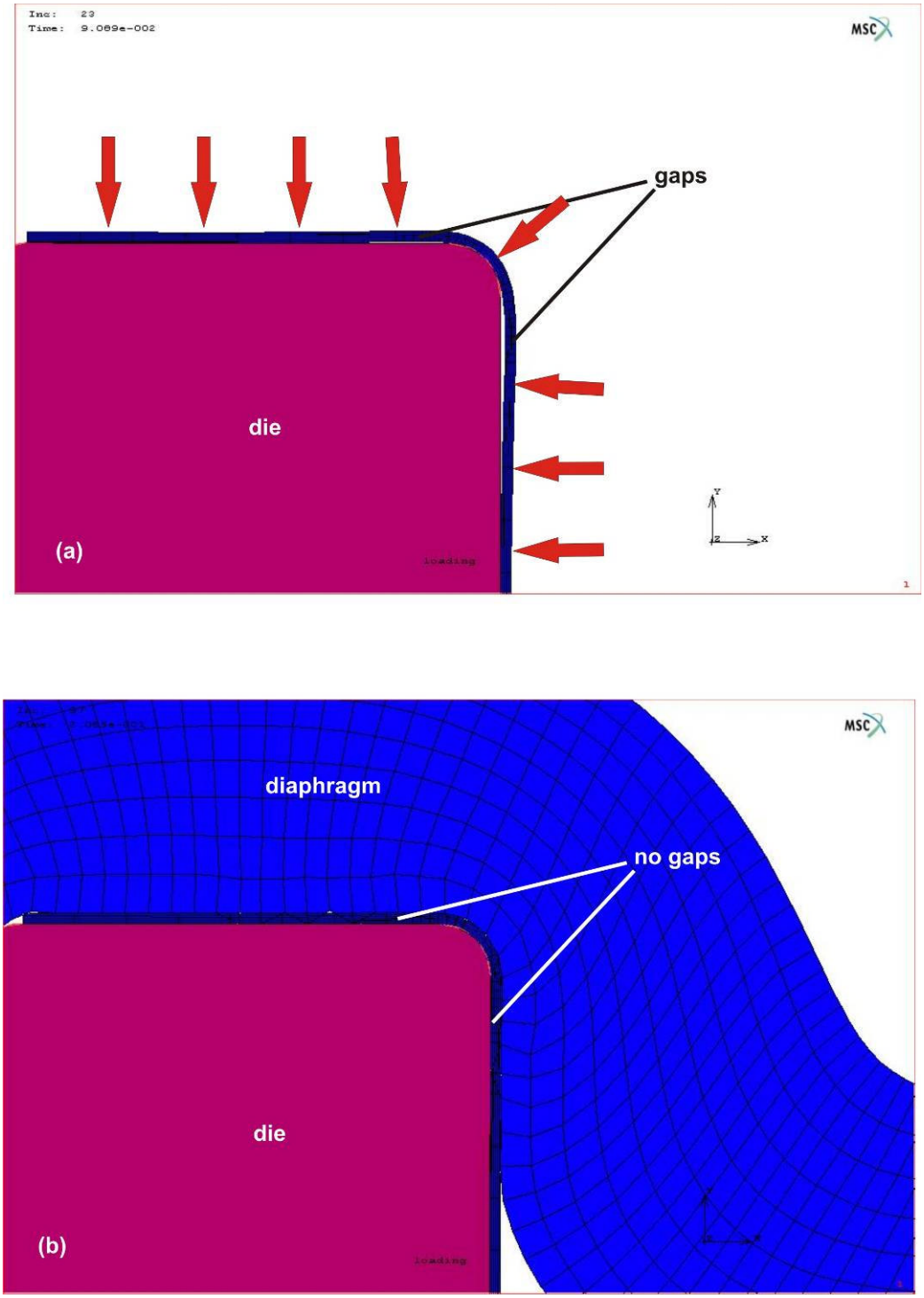

Figure 5.17 The change in the sheet deformation with the insertion of the diaphragm to the model. (a) The analysis without diaphragm ending with two gap formations (b) No occurrence of gaps with the analysis including the diaphragm

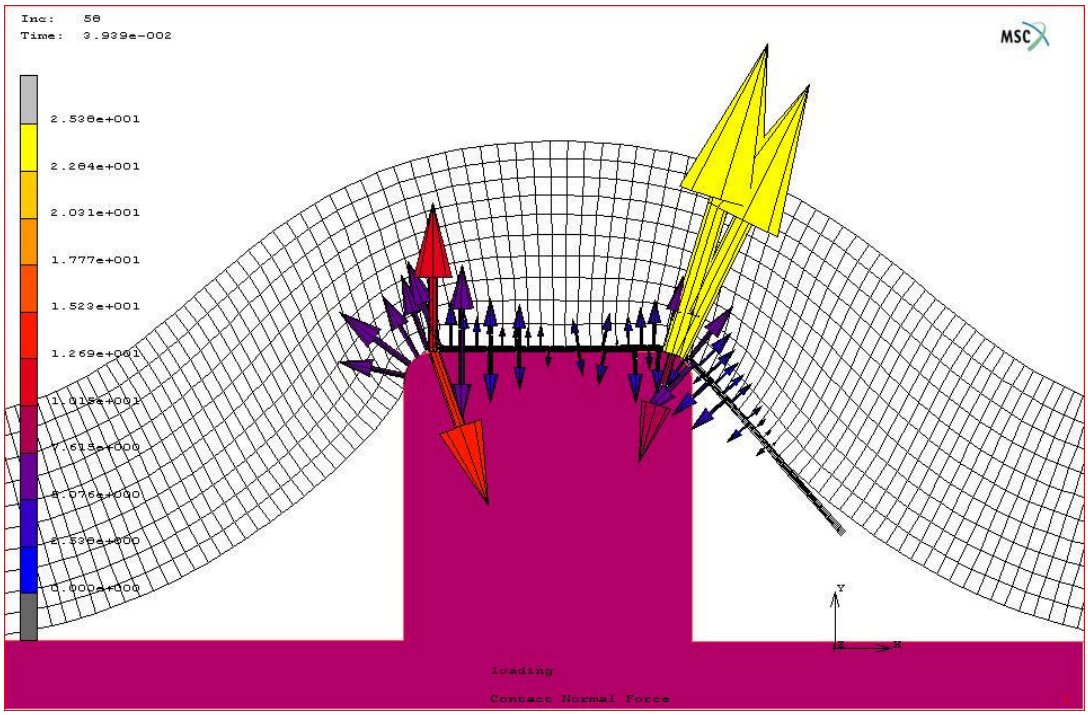

Figure 5.18 Normal contact force distribution in the straight flange bending analysis. The arrows are sized according to their magnitudes.

Table 5.5 Springback angle results of the two-dimensional, with diaphragm, solid elements, static-implicit model of the straight flange bending specimen.

forming pressure (*p*) [MPa]	**die bend radius (*r*) [mm]**	**blank thickness (*t*) [mm]**	**springback [degrees]**
10	2.5	0.6	7.7
10	2.5	1	6
10	2.5	1.6	4.3
10	2.5	2	-
10	5	0.6	12.7
10	5	1	9.4
10	5	1.6	6.9
10	5	2	6.4

10	7.5	0.6	17.4
10	7.5	1	12.2
10	7.5	1.6	9.2
10	7.5	2	8
40	2.5	0.6	10
40	2.5	1	7.3
40	2.5	1.6	5
40	2.5	2	-
40	5	0.6	15
40	5	1	11.2
40	5	1.6	8.1
40	5	2	7.5
40	7.5	0.6	20
40	7.5	1	14.4
80	7.5	1.6	10.5
80	7.5	2	9.4
80	2.5	0.6	9.7
80	2.5	1	7
80	2.5	1.6	5
80	2.5	2	-
80	5	0.6	15.3
80	5	1	11.1
80	5	1.6	7.8
80	5	2	7.3
80	7.5	0.6	19.9
80	7.5	1	14.5
80	7.5	1.6	10.4
80	7.5	2	9.5

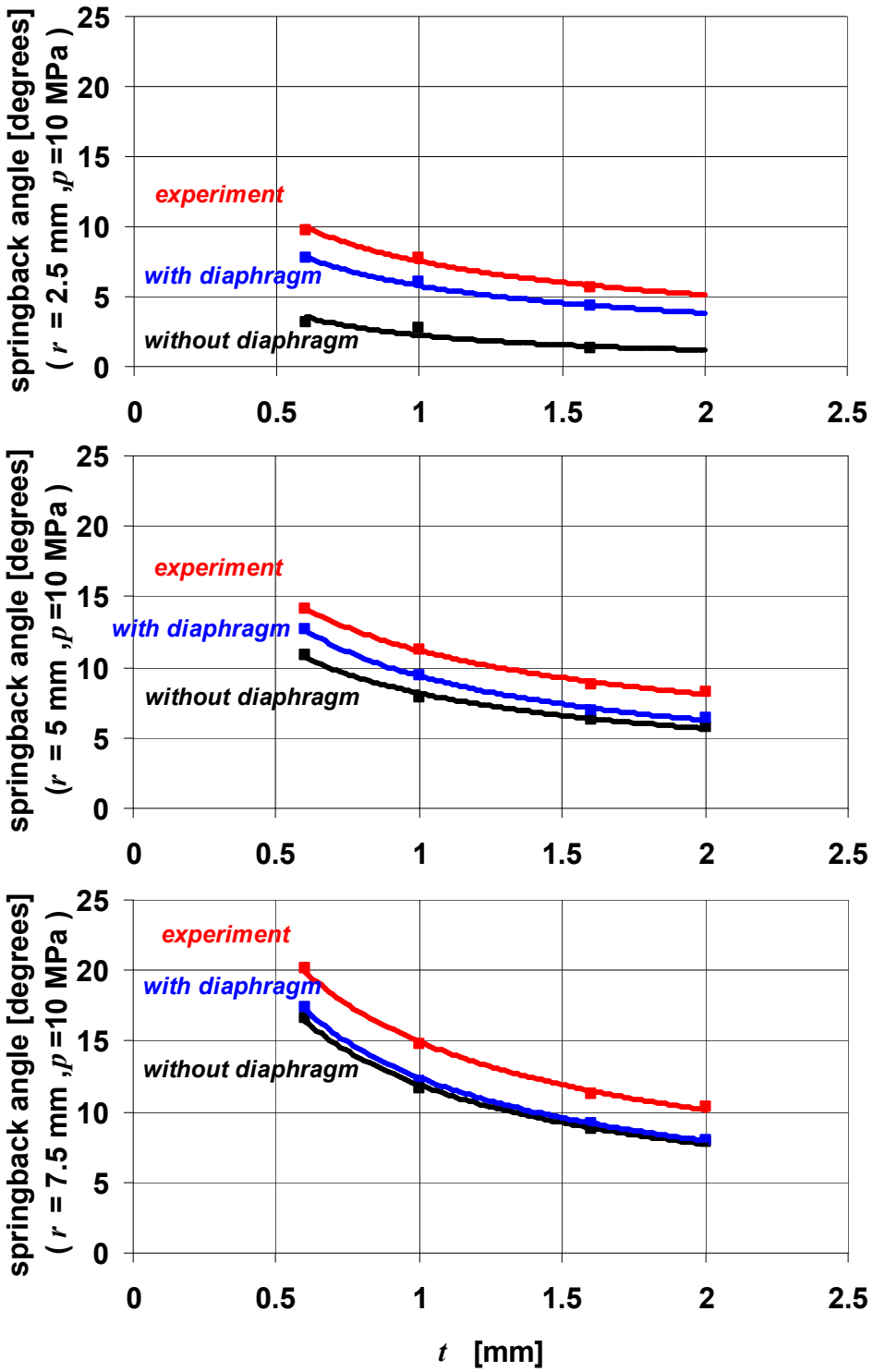

Figure 5.19 Comparison of the springback angle results of the two-dimensional, without diaphragm, solid elements, static-implicit model of the straight flange bending specimen with the same model done with diaphragm and also with the experimental results.

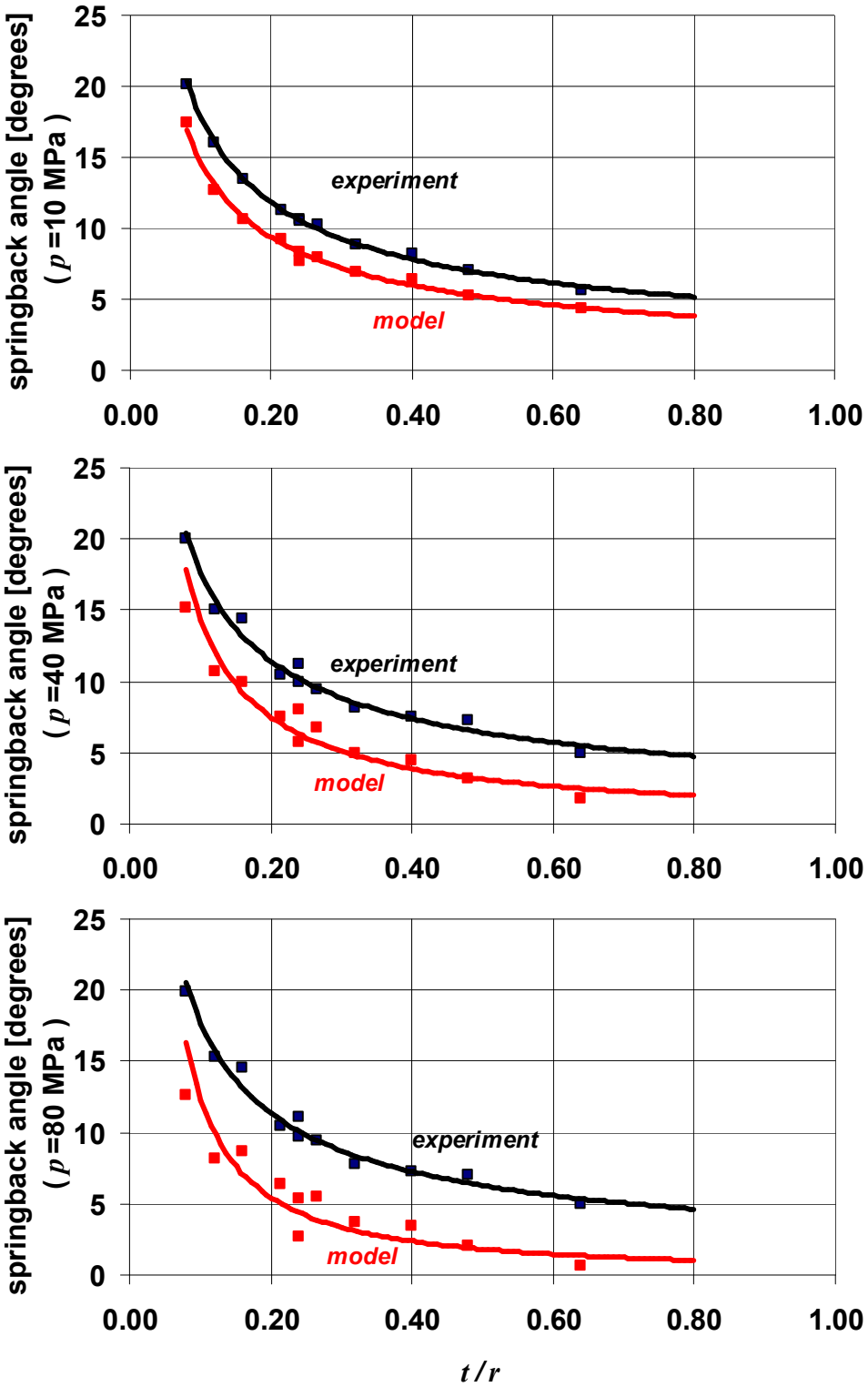

Figure 5.20 Comparison of the springback angle results of the two-dimensional, with diaphragm, solid elements, static-implicit model of the straight flange bending specimen with experimental results.

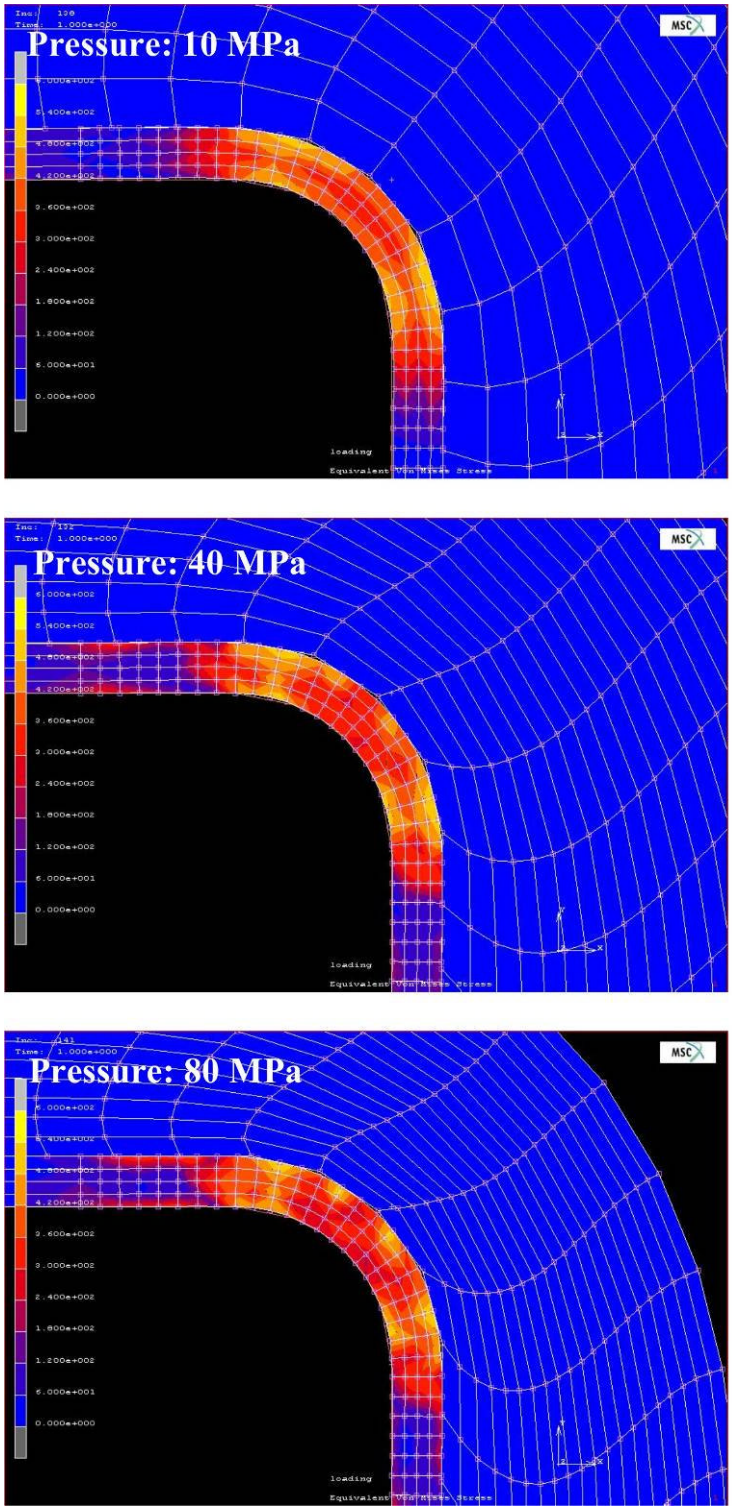

Figure 5.21 High local stresses observed in the bend region with increasing pressure for the simulation of straight flange bending specimen.

In the next section, a full model will be prepared which is three-dimensional and with diaphragm. Dynamic-explicit scheme will be used in this model since static-implicit scheme has convergence problems with three-dimensional analyses.

5.2.6 Three-Dimensional Models with Diaphragm using Shell Elements and Dynamic-Explicit Scheme

Implicit scheme has convergence problems with three-dimensional models including the diaphragm. Some details like the corners of dies and blank edges are complex contact areas between the diaphragm-die and diaphragm-blank. To handle contact convergence in those areas, small time steps are needed and that is the nature of the explicit time integration scheme. Therefore, three-dimensional models are prepared with using dynamic-explicit code LS-DYNA.

Figure 5.22 shows the three bodies in the model: The die including the tray (rigid), the blank (plastically deformable) and the diaphragm (elastically deformable). The blank is discretized

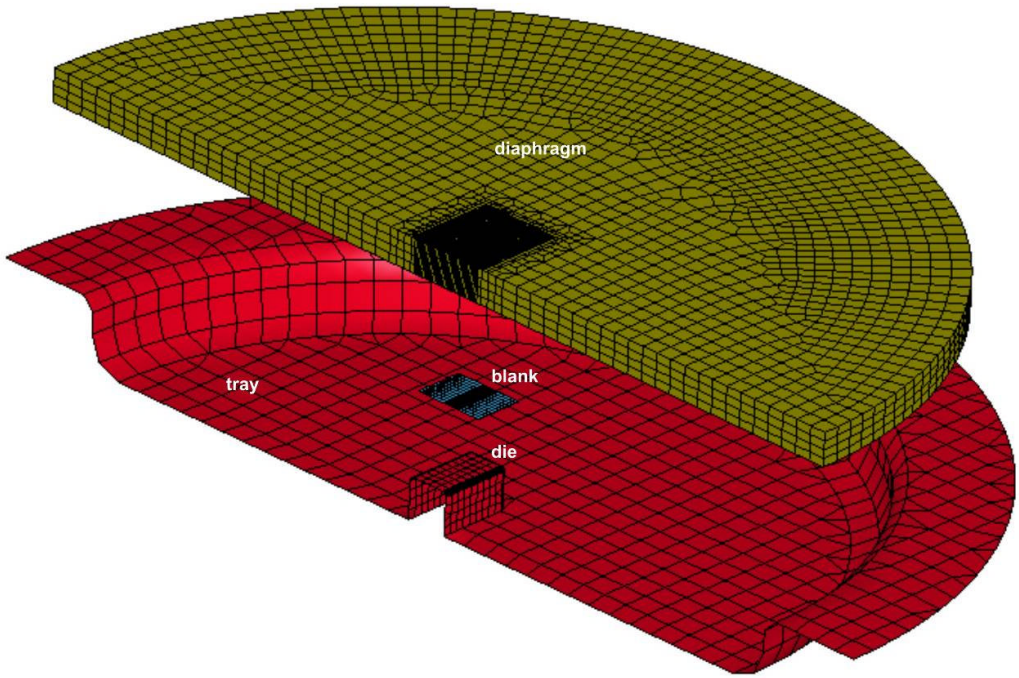

Figure 5.22 Three-dimensional, with diaphragm, shell elements, dynamic-explicit model of the straight flange bending experiment (LS-DYNA).

with full integrated shell elements using 5 integration points through the thickness. Reduced integrated constant stress solid elements are used for the diaphragm. The mesh density is increased in the critical areas like the bend region of the blank and the center of the diaphragm where the die is placed. The boundary conditions are hinged peripheral nodes of the diaphragm, pinned nodes of the blank at the guide pins, the symmetry conditions at the half plane and finally the pressure load on the diaphragm.

MAT_PIECEWISE_LINEAR_PLASTICITY (Material Type 24) is defined for the blank material by using effective stress vs effective plastic strain curve obtained form uniaxial tensile test. MAT_MOONEY-RIVLIN_RUBBER (Material Type 27) with two constants is used for the diaphragm material. These constants are obtained from the uniaxial tensile test again.

Stages are defined for the load curve (pressure vs time) in which slope is increased gradually. The aim in doing this is to shorten the analysis time as much as possible while maintaining the quasi-static behavior. Since the diaphragm becomes more and more stationary as pressure increases, the load speed can be increased without having negative effect on the quasi-static analysis. However, it should be checked that no big dynamic effects occurred while artificially speeding up the process and this check is done by comparing the kinetic energy-internal energy ratio of the sheet. Figure 5.23 shows the loading curve used in this analysis and the kinetic-internal energy curves.

In addition, some mass is added to the blank in order to increase the time step and thereby shorten the analysis time. A critical time step value is specified and the mass is added to the elements that has time steps lower than this critical value. Care should be taken by doing this since it also increases the dynamic behavior of the sheet. Again, a check of the kinetic-internal energy ratio is needed (Figure 5.24).

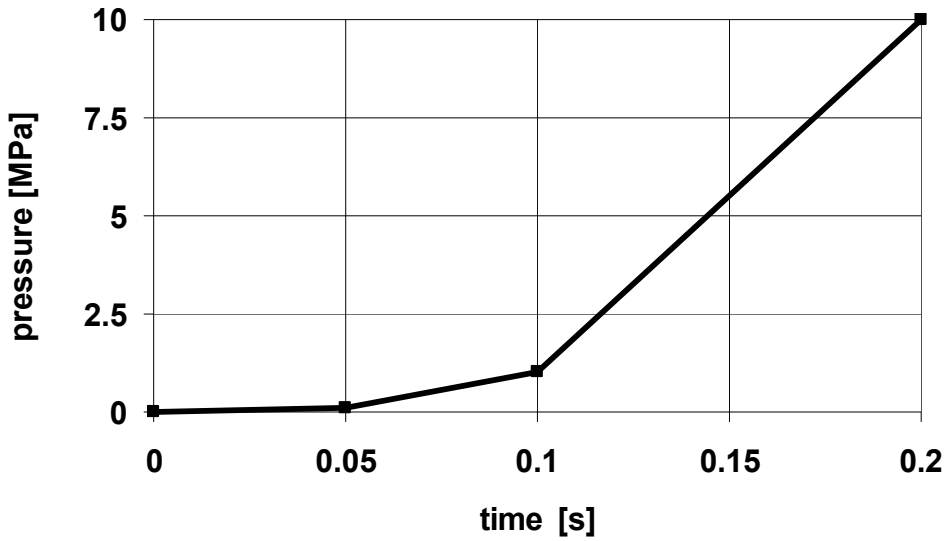

Figure 5.23 The load curve used in the three-dimensional, with diaphragm, shell elements, dynamic-explicit model of the straight flange bending experiment.

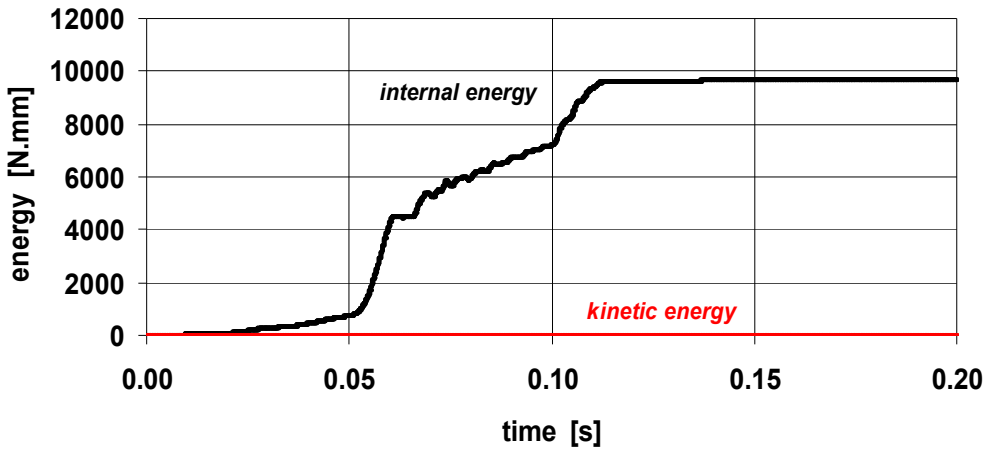

Figure 5.24 The curves of internal energy and kinetic energy of the blank in the three-dimensional, with diaphragm, shell elements, dynamic-explicit model of the straight flange bending experiment.

The challenging part in modeling this process is defining contact parameters between two deformable and one rigid body all being mutually in contact with each other. The penalty method is used for the implementation of the contact algorithm in which contact stiffness is calculated by considering the slave side nodes with area or mass weighted option (PENOPT=4 in CONTROL_CONTACT card). Special scaling should be done for the contact stiffness between the diaphragm and the die, and also between the diaphragm and the blank in order to compensate the bulk modulus differences between these materials (bulk modulus for aluminum is taken as 71667 MPa and for rubber 50 MPa; for the rigid die the same bulk modulus as for aluminum is taken). FORMING_ONE_WAY_SURFACE_TO_SURFACE contact type is defined between blank-die and diaphragm-die in which slave side is blank and diaphragm respectively. It is advisable to use a double sided contact (no slave, no master) if the bodies are both deformable. Therefore, AUTOMATIC_SURFACE_TO_SURFACE contact type is used for the contact between diaphragm-blank. The problem with penalty contact method is that the penetrations of the blank nodes to the die surface are not exactly equal and at high pressures, this inequality becomes more clear that disruptions are seen in the pattern of strain and stress distributions in the bend region. This phenomenon causes the bad prediction of springback angles at higher pressures (higher than 10 MPa).

Coulomb friction model is used for contacting parts. Values of 0.2 and 0.9 are used for the friction coefficients between aluminum-aluminum and rubber – aluminum, respectively.

For springback calculation, implicit scheme is used [6].

Oscillations are observed during the first contact between diaphragm and blank. One can get rid of those by applying numerical mass damping. Higher values may lead instabilities and should be avoided.

Springback results of this model are given in Table 5.6. Comparison with experimental results is given in Figure 5.25. Maximum error of the model is 1.5 degrees, minimum error is 0.1 degrees and average error is 0.7 degrees.

Table 5.6 Springback angle results of the three-dimensional, with diaphragm, shell elements, dynamic-explicit model of the straight flange bending specimen.

forming pressure (*p*) [MPa]	**die bend radius (*r*) [mm]**	**blank thickness (*t*) [mm]**	**springback [degrees]**
10	2.5	0.6	9.8
10	2.5	1	6
10	2.5	1.6	5.1
10	2.5	2	-
10	5	0.6	14.6
10	5	1	10.6
10	5	1.6	7.8
10	5	2	6.7
10	7.5	0.6	20
10	7.5	1	13.6
10	7.5	1.6	10.2
10	7.5	2	8.9

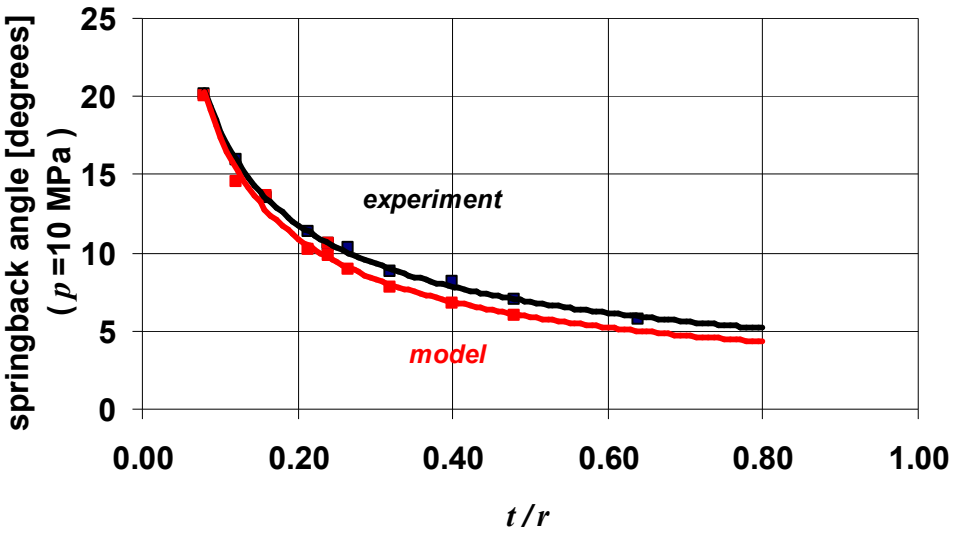

Figure 5.25 Comparison of the springback angle results of the three-dimensional, with diaphragm, shell elements, dynamic-explicit model of the straight flange bending specimen with experimental results.

5.3 Simulation of Contoured Flange Bending Experiment

As described in Chapter 4, this experiment is the 90 degrees bending of a rectangular blank over a contoured die (Figure 5.26). For this specimen the wrinkle formation is used as the basic parameter for the assessment. The deformation is so complex that simple two-dimensional models can not be established for this specimen. Analyses have made with and without diaphragm modelled and the need for the diaphragm is observed again for the numerical modelling of this process.

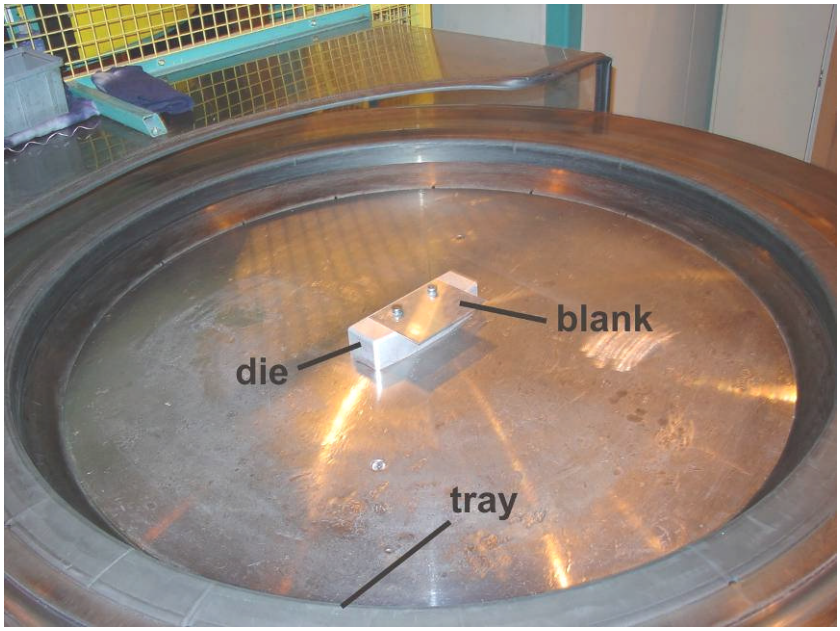

Figure 5.26 Contoured Flange Bending Experiment.

5.3.1 Three-Dimensional Models without Diaphragm using Shell Elements and Dynamic-Explicit Scheme

This model is identical to the model in Section 5.2.3 except the geometry of the die. The straight die is replaced by the contoured one. Figure 5.27 shows this model. Another difference is that adaptive meshing is defined for the blank in order to capture the curvature of tool and also in order to capture wrinkling. In this analysis the refinement level is three which means elements are split to four for two times. The critical element edge length is decreased to 1.25 mm from 5 mm in two stages.

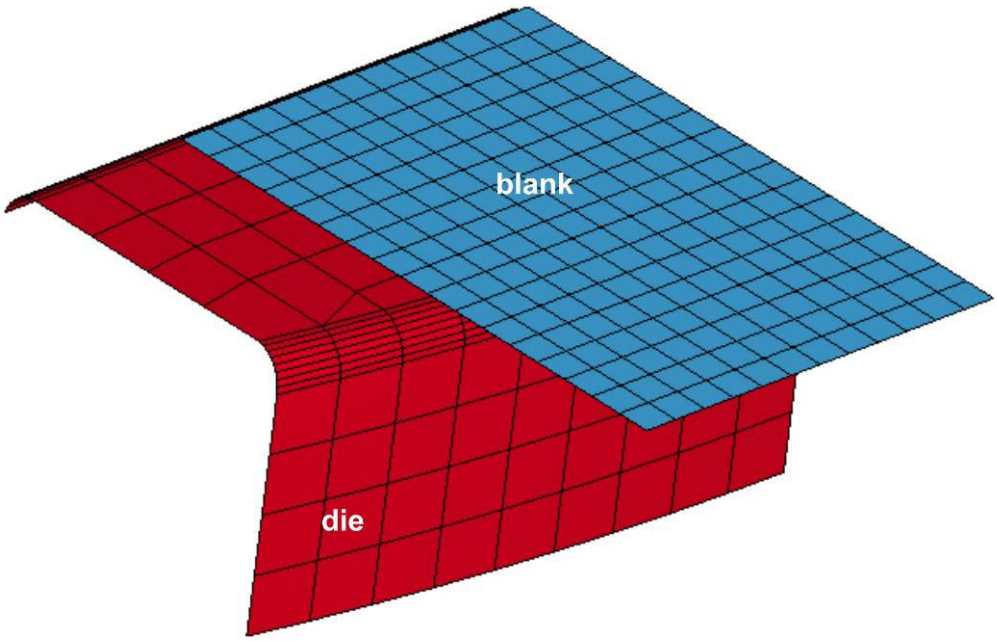

Figure 5.27 Three-dimensional, without diaphragm, shell elements, dynamic-explicit model of the contoured flange bending experiment (LS-DYNA).

While looking to the result (Figure 5.28), no wrinkling is observed which is not the real case in the physical experiment (t=1 mm, r=5 mm, p=10 MPa). This result emphasizes the need for the diaphragm modeling.

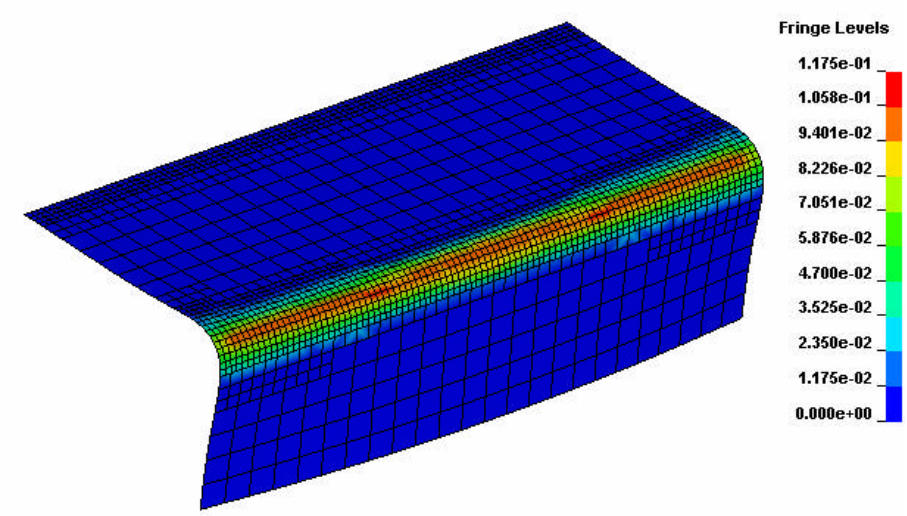

Figure 5.28 Plastic strain contour plot of the blank after forming belonging to the three-dimensional, without diaphragm, shell elements, dynamic-explicit model of the contoured flange bending experiment.

5.3.2 Three-Dimensional Models with Diaphragm using Shell Elements and Dynamic-Explicit Scheme

This model is identical to the model in Section 5.2.6 except the geometry of the die. The straight die is replaced by the contoured one. Also, adaptive meshing is used for the blank. Figure 5.29 shows this model.

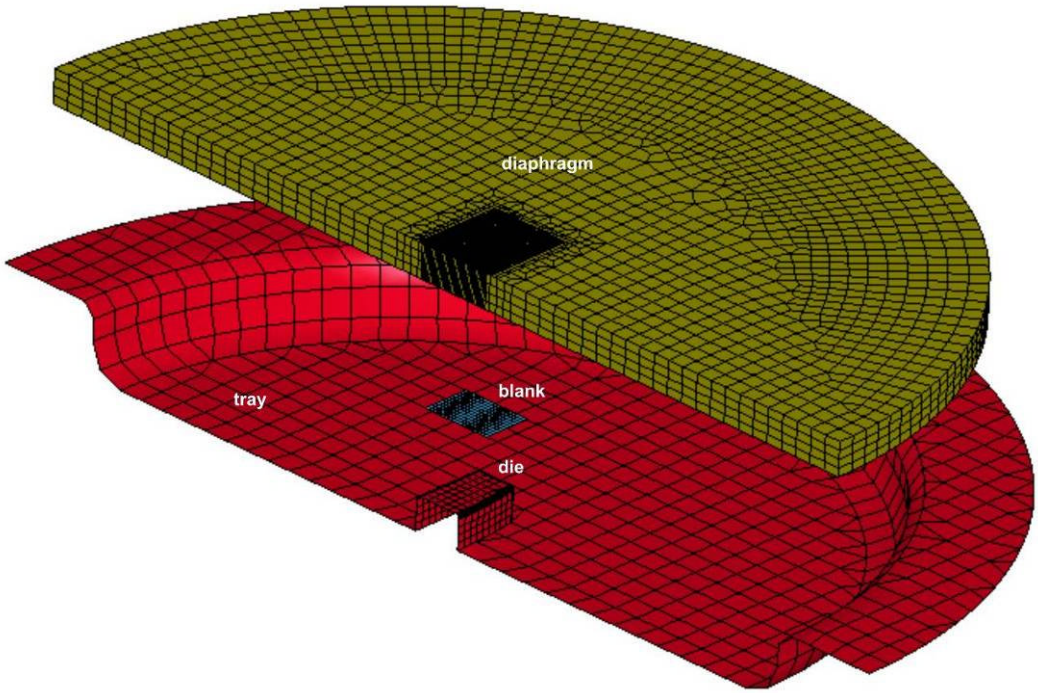

Figure 5.29 Three-dimensional, with diaphragm, shell elements, dynamic-explicit model of the contoured flange bending experiment (LS-DYNA).

The results are shown in Figure 5.30 comparing with experimental results. They show good agreement with experimental results.

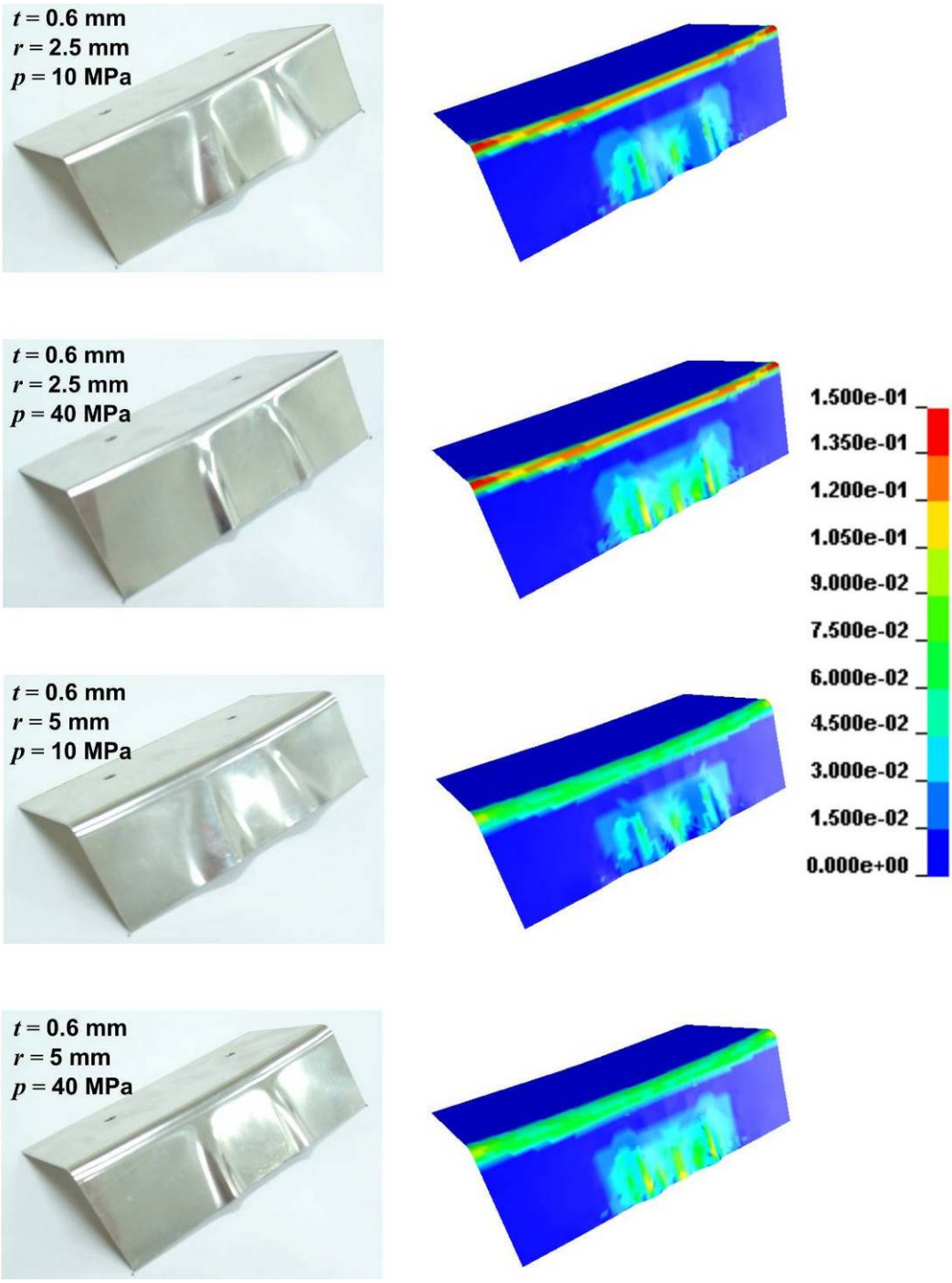

Figure 5.30 Plastic strain contour plot of the blank after forming belonging to the three-dimensional, with diaphragm, shell elements, dynamic-explicit model of the contoured flange bending experiment.

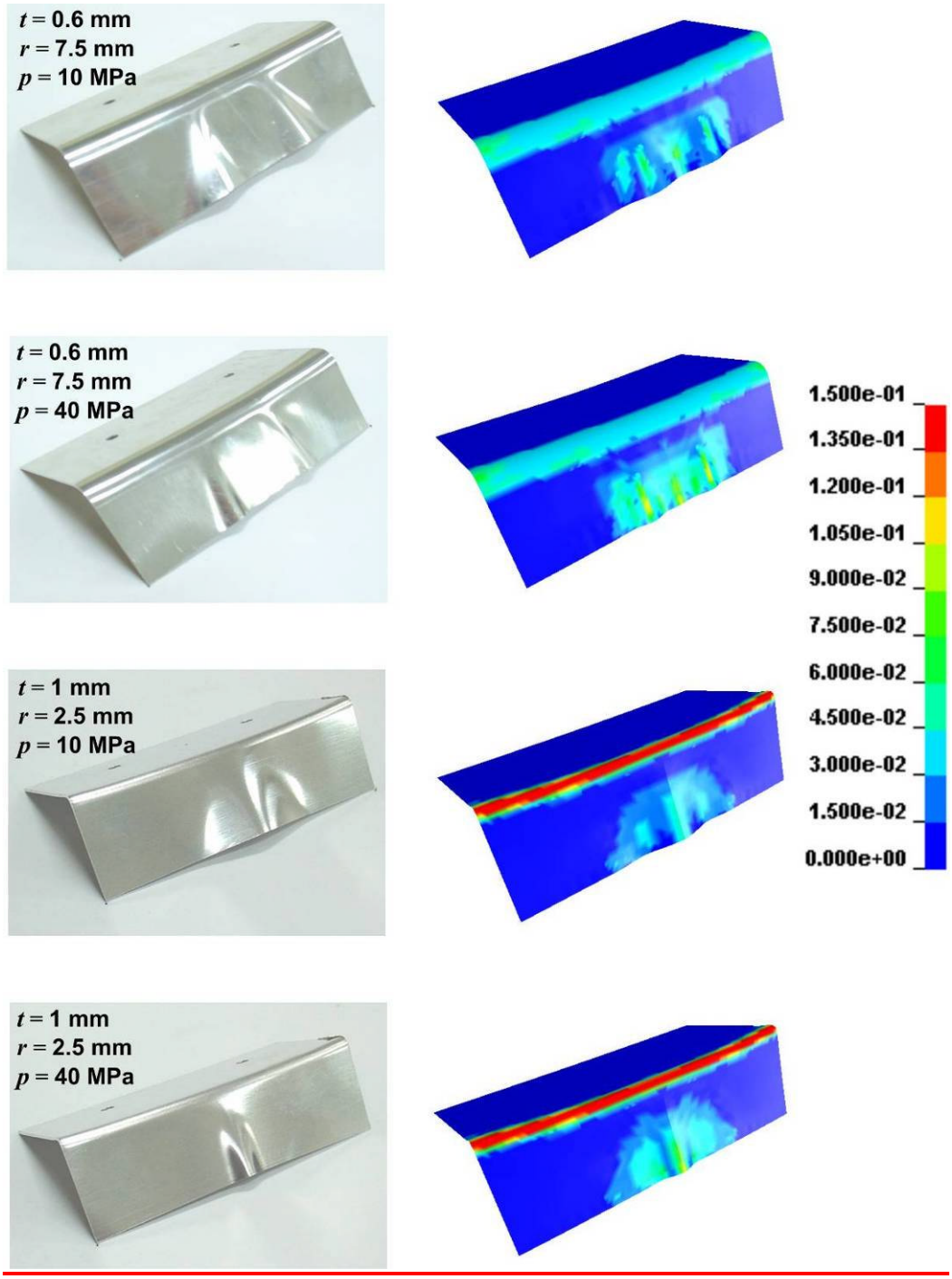

Figure 5.30 (continued)

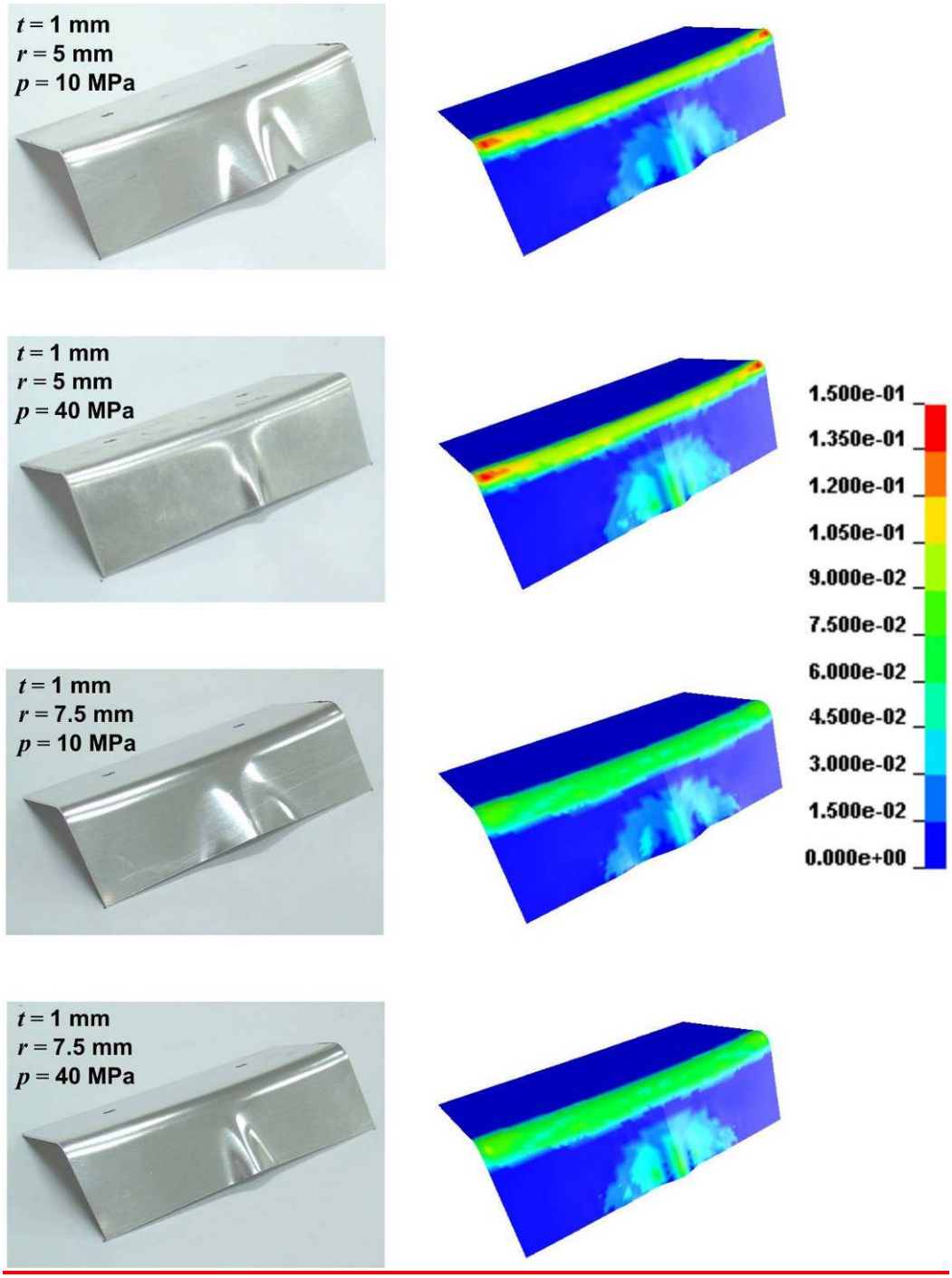

Figure 5.30 (continued)

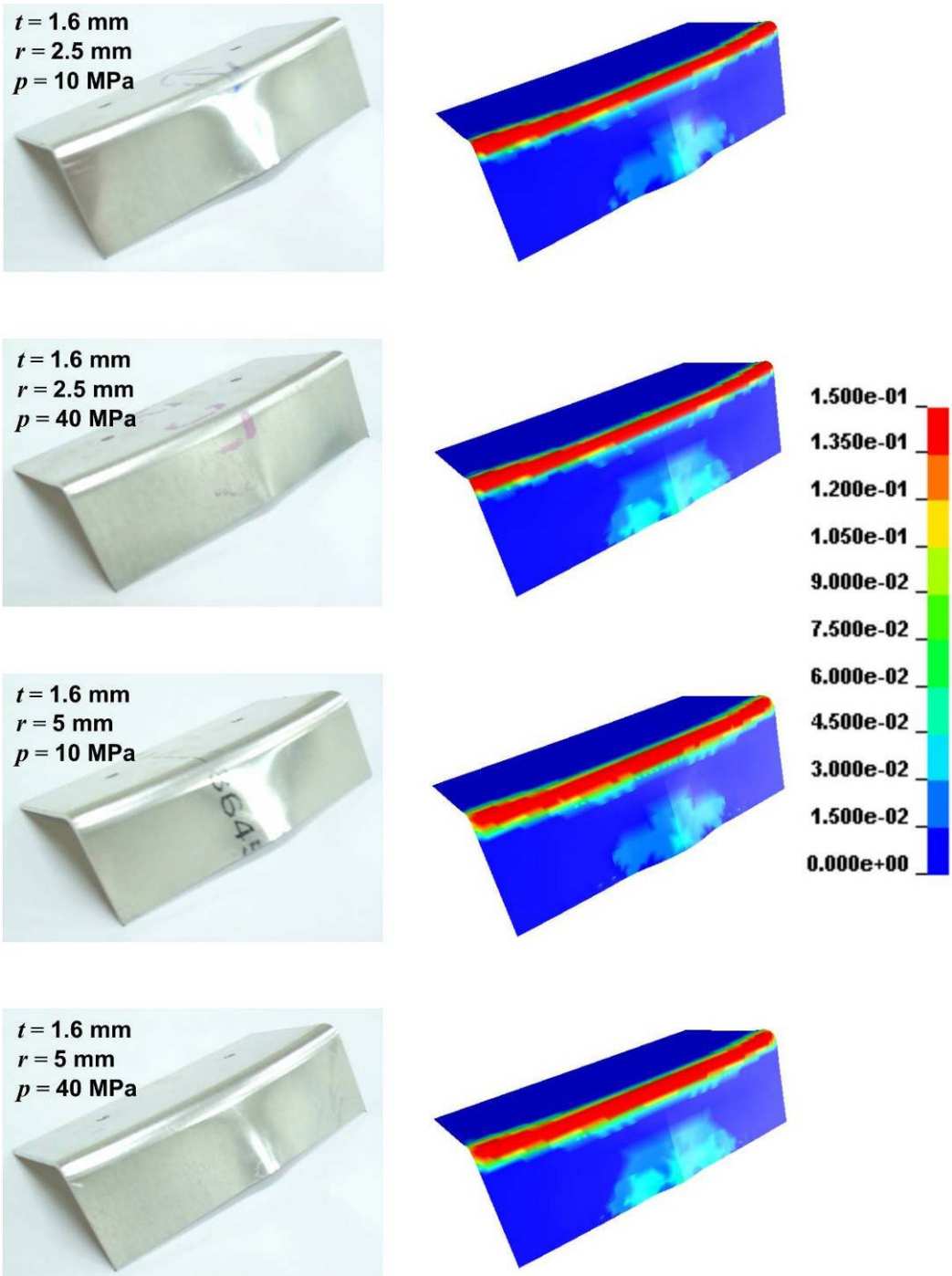

Figure 5.30 (continued)

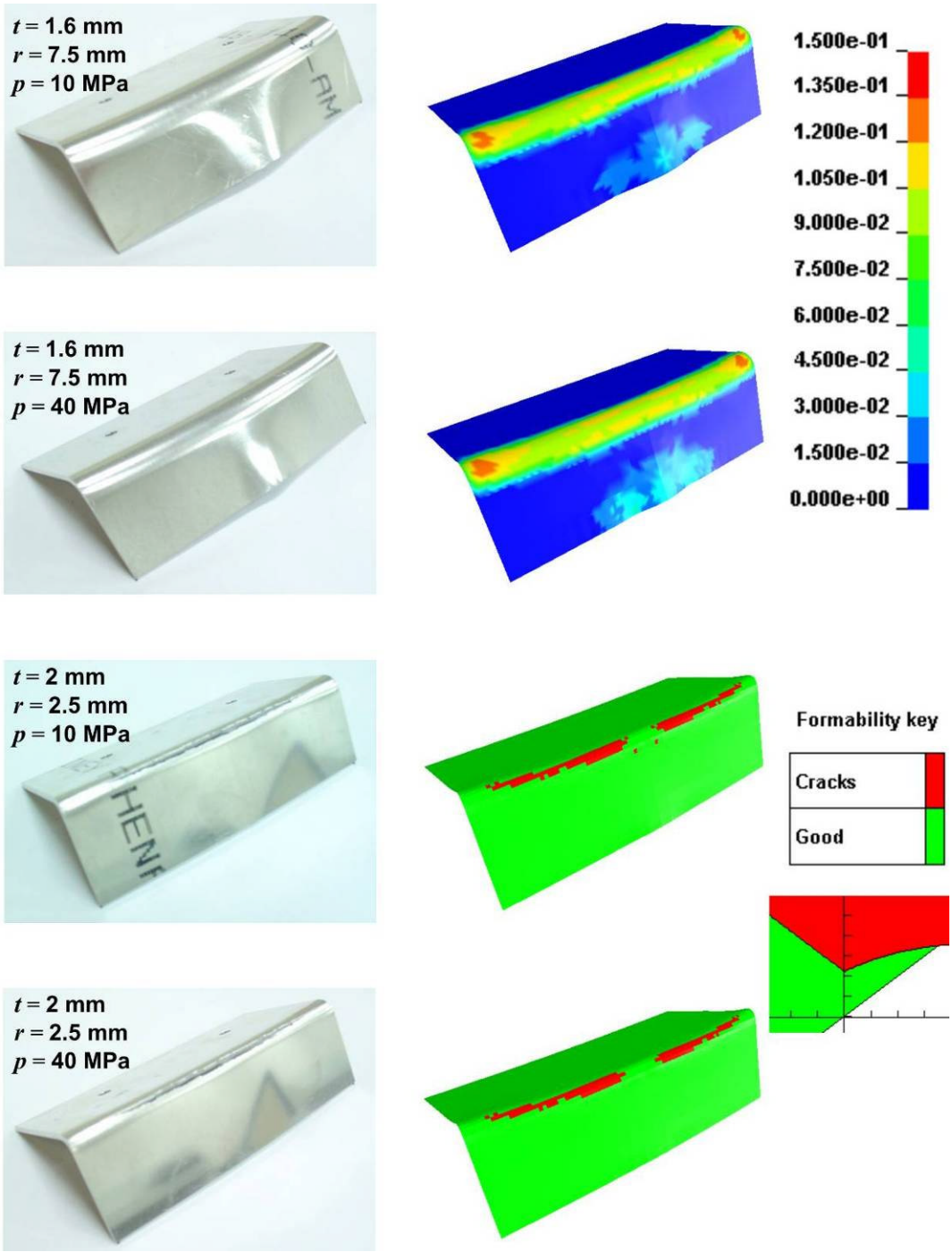

Figure 5.30 (continued)

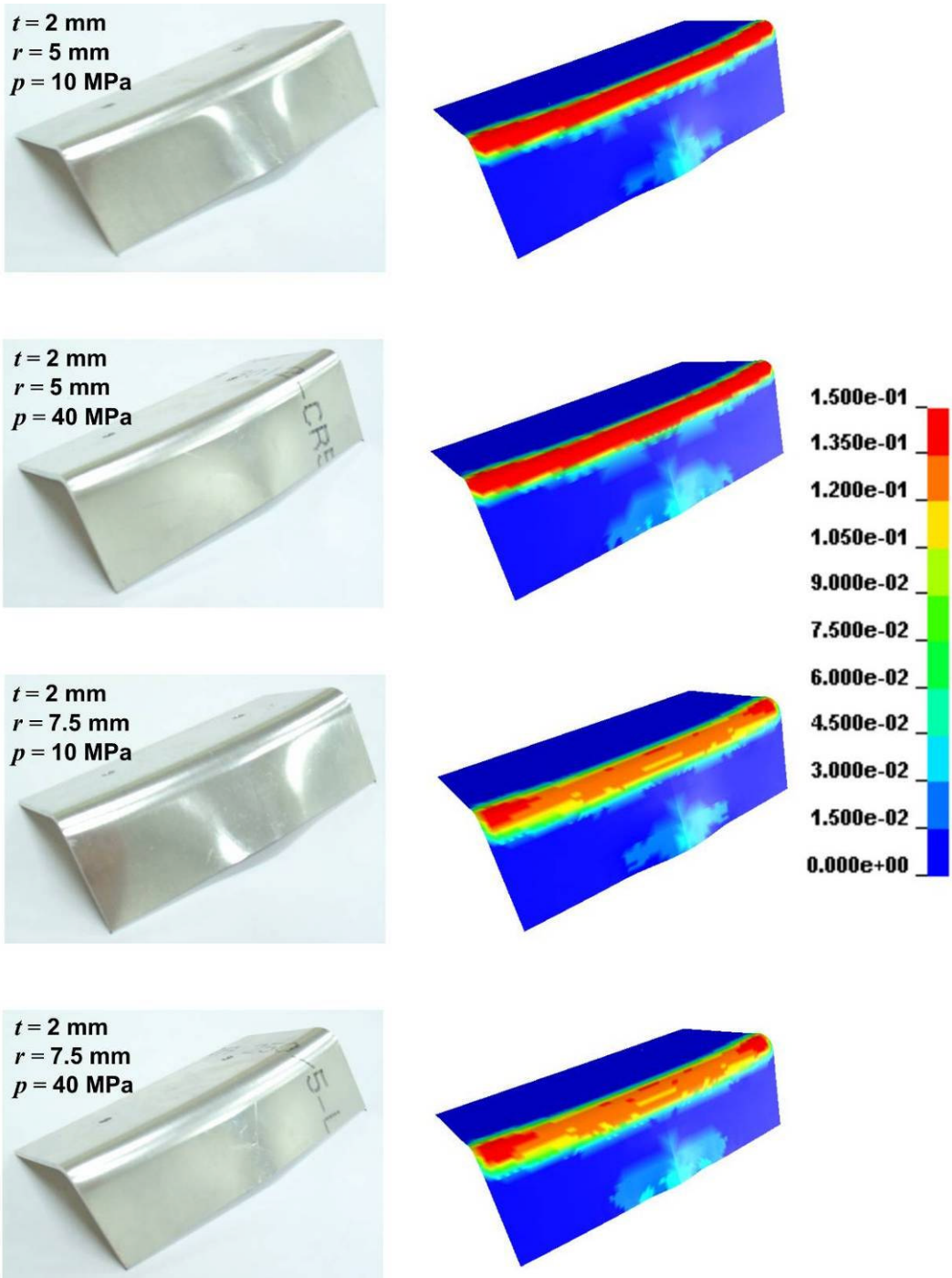

Figure 5.30 (continued)

5.4 Simulation of Circular Bulging Experiment

As described in Chapter 4, this experiment is the bulging of a circular sheet over a circular die with a hole at center (Figure 5.31). Problem can be simplified by using two-dimensional axisymetric assumption. Firstly, direct pressure is applied onto the sheet and then, rubber diaphragm is added to the model. In addition, full three-dimensional models are established for generalizing the problem. The defect of this specimen is that it splits at a certain pressure. This fracture point and bulge depths at different forming pressures are used as the basic parameters for the assessment.

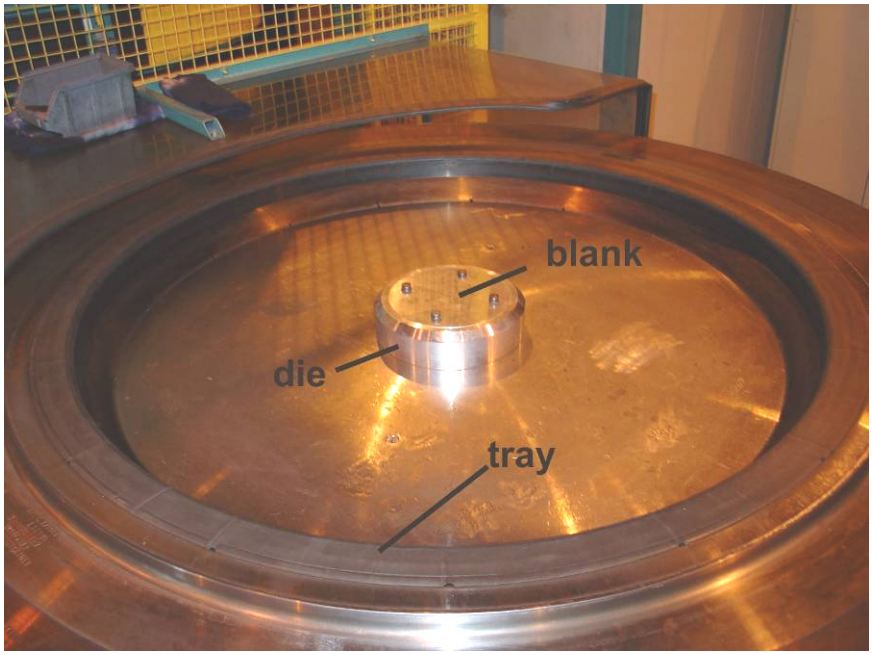

Figure 5.31 Circular Bulging Experiment.

5.4.1 Two-Dimensional Models without Diaphragm using Solid Elements and Static-Implicit Scheme

This model is identical to the model in Section 5.2.1 except that this is an axisymetric application and the geometry of the die and blank is circular. Figure 5.32 shows this model. The results are given in Table 5.7. Comparisons with experimental results are given in Figure 5.33. If the error of the model is defined as the difference of the bulge depth values of the model and experiment, max error is 5.1 mm, min error is 0.4 mm and the average error is 1.3 mm.

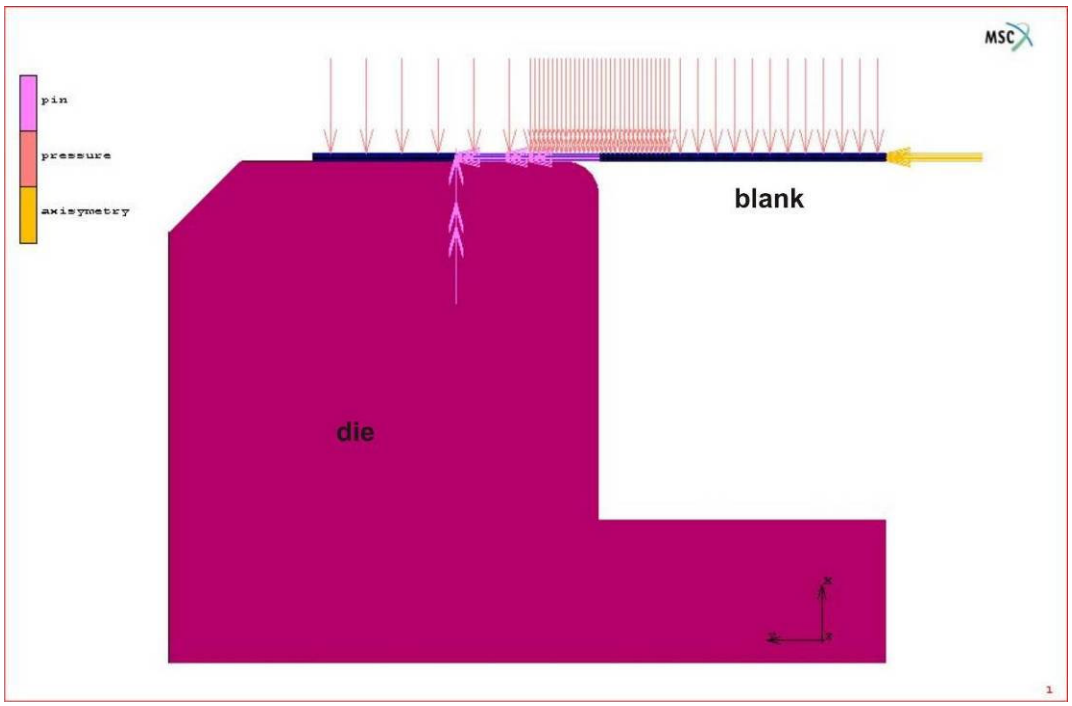

Figure 5.32 Two-dimensional, without diaphragm, solid elements, static-implicit model of the circular bulging experiment (MARC-MENTAT).

Table 5.7 Bulge depth results for two-dimensional, without diaphragm, solid elements, static-implicit model of the circular bulging specimen.

blank thickness (*t*) [mm]	**forming pressure (*p*) [MPa]**	**bulge depth [mm]**
0.6	10	splits
0.6	12.5	splits
1	10	11.4
1	12.5	14.4
1	15	20.4
1	17.5	splits
1	20	splits
1.6	10	7.1
1.6	12.5	8.9
1.6	15	10.7
1.6	17.5	12.4
1.6	20	14.4
2	10	5.7
2	12.5	7.1
2	15	8.5
2	17.5	10.0
2	20	11.3

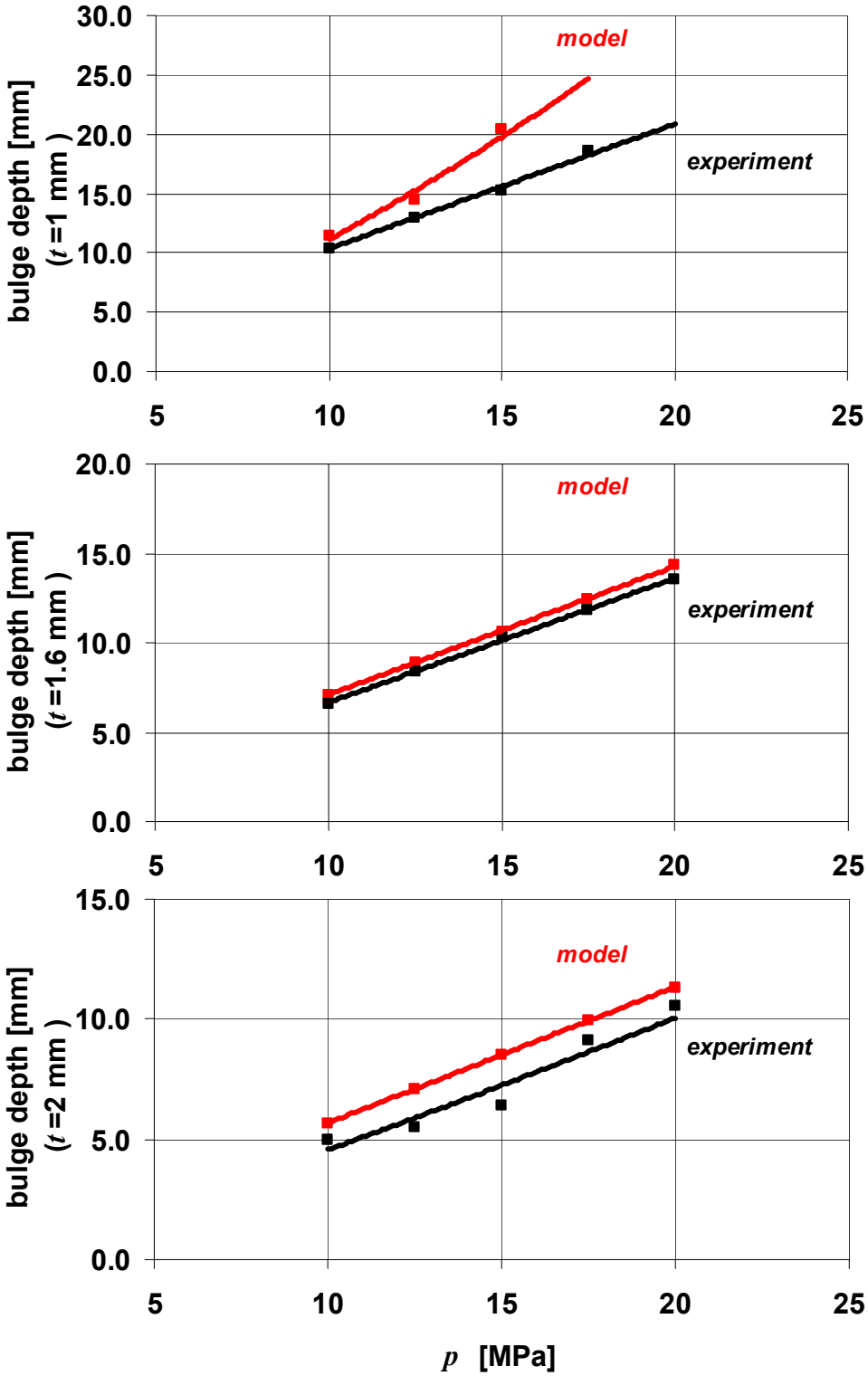

Figure 5.33 Comparison of the bulge depth results of the two-dimensional, without diaphragm, solid elements, static-implicit model of the circular bulging specimen with experimental results.

5.4.2 Two-Dimensional Models with Diaphragm using Solid Elements and Static-Implicit Scheme

This model is identical to the model in Section 5.2.5 except that this is an axisymetric application and the geometry of the die is circular. Figure 5.34 shows this model. The results are given in Table 5.8. Comparisons with experimental results are given in Figure 5.35. For the model, max error is 1.4 mm, min error is 0.1 mm and the average error is 0.5 mm. This result emphasizes the need for diaphragm modeling once again.

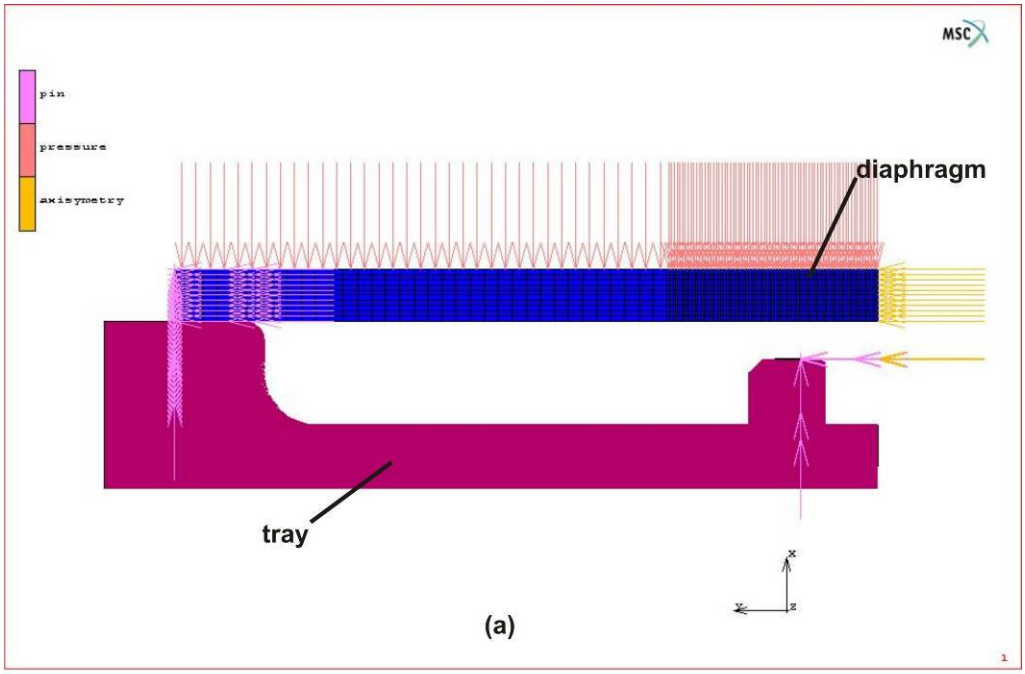

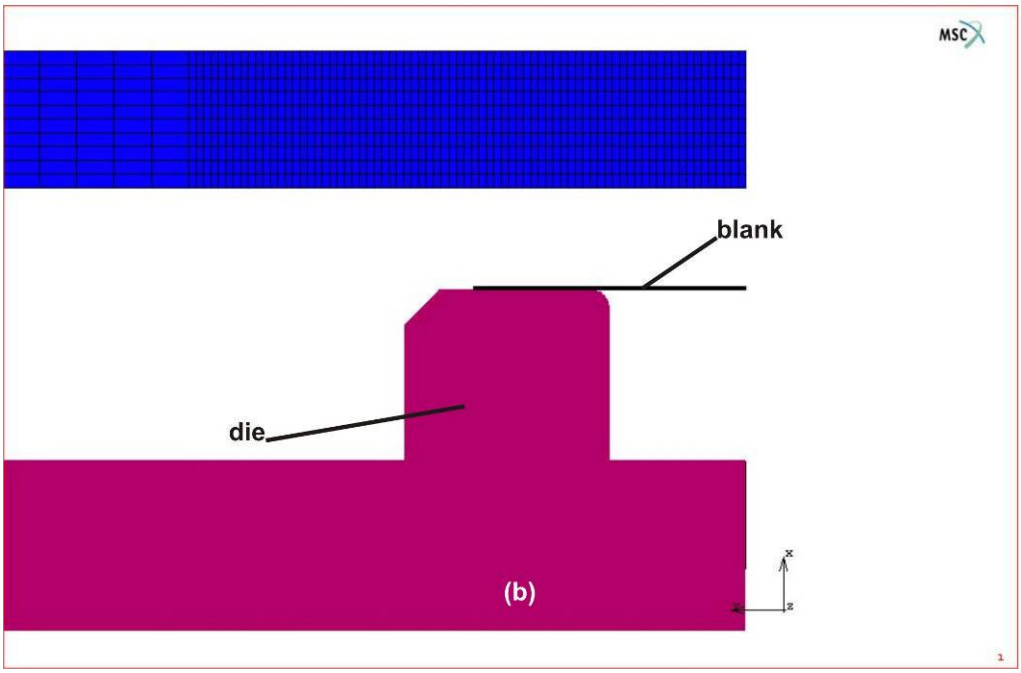

Figure 5.34 Two-dimensional, with diaphragm, solid elements, static-implicit model of the circular bulging experiment (MARC-MENTAT). (a) whole model (b) zoom to the die and blank.

Table 5.8 Bulge depth results for two-dimensional, with diaphragm, solid elements, static-implicit model of the circular bulging specimen.

blank thickness (*t*) [mm]	**forming pressure (*p*) [MPa]**	**bulge depth [mm]**
0.6	10	15.7
0.6	12.5	splits
1	10	9.8
1	12.5	12.2
1	15	14.9
1	17.5	19.0
1	20	splits
1.6	10	6.4
1.6	12.5	8.0
1.6	15	9.6
1.6	17.5	11.1
1.6	20	12.7
2	10	5.2
2	12.5	6.5
2	15	7.8
2	17.5	9.1
2	20	10.3

,

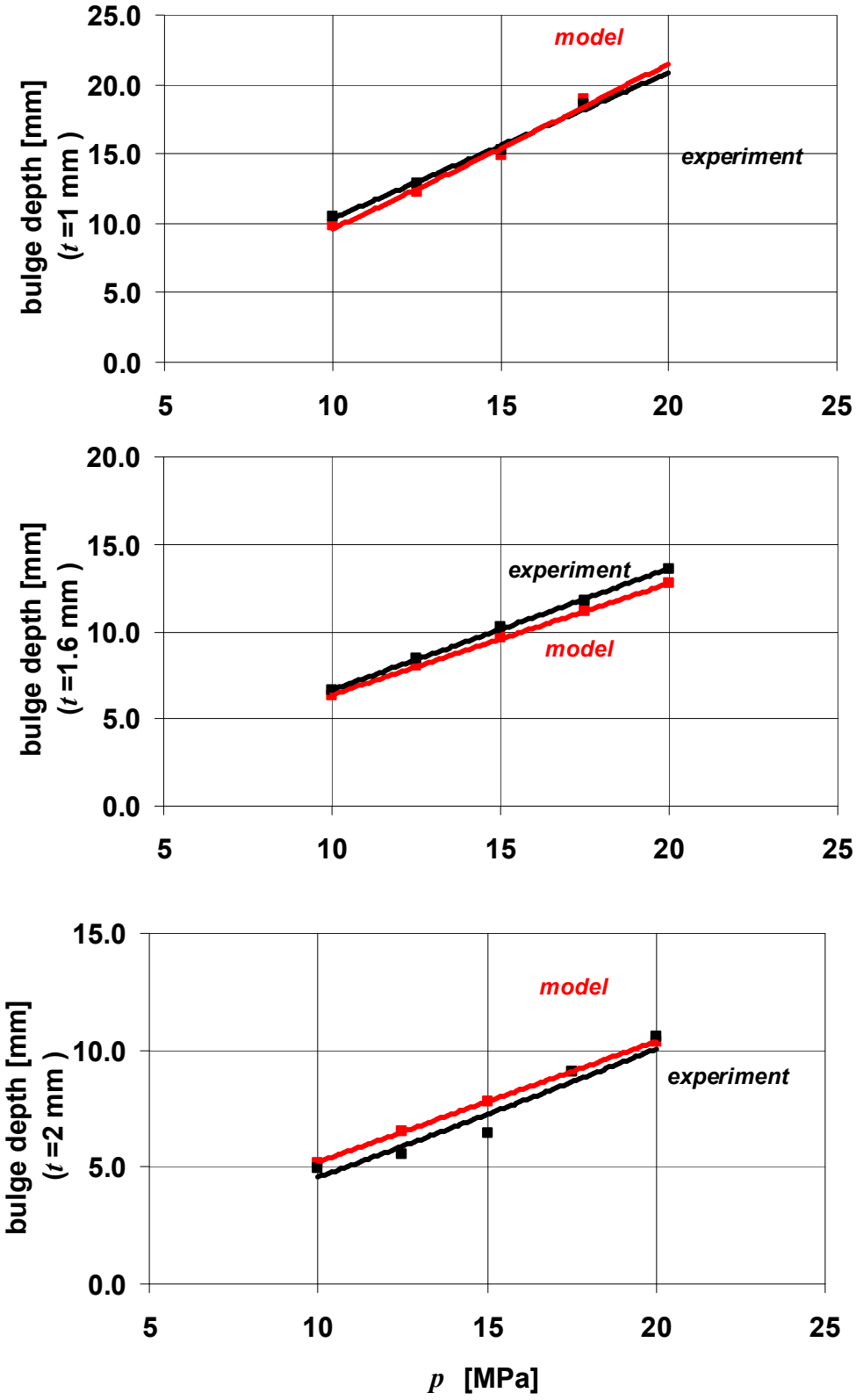

Figure 5.35 Comparison of the bulge depth results of the two-dimensional, with diaphragm, solid elements, static-implicit model of the circular bulging specimen with experimental results.

5.4.3 Three-Dimensional Models with Diaphragm using Shell Elements and Dynamic-Explicit Scheme

This model is identical to the model in Section 5.2.6 except that this is a quarter model and the geometry of the die is circular. Also, adaptive meshing is used for the blank. Figure 5.36 shows this model. The results are given in Table 5.9. Comparisons with experimental results are given in Figure 5.37. For the model, max error is 1.4 mm, min error is 0.4 mm and the average error is 0.9 mm.

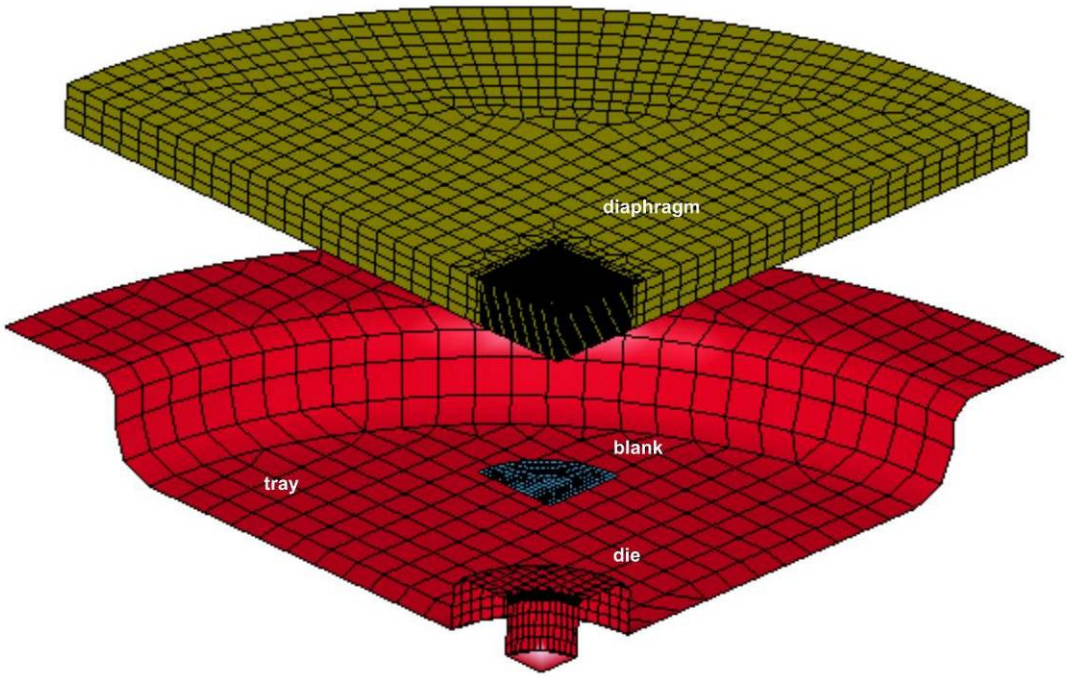

Figure 5.36 Three-dimensional, with diaphragm, shell elements, dynamic-explicit model of the circular bulging experiment (LS-DYNA).

Table 5.9 Bulge depth results for three-dimensional, with diaphragm, solid elements, dynamic-explicit model of the circular bulging specimen.

blank thickness (*t*) [mm]	**forming pressure (*p*) [MPa]**	**bulge depth [mm]**
0.6	10	14.4
0.6	12.5	19.5
0.6	15	splits
1	10	9.2
1	12.5	11.7
1	15	14.4
1	17.5	17.6
1	20	splits
1.6	10	5.9
1.6	12.5	7.5
1.6	15	9.2
1.6	17.5	10.8
1.6	20	12.5
2	10	4.4
2	12.5	5.9
2	15	7.4
2	17.5	8.6
2	20	10.0

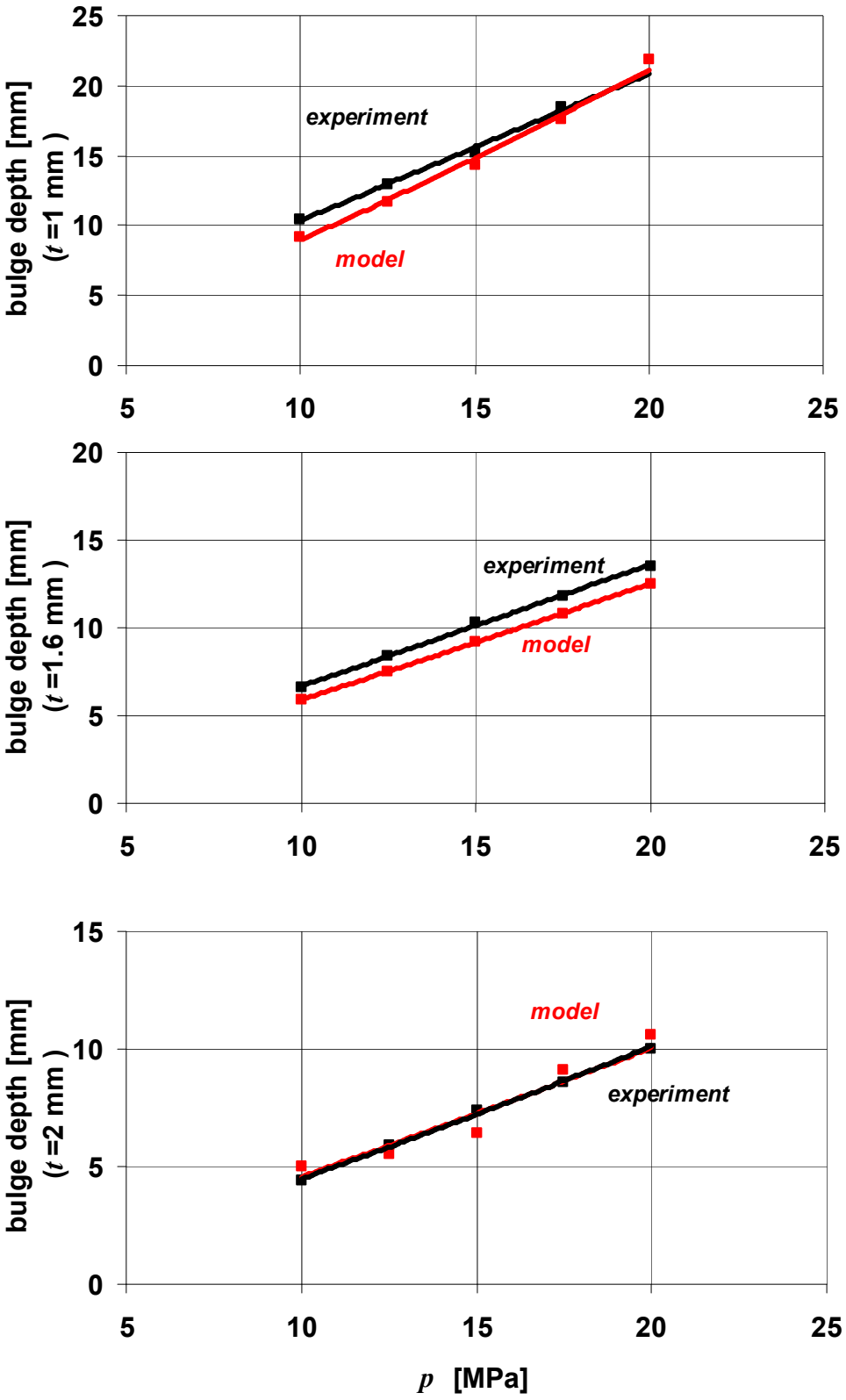

Figure 5.37 Comparison of the bulge depth results of the three-dimensional, with diaphragm, shell elements, dynamic-explicit model of the circular bulging specimen with experimental results.

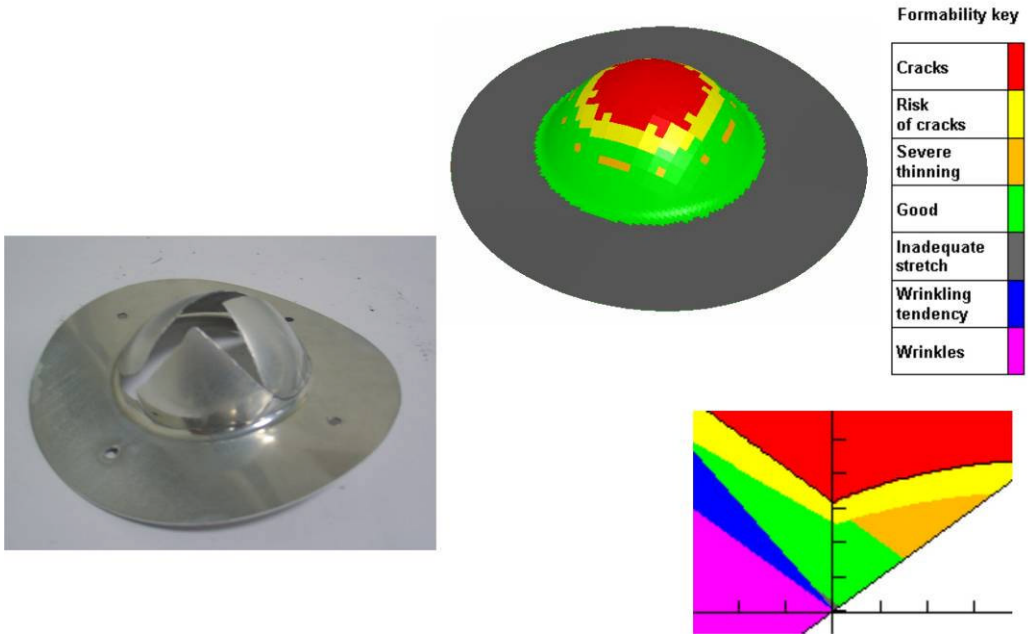

Figure 5.38 Fracture of the circular bulging specimen and its numerical model showing the split region defined by a FLD plot.

CHAPTER 6

CASE STUDIES

6.1 Introduction

In the previous chapter, the numerical analyses of simple experimental parts are done successfully. However, real aircraft parts are more complex and they need to be investigated in order to prove the success of the model. Hence, this chapter is devoted to the real applications. Three aircraft parts are selected that each has one of the defects of springback, wrinkling and splitting. Their numerical models are established and analyses are made. Results are then compared with real formed parts.

6.2 Case Study 1: Springback

This part is a connector part in the upper shell of the Agusta AB-139 aircraft (Figure 6.1). Connector parts typically have joggles on their flanges to allow stepped transitions between assembled parts. For the manufacturing of these parts, springback prediction is essential. Figure 6.2 shows this part after forming in the flexform press. Joggles, which can be defined as steps on the surface, make the deformation of the sheet complicated and empirical methods can not be used to predict the springback. and numerical analysis is needed for predicting the springback angles at different regions of the part.

The material of the blank is Al 2024-T3 and the data is given in Table 6.1. The blank has a thickness of 1.27 mm and the part is formed up to 80 MPa.

Using the CAD data of the die and blank, the model is prepared. Three-dimensional, with diaphragm, shell elements, dynamic-explicit model is used for the analysis (Section 5.2.6). Figure 6.3 shows this model.

Figure 6.1 The location of the part case 1 in the upper shell of Agusta AB-139 aircraft.

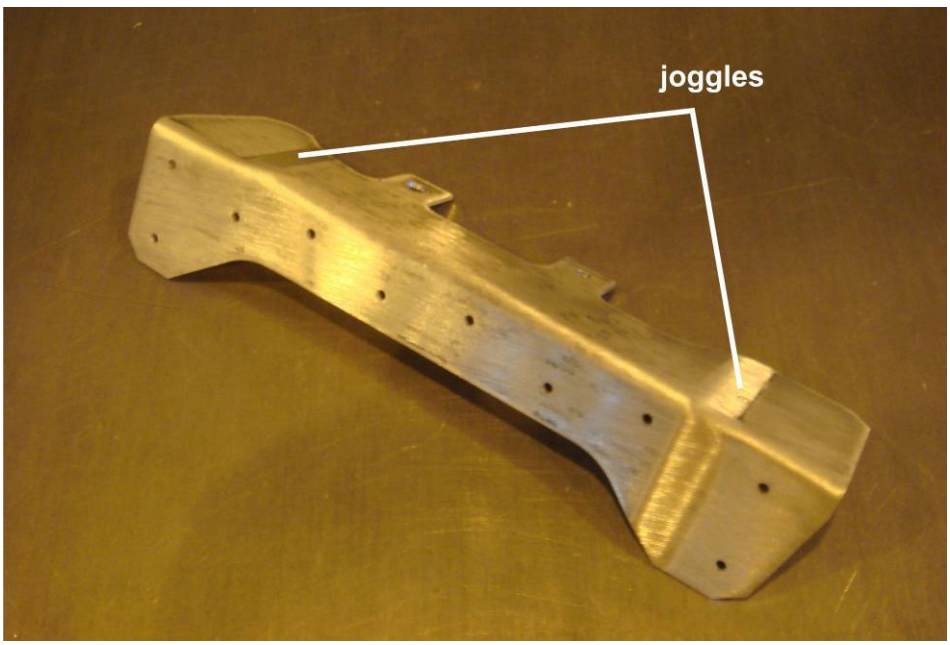

Figure 6.2 Springbacked part after forming in the flexform press.

Table 6.1 Material Properties of Al 2024-T3

Density	Young's Modulus	Poisson's Ratio	Yield Strength	Strength Coefficient (C)	Strain Hardening Exponent (n)
2.7e-9 tonnes/mm3	73100 MPa	0.33	275 MPa	628 MPa	0.119

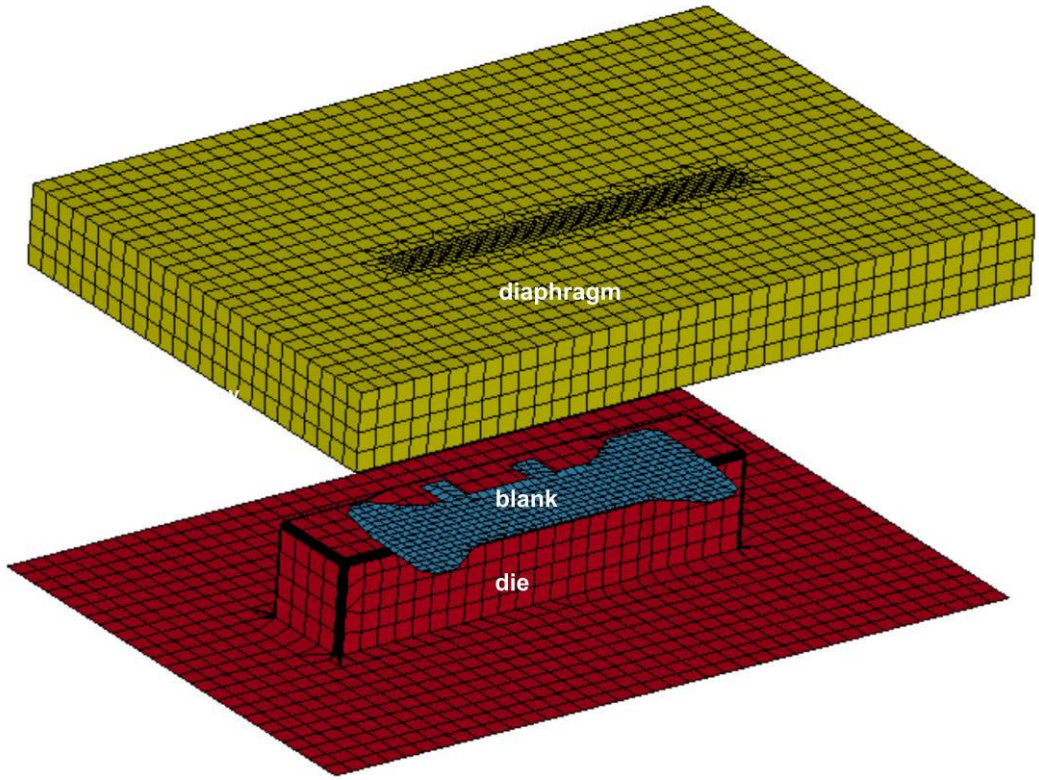

Figure 6.3 Numerical model of springbacked part

The tray of the press is not fully modeled. Only the die and the diaphragm piece over the die is modeled. This assumption is valid if enough distance is left from the blank to the boundaries. The blank is fixed from the guide pins. Adaptive meshing

is used for the blank. Finer mesh is used for the diaphragm in the bend region. Although the real part is formed up to 80 MPa, the analysis is done up to 10 MPa since this model has problems (due to the penalty contact) in springback prediction with higher pressures. However, springback results are still valid because of the negligible change in the springback angle as the forming pressure is increased to higher values. After forming analysis, springback calculation is done by using implicit method. The part after springback is shown in Figure 6.4 with angle values on it.

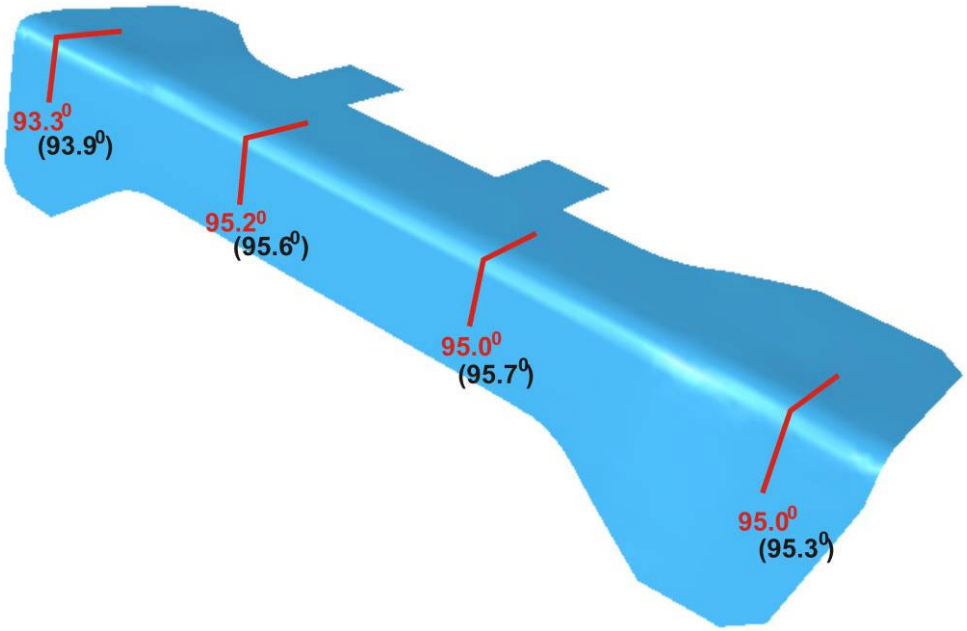

Figure 6.4 Comparison of the springback angles between the experiment and the model belonging to the springbacked part (The values in parenthesis are the experimental results).

Springback angles of this part are predicted with an average error of 0.5 degrees and that is acceptable considering the tolerances stated for this aircraft project.

The designed part has 90 degrees bend angles and springback causes the deviation from 90 degrees. The die should be compensated with a spring-forward method in

order to obtain the desired part. Since the flange of the part is not straight, empirical formulas are useless and numerical analysis is needed for this compensation.

6.3 Case Study 2: Wrinkling

This part is used in the cockpit of the McDonnell Douglas 902 helicopter (Figure 6.5). It has a contoured flange having a 130 degrees bend angle. This feature makes this part difficult to form and severe wrinkles are observed after forming in the flexform press (Figure 6.6).

The material of the blank is Al 2024-T0 and the data is given in Table 6.2. The blank has a thickness of 1mm and the part is formed up to 5 MPa.

Figure 6.5 The location of the part case 2 in the cockpit of McDonnell Douglas 902 helicopter

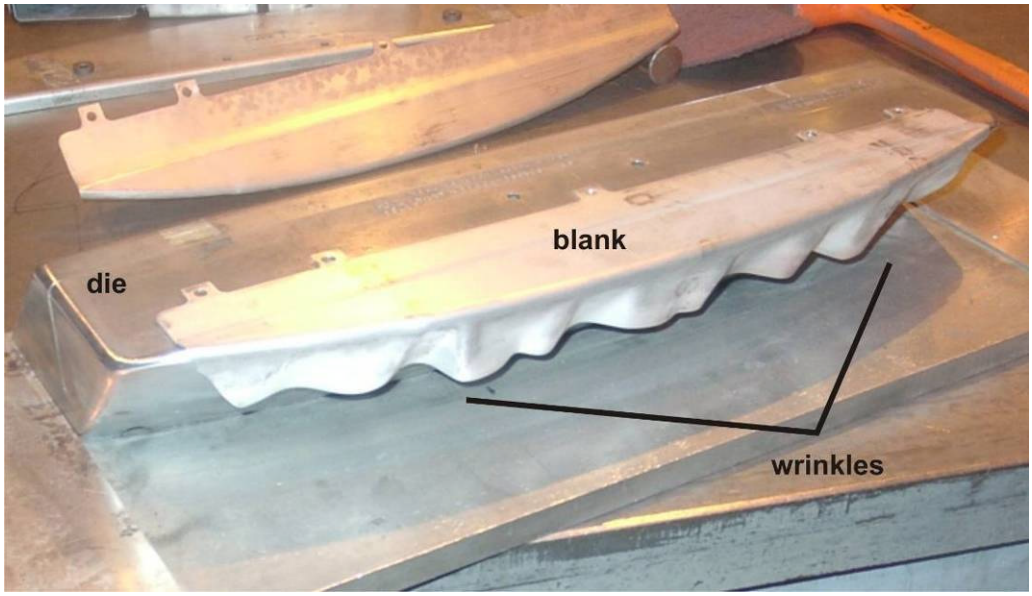

Figure 6.6 Wrinkled part after forming in the flexform press.

Table 6.2 Material Properties of Al 2024-T0

Density	Young's Modulus	Poisson's Ratio	Yield Strength	Strength Coefficient (C)	Strain Hardening Exponent (n)
2.7e-9 tonnes/mm3	73100 MPa	0.33	75 MPa	266 MPa	0.134

Using the CAD data of the die and blank, the model is prepared. Three-dimensional, with diaphragm, shell elements, dynamic-explicit model is used for the analysis (Section 5.2.6). Figure 6.7 shows this model. Since the part is symmetric half model is used. The blank is fixed from the guide pins. Adaptive meshing is used for the blank. Finer mesh is used for the diaphragm in the bend region. The formed part is shown in Figure 6.8.

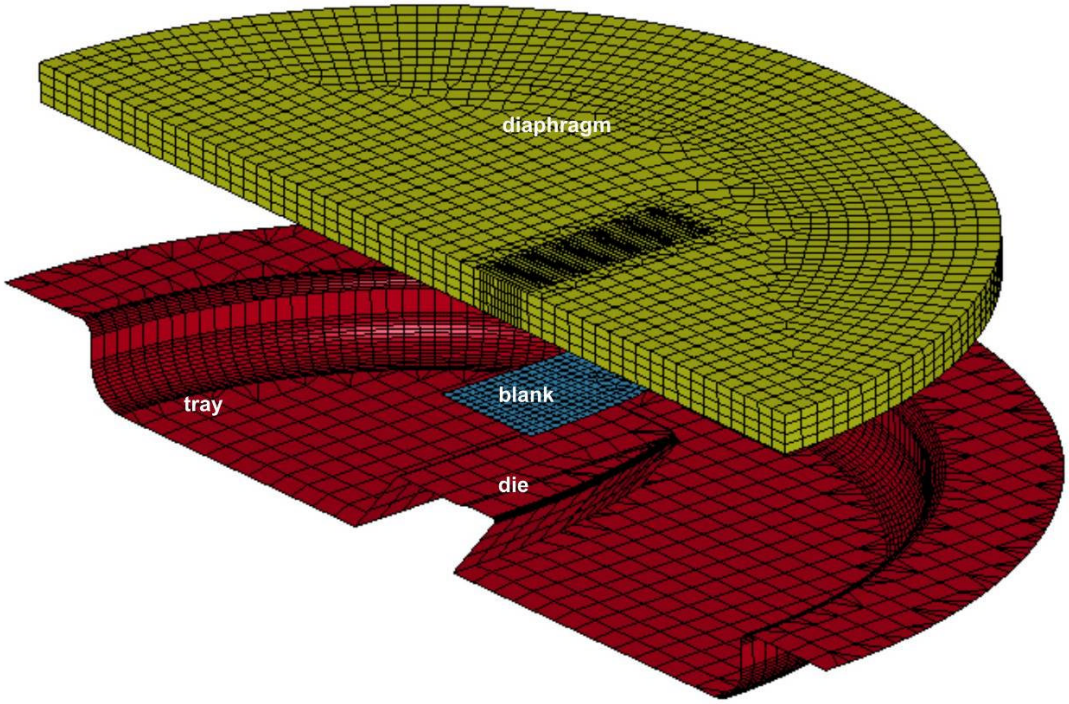

Figure 6.7 Numerical model of wrinkled part

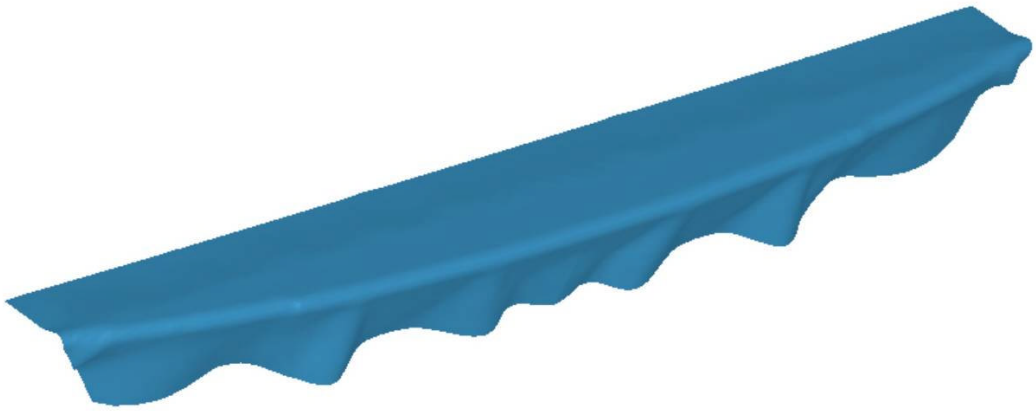

Figure 6.8 Wrinkled part after forming in the flexform press.

The resulting shape is very similar to the real part but has some differences. Expecting the exact shape from the model is unreasonable since the physical parts themselves have differences although they are formed at the same conditions.

Wrinkles can be prevented by changing the blank geometry so that some region of the blank contacts with the tray avoiding high compressive stresses. However, an additional trim operation is needed to exclude the excess material for the net shape in that case.

6.4 Case Study 3: Splitting

This part is used in the horizontal stabilizer of Sikorsky UH-60 helicopter (Figure 6.9).

Figure 6.9 The location of the part case 3 in the horizontal stabilizer of Sikorsky UH-60 helicopter

It is like a deep drawn part and is split after forming in the flexform press (Figure 6.10).

Figure 6.10 Split part after forming in the flexform press.

The material of the blank is Al 6061-T0 and the data is given in Table 6.3. The blank has a thickness of 1.27 mm and the part is formed up to 80 MPa.

Table 6.3 Material Properties of Al 6061-T0

Density	Young's Modulus	Poisson's Ratio	Yield Strength	Strength Coefficient (C)	Strain Hardening Exponent (n)
2.7e-9 tonnes/mm3	68900 MPa	0.33	55 MPa	224 MPa	0.209

Using the CAD data of the die and blank, the model is prepared. Three-dimensional, with diaphragm, shell elements, dynamic-explicit model is used for the analysis (Section 5.2.6). Figure 6.11 shows this model.

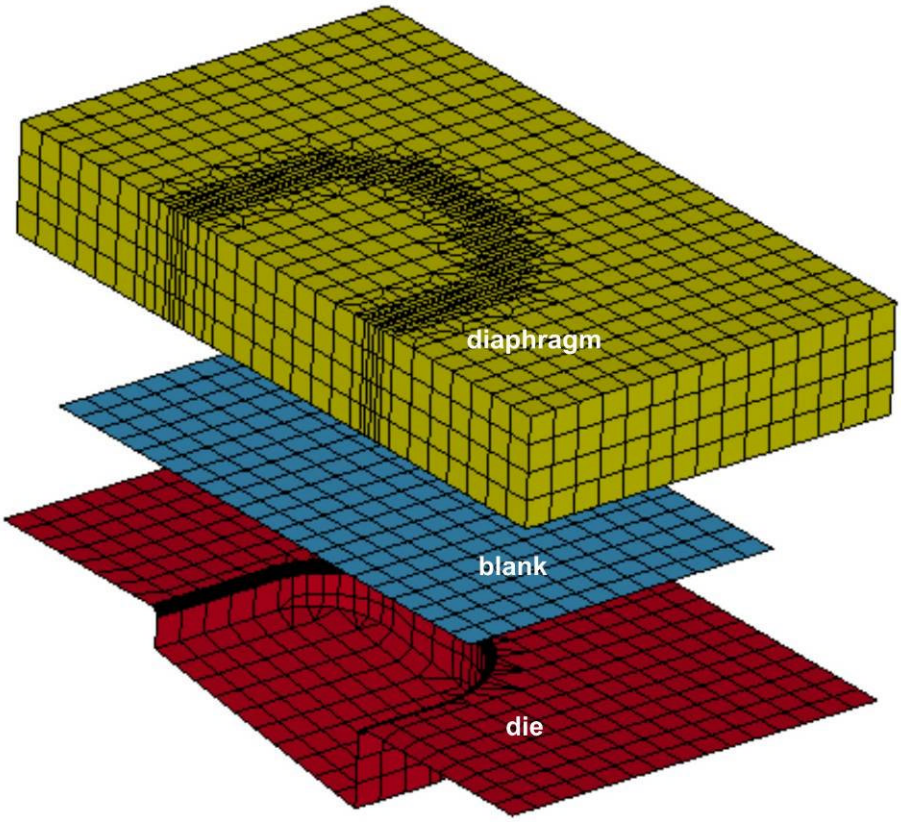

Figure 6.11 Numerical model of split part

Since the part is symmetric, half model is used. Only the die and the diaphragm piece over the die is modeled. This assumption is valid if enough distance is left from the blank to the boundaries. No guide pins are used for this part since the sheet must slide over the die in order to fill the deep regions. Adaptive meshing is used for the blank. Finer mesh is used for the diaphragm in the bend region. The formed part is shown in Figure 6.12 with a FLD plot. Keeler and Goodwin's empirical formula is used for the determination of FLC.

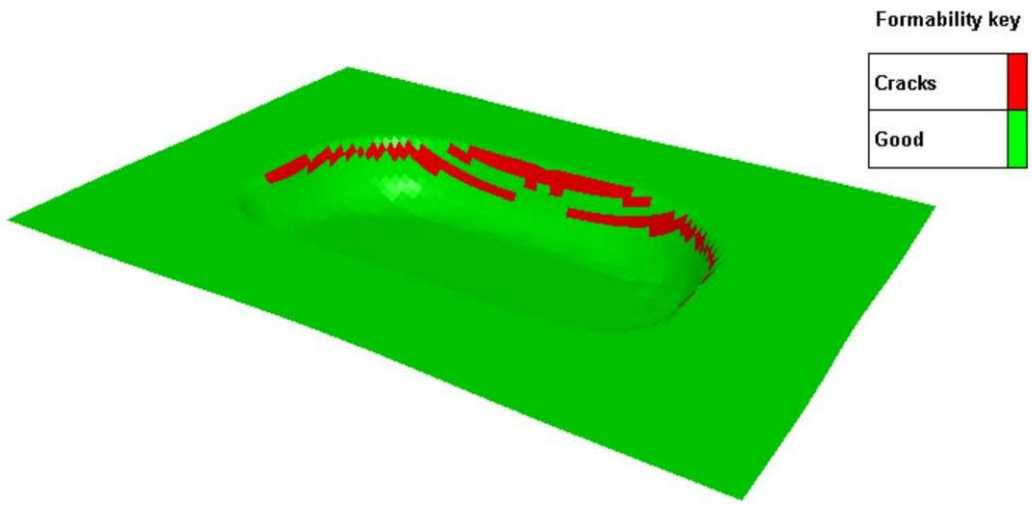

Figure 6.12 Split part after forming in the flexform press.

Figure shows that the split region is predicted well by the model. To avoid the splitting of this specimen, friction forces should be decreased and this can be done by using some lubricant and nylon between the blank and the die.

CHAPTER 7

CONCLUSIONS & FUTURE WORK

The aim of this study is to obtain a general numerical model which predicts the defects of the sheets before forming in the flexform press and to adjust the process parameters and make the necessary design changes of the dies and blanks accordingly.

Basic experiments are designed and conducted as straight flange bending, contoured flange bending and circular bulging representing the defects of springback, wrinkling and splitting respectively. Experiments are conducted in order to detect the effects of experimental parameters such as blank thickness, forming pressure, etc. to the final shape of sheets and also in order to validate the finite element results. Experimental results show that:

1- Springback angle in straight flanging depends on the forming pressure p and blank thickness-die bend radius ratio t/r for a given material. It decreases as t/r increases leading to splitting of the specimen at a certain t/r. It also decreases as the forming pressure increases, but after certain forming pressure, no change is observed.

2- Wrinkle formation in contoured flanging mainly depends on the blank thickness t. Die bend radius r has almost no effect on the wrinkle shape. Increasing forming pressure decreases the wrinkle size, but no change is observed after certain forming pressure.

3- Splitting in circular bulging depends on the blank thickness t and forming pressure p. Splitting occurs with increasing forming pressure and decreasing blank thickness.

Numerical analyses of physical experiments are done with various two and three-dimensional models, with and without diaphragm, using explicit and implicit approach for time integration and using solid and shell elements for the blank. Numerical results show that:

1- In all the analyses, rubber diaphragm should be modeled in order the capture the correct shape of the formed sheet.

2- Shell elements can be used instead of solids for the blank and dynamic-explicit scheme can be used instead static-implicit scheme for the time integration.

3- For springback prediction, mesh structure is very essential and enough number of elements should be used for the blank through the thickness and along the bend radius.

4- Penalty contact algorithm is useless for high pressures (higher than 10 MPa) especially for springback prediction since disruptions are seen in the pattern of strain and stress distributions in the bend region at higher pressures.

5- When using constraint contact algorithm, the deviation between the experimental and numerical springback results increases as the forming pressure increases since the discretization of the rubber diaphragm causes high local stress regions at higher pressures (higher than 10 MPa) leading to bad springback results.

Eventually, the three-dimensional model with diaphragm using shell elements for the blank and dynamic-explicit scheme for the time integration is chosen as the general model for this process. If the numerical results are compared with experimental results, it is seen that this model is successful. For springback prediction, the average error is 0.7 degrees which is acceptable for most of the applications. For wrinkling, it can predict the number of wrinkles and size well. For

bulge depth prediction, the average error is 0.9 mm which is also acceptable for most of the applications.

Then, this general model is used for the analyses of three selected aircraft sheet parts and success of the model in the real life applications is proved.

On the other hand, there are numerous subjects that should be investigated for future work:

1- In this study, isotropic material models are used since the material used in the experiments is nearly isotropic. However, for a general solution anisotropic behavior of sheet metals should be considered by using other material models.

2- In this study, penalty contact algorithm is used for dynamic-explicit solutions but this algorithm has problems at high pressures. Therefore, different algorithms should be investigated that are working well with dynamic-explicit method at high pressures.

3- For material characterization of the sheet , simple uniaxial tensile tests are conducted. For a complete characterization, hydraulic bulge tests and forming limit tests are required.

4- Friction between contacting pairs are modeled by using Coulomb's law and friction coefficients are chosen according to the previous studies. Tests like strip tests should be conducted in order to detect the correct behavior of friction forces between rubber diaphragm and aluminum sheet especially.

5- This study is focused on the prediction of the defects of the sheets, but for a complete work it is also required to study on the prevention techniques of these defects like die compensation for springback and changing blank geometry for wrinkle prevention, etc.

REFERENCES

[1] Z. Marciniak, J.L. Duncan, S. J. Hu: Mechanics of Sheet Metal Forming, Butterworth-Heinemann, London, 2002

[2] D. Ling, J. L. Babeau, A. Vaizian, F. E. Khaldi: Best Practice Methodology for Springback Prediction and Compensation, Proceedings of IDDRG 2007, Györ-Hungary

[3] K. Siegert and S. Wagner: TALAT Lecture 3701-Formability Characteristics of Aluminium Sheet, Insitut für Umformtechnik, Universität Stuttgart,1994

[4] H. Palaniswamy, G. Ngaile, T. Altan: Optimization of blank dimensions to reduce springback in the flexforming process, J. Mat. Process. Tech. 146 (2004), p.28-34.

[5] P. Kulkarni, S. Prabhakar: Influence of the Effect of strain Rates on Springback in Aluminum 2024 (ISO AlCuMg1), 4th European Ls-Dyna Users Conference.

[6] L. Noels, L. Stainier, J.Ponthot: Combined implicit-explicit time integration algorithms for the numerical simulation of sheet metal forming, J. Comp. and App. Math. 168 (2004), p. 331-339.

[7] Lembit M. Kutt, Allan B. Pifko, Jerrell A. Nardiello, John M. Papazian: Slow-Dynamic Finite Element Simulation of Manufacturing Processes, Computers & Structures Vol. 66, No. 1 (1998) , p. 1-17.

[8] H.Ali Hatipoğlu, A. Erman Tekkaya: Modeling Flexforming Process with Finite Element Method, Key Eng. Materials Vol. 344 (2007), p. 469-476

[9] F. Vollersten, R. Breede, M. Beckman: Process Layout and Forming Results from Deep Drawing Using Pressurized Membranes, Department for Metal Forming Technologies (LUF), University of Paderborn, Germany, 2001

[10] Dr. Daniel E. Green: Summary Report of A/SP Hydroforming Work, Industrial Research & Development Institute (IRDI), 2004

[11] PAM-STAMP 2G User's Guide, ESI-Software, France, 2007

[12] MARC-MENTAT Vol. A, Vol. B, MSC-Software, U.S.A., 2005

[13] A. Stühmeyer: LS-DYNA Introductory Class, CADFEM, 2006

[14] C. D. Joseph: Experimental Measurement and Finite Element Simulation of Springback in Stamping Aluminum Alloy Sheets for Auto-Body Panel Application, Mississippi State University, 2003

[15] N. E. Abedrabbo: Experimental and Numerical Investigation of Stamp Hydroforming and Ironing of Wrinkling in Sheet Metal Forming, Michigan State University, 2002

[16] R. S. Pandya: Prediction of Variation in Dimensional Tolerance Due to Sheet Metal Hydroforming Using Finite Element Analysis, Sardar Patel University, India, 2002

[17] A. E. Tekkaya: Finite Element Analysis in Solid Mechanics, Lecture Notes, Middle East Technical University, Ankara, 2002

[18] B. N. Maker, X. Zhu: Input Parameters for Springback Simulation Using LS-DYNA, Livermore Software Technology Corporation, 2001

[19] S.H. Zhang, J. Danckert: Development of Hydro-mechanical Deep Drawing, Journal of Material Processing Technology, 83 (1998), p. 14-25

[20] MARC-MENTAT Experimental Elastomer Analysis, MSC-Software, U.S.A., 2005

[21] LS-DYNA 970 Theory Manual, Livermore Software, U.S.A., 1998

[22] J. Tirosh, A. Shirizly, S. Yossifon: On Recent Progress in Deep Drawing Processes by Fluid-Pressure Assisted Methods, Adv. Technol. Plast. 1996, Proc. 5th Int. Conf. on Technology and Plasticity, Columbus, OH, 7-10 October, p. 707-710

[23] E. Buerk: Hydromechanical drawing, Sheet Met. Ind, March 1967, p. 182-188

[24] T.G. Johannisson: Flexforming-High Pressure Sheet Metal Forming, ABB Rev.6, 1989, p. 3-10

[25] D. Banabic, H.J. Bunge, K. Pöhlandt, A.E. Tekkaya: Formability of Metallic Materials", Springer, Berlin, 2000

[26] W.I. Lankford, S.C. Snyder, J.A. Bauscher: New Criteria for Predicting the Press Performance of Deep Drawing Sheets, Trans. ASM, 42 (1950), pp 1196-1232

[27] D. M. Woo: On the Complete Solution of the Deep Drawing Problem, Int. J. Mech. Sci., 10 (1968), pp 83 - 94

APPENDIX A

TECHNICAL DRAWINGS OF DIES & BLANKS OF BASIC EXPERIMENTS

The following figures show the technical drawings of dies and blanks used in the basic experiments mentioned in Chapter 4.

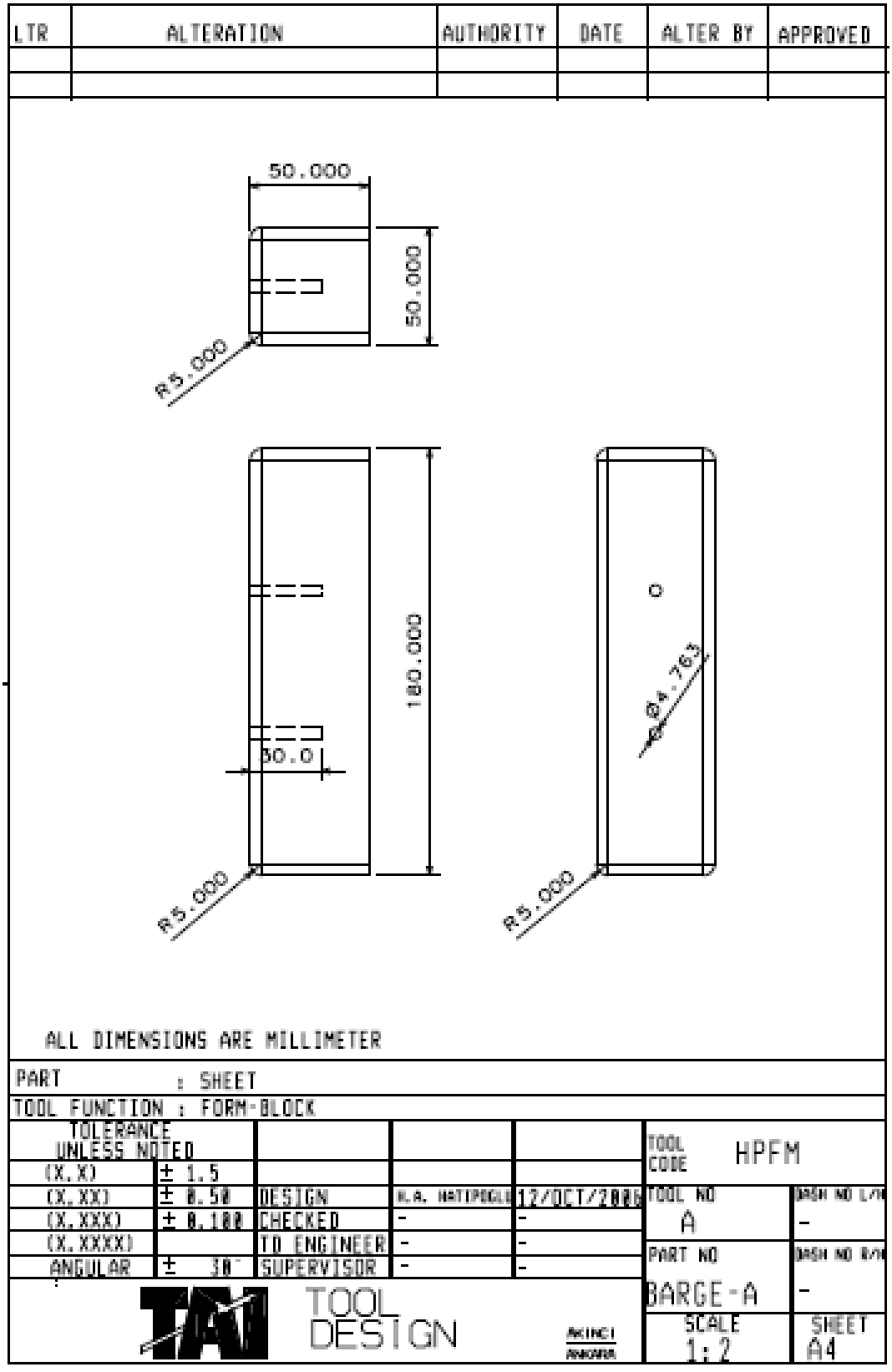

Figure A.1 Technical drawing of the die used in the straight flanging experiment

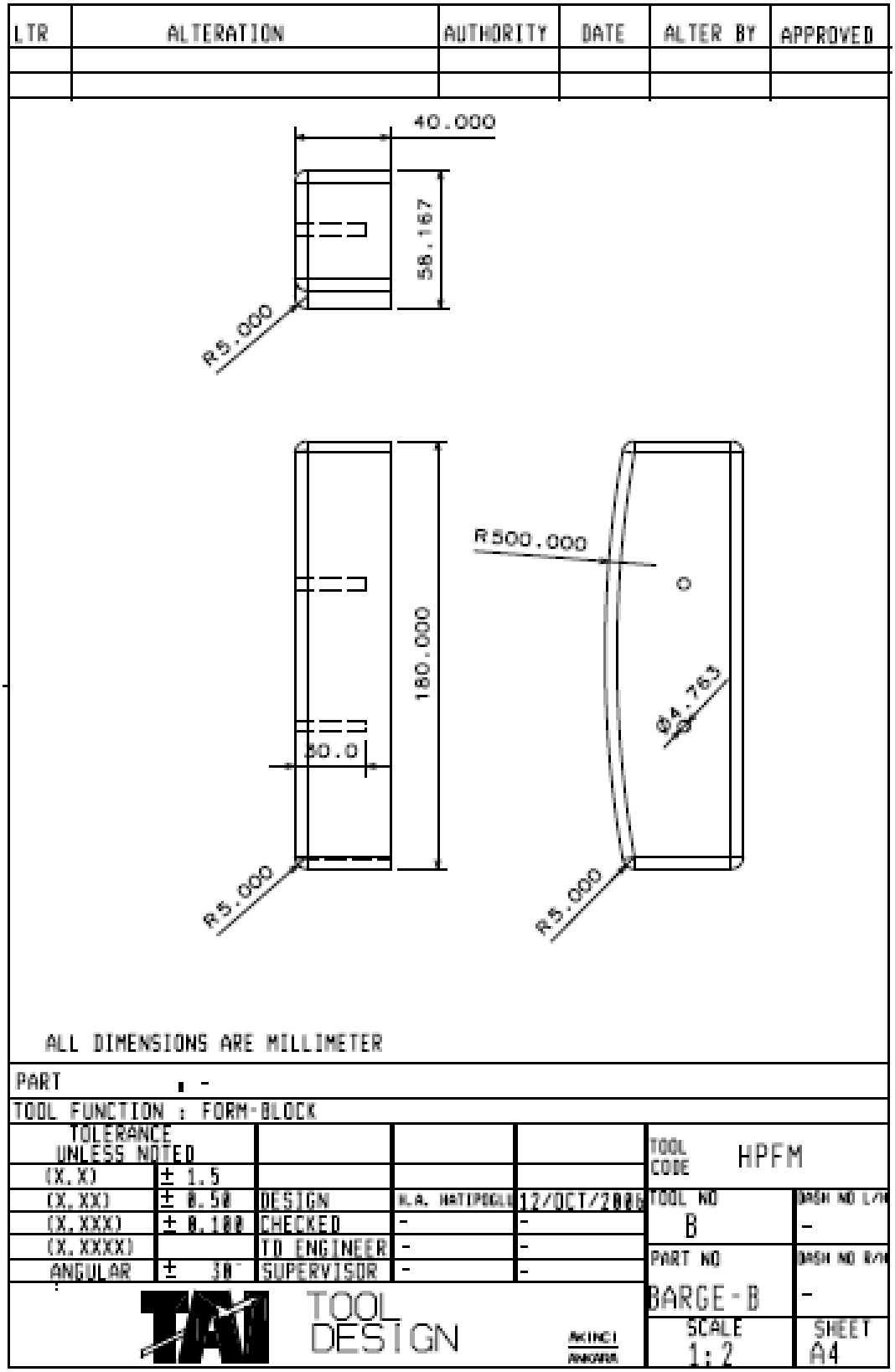

Figure A.2 Technical drawing of the die used in the contoured flanging experiment.

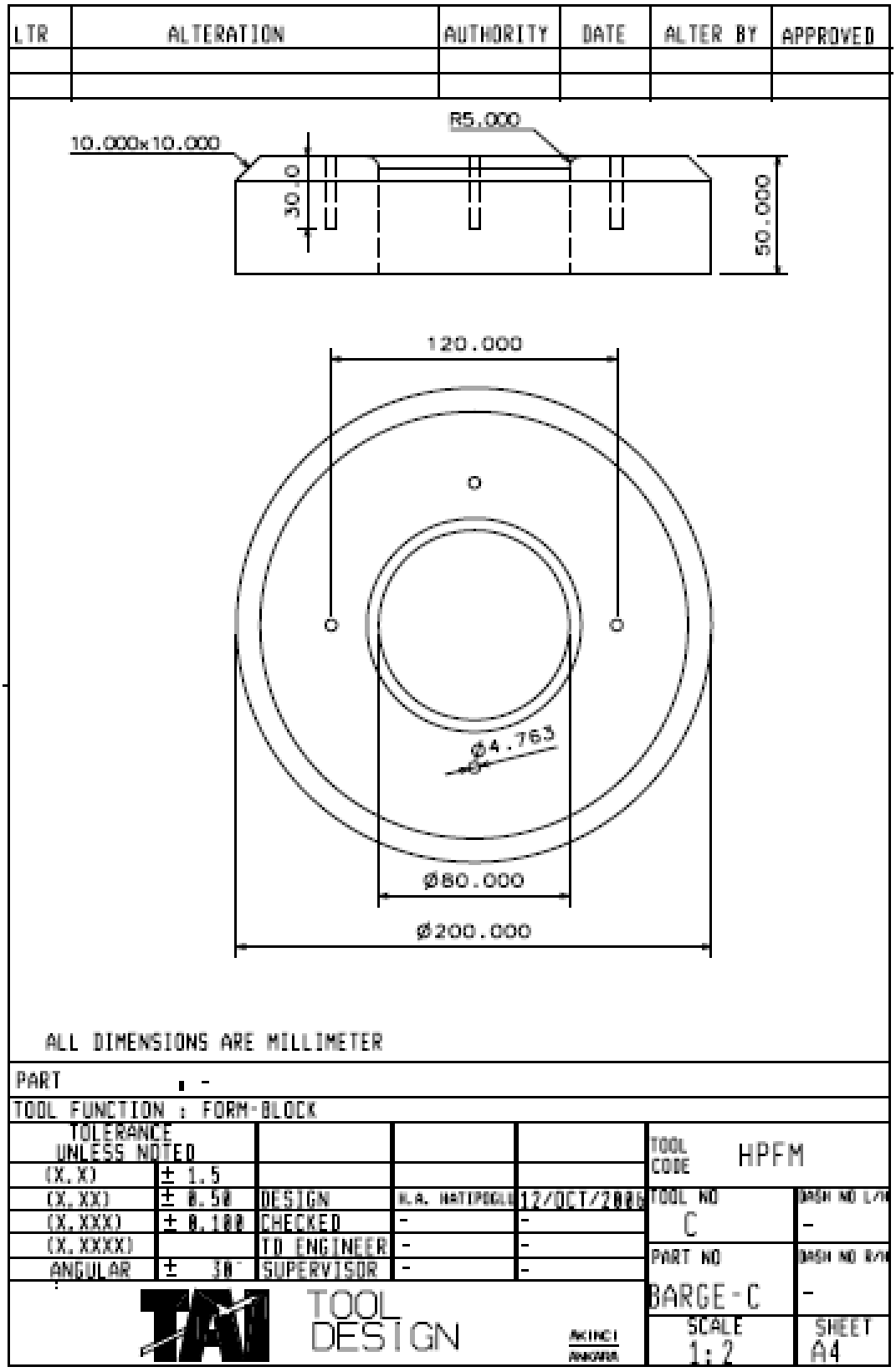

Figure A.3 Technical drawing of the die used in the circular bulging experiment.

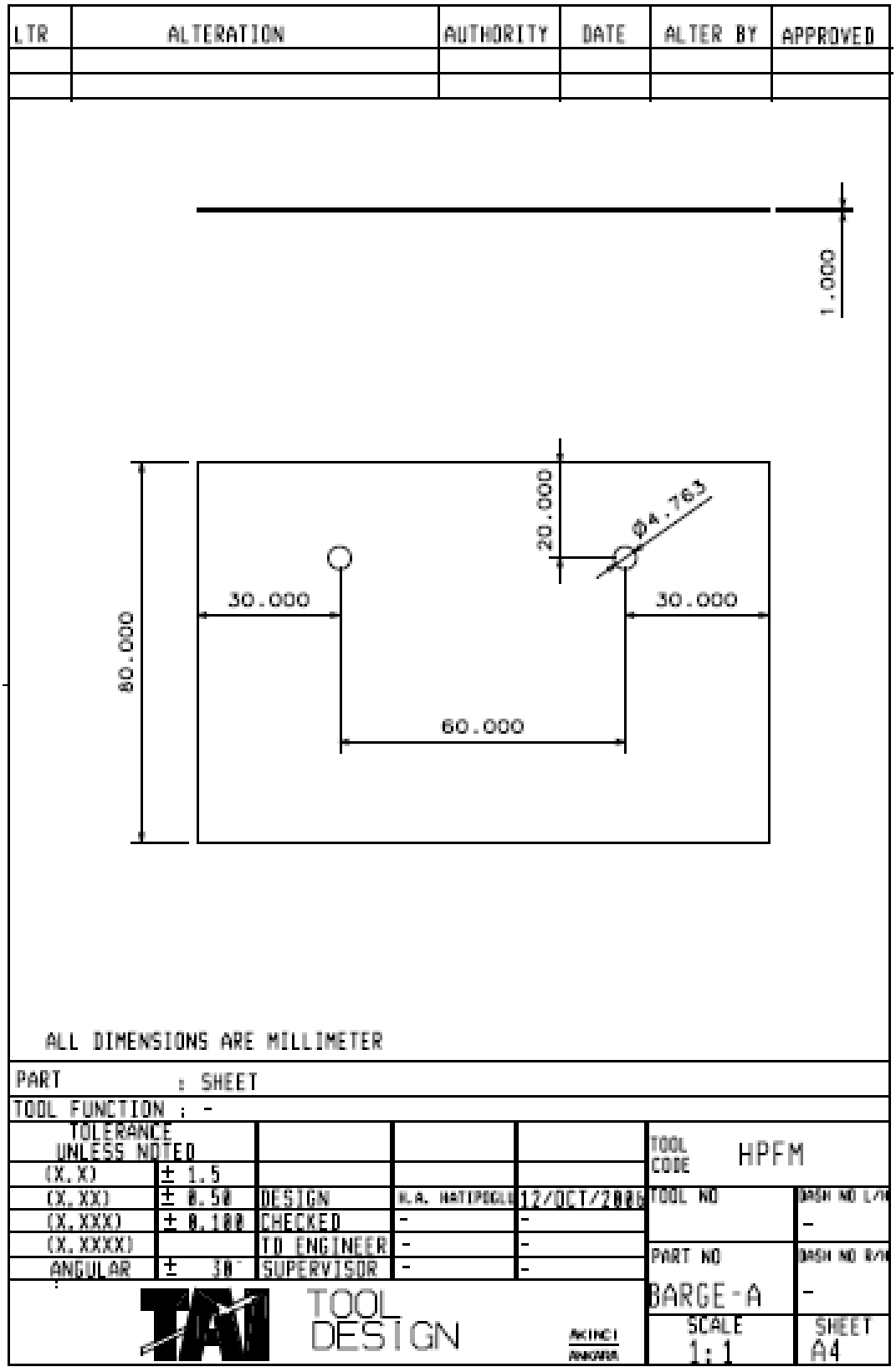

Figure A.4 Technical drawing of the blank used in the straight flanging and contoured flanging experiment.

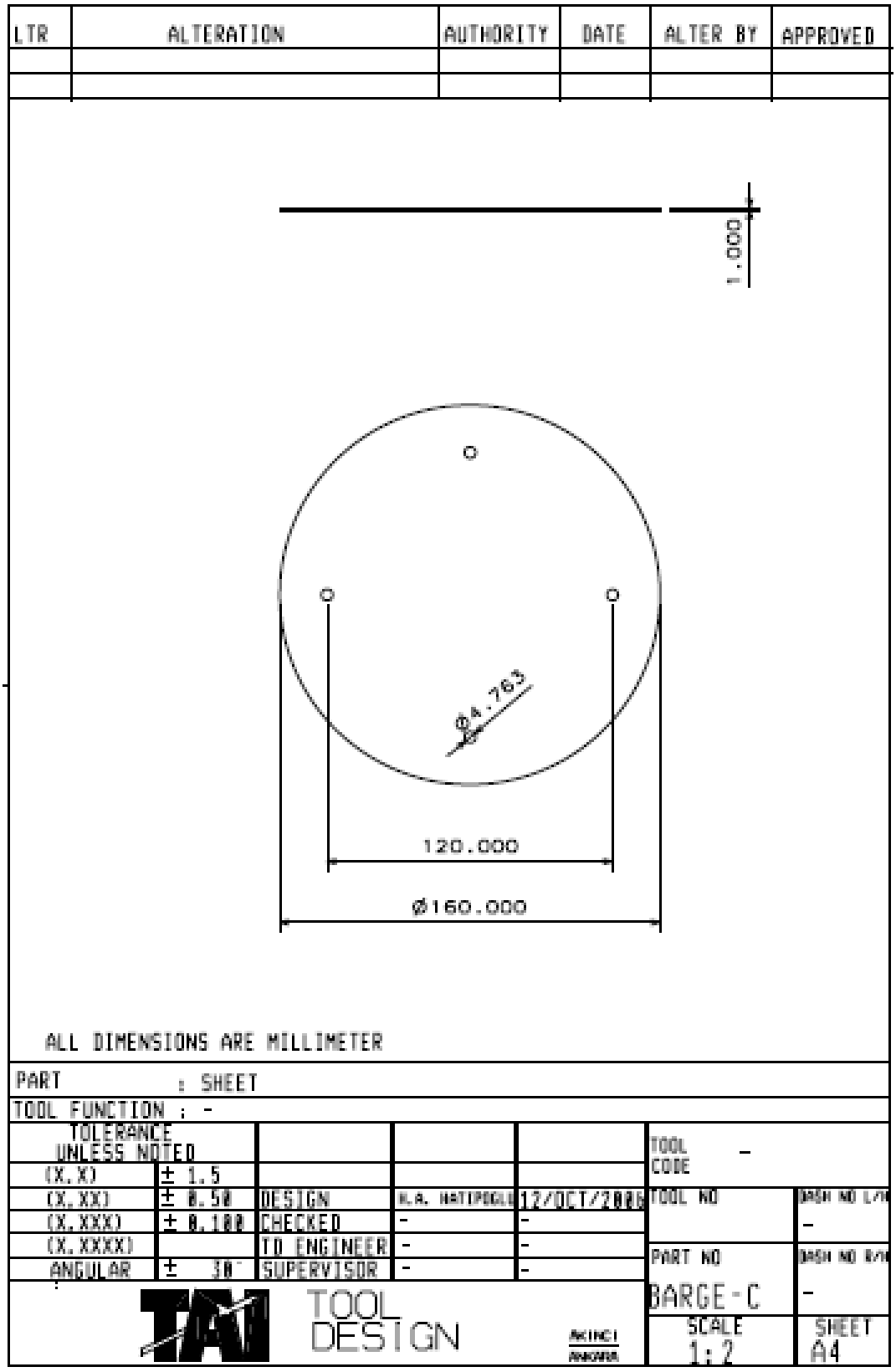

Figure A.5 Technical drawing of the blank used in the circular bulging experiment.

APPENDIX B

INFORMATION ABOUT ALCLAD ALUMINUM 2024- T3 ALLOY

2024 is a heat-treatable Al-Cu alloy that is available in a wide variety of product forms and tempers. Among those tempers, T3 corresponds to solution heat treated, cold worked and naturally aged to a substantially stable condition. Solution heat treatment is a high temperature process; usually close to the alloys melting point, at around 500°C. After heating to the solution treatment temperature, the part must be quenched to trap all the alloying elements in what is called a 'solid solution'. Usually the quenchant is water or a polymer. The high temperatures and severe quenching involved usually means this process causes a large amount of distortion. Sometimes aluminum alloys are solution treated at the mill or extrusion plant by quenching as the aluminum exits the tooling in order to control distortion. Immediately after quenching the metal is completely soft so there is an opportunity to straighten before aging occurs. Cold work is done by a flattening or straightening operation to strengthen the product. Natural aging involves leaving the material at room temperature for a period of time after solution treatment. Some of the dissolved alloying elements precipitate out of the solid solution and cause an increase in strength. This is a slow process as most alloys require about 96 hours to achieve full strength by natural aging.

2024-T3 is characterized by high ratios of tensile to yield strength and high fracture toughness and resistance to fatigue. It is used in aircraft fittings, gears and shafts, bolts, clock parts, computer parts, couplings, fuse parts, hydraulic valve bodies, missile parts, munitions, nuts, pistons, rectifier parts, worm gears, fastening devices, veterinary and orthopedic equipment, structures. Figure B.1 shows the uniaxial tensile data of Alclad Aluminum 2024-T3 with different rolling directions, different speeds and different sheet thicknesses.

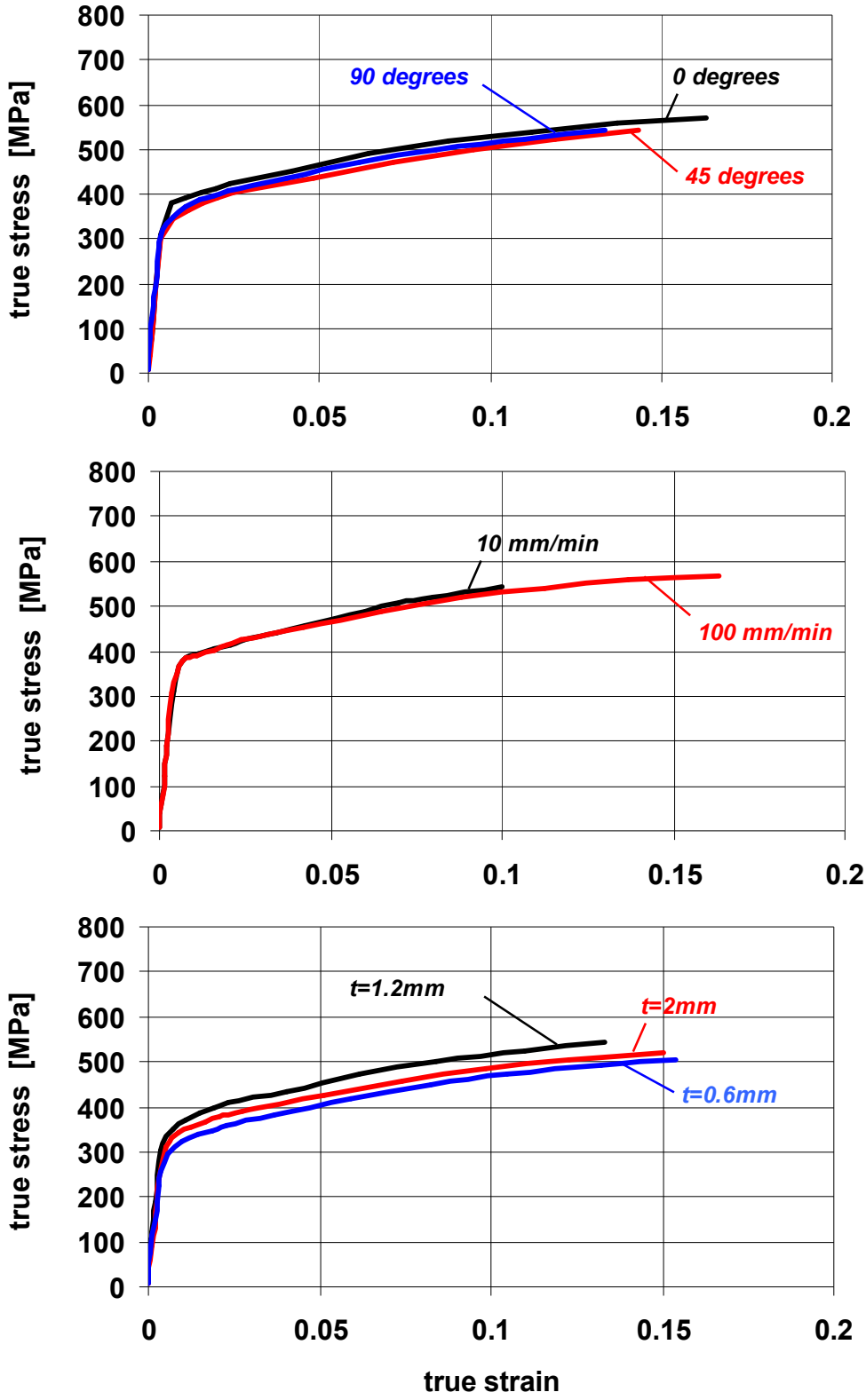

Figure B.1 Uniaxial tensile data of Alclad Aluminum 2024-T3 with different rolling directions, different speeds and different sheet thicknesses.

APPENDIX C

ANALYTICAL SOLUTION OF THE CIRCULAR BULGING EXPERIMENT

For the circular bulging experiment mentioned in Chapter 4, an analytical formulation is suggested [17] in order to predict the bulge depth of the specimen as:

$$p = 4.\left\{ C\left[\ln\left(\left(\frac{a^2}{a^2 + h^2} \right)^{-2} \right) \right]^n \right\}.t\frac{a^4 h}{\left(a^2 + h^2\right)^3} \tag{C.1}$$

Where,

p : forming pressure [MPa]

C : hardening coefficient [MPa]

n : hardening exponent

a : blank radius [mm]

t : blank thickness [mm]

h : bulge depth [mm]

From Eqn. C.1, h is calculated implicitly for given p, C, n, a and t.

Table C.1 gives the bulge depth results for different p and t values. Figure C.1 compares the analytical results with the numerical model results in section 5.4.1 which is two-dimensional, without diaphragm, solid elements and static-implicit.

Table C.1 Bulge depth results for the analytical model of the circular bulging specimen.

blank thickness (*t*) [mm]	**forming pressure (*p*) [MPa]**	**bulge depth [mm]**
0.6	10	splits
1	10	11.2
1	12.5	15.4
1	15	splits
1.6	10	6.9
1.6	12.5	8.6
1.6	15	10.4
1.6	17.5	12.5
1.6	20	15.4
2	10	5.7
2	12.5	6.9
2	15	8.2
2	17.5	9.6
2	20	11.2

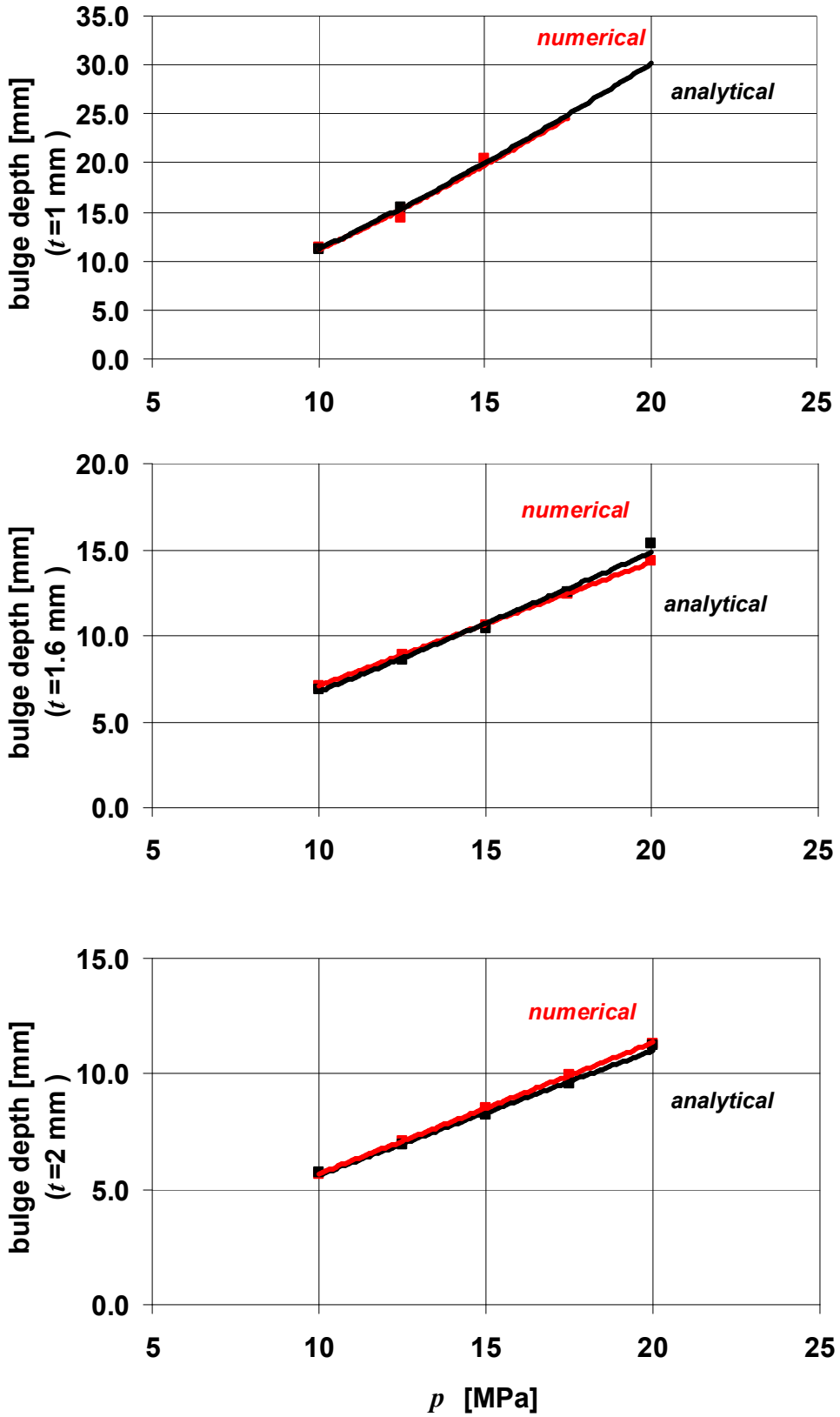

Figure C.1 Comparison of the bulge depth results of the two-dimensional, without diaphragm, solid elements, static-implicit model of the circular bulging specimen with analytical results